

Wave-current modeling in the Irish Sea and coastal flood impacts

JENNY M. BROWN, JUDITH WOLF, ALEJANDRO J. SOUZA, ROGER PROCTOR

Proudman Oceanographic Laboratory, 6 Brownlow Street, Liverpool L3 5DA UK
email: jebro@pol.ac.uk, jaw@pol.ac.uk, ajso@pol.ac.uk, rp@pol.ac.uk

Keywords: surge, wave-current interaction, POLCOMS, WAM; Irish Sea

ABSTRACT

It is believed that in the future the intensity and frequency of extreme coastal flooding events will increase as a result of climate change. The Coastal Flooding by Extreme Events (CoFEE) project is investigating the flood risks in the eastern Irish Sea. This study area includes most of England's coastal types and the project focuses on the management of the Sefton coast with its mobile dunes. The present and future flood risk posed by extreme events is being investigated using advanced modeling. Following from the model results presented here, a 10-year simulation (1996–2006) using a nested model system to simulate the wave-current interaction will be performed and validated. These data can then be used to investigate the potential of coastal flooding by waves in the study area.

In order to accurately simulate the waves in the study area, we have set up a one-way nested approach from a 1° North Atlantic model, through a 1.8-km Irish Sea model, to a 180-m Liverpool Bay model, using the state-of-the-art 3rd-generation spectral Wave Model (WAM), so that any influence that swell might have in the study area will be correctly represented. At the medium resolution Irish Sea model, using a POLCOMS-WAM coupled model, we examine the effects of wave-current interaction on the prediction of surges and waves at the coast compared with available data.

Introduction

Future extreme coastal flooding events are expected to increase (in intensity and frequency) as a result of climate change. The Coastal Flooding by Extreme Events (CoFEE) project is investigating present and future flood risks in Liverpool Bay and especially along the Sefton coastline. The flood risk posed by extreme events is being investigated using advanced modeling over a 10-year period (1996–2006).

We use POLCOMS-WAM as a wave-current coupled modeling system in a one way nested framework from ~12 km to 1.8 km. To test the accuracy of the modeling system two extreme storm events 12th November 1977 (Jones and Davies, 1998) and 18th January 2007 have been simulated to validate and tune the model to allow accurate surge elevations to be predicted in the eastern Irish Sea.

Methods

In order to accurately simulate the waves in the study area, a one-way nested approach has been set up. For waves a 1° North Atlantic model forces the boundary of a 1.8-km Irish Sea model (Figure 1a), using the state-of-the-art 3rd-generation spectral Wave Model (WAM). Any influences that swell might have in the study area will therefore be correctly represented. To capture the external surge-tide effects generated outside of the Irish Sea a one-way nested approach from a 1/9° latitude by 1/6° longitude (~12 km) model to the 1.8-km Irish Sea model has been applied. For the 1977 surge event the Proudman Oceanographic Laboratory Coastal Ocean Modelling System (POLCOMS) Atlantic Margin Model (Figure 1b) was used to provide the boundary forcing, but in the 2007 event POL's operational Continental Shelf surge model (CS3) was applied (Figure 1c) since this model has been tuned to accurately predict storm surge events around the UK. In the Irish Sea POLCOMS-WAM was used to simulate the wave-current interaction to accurately predict the two surge events.

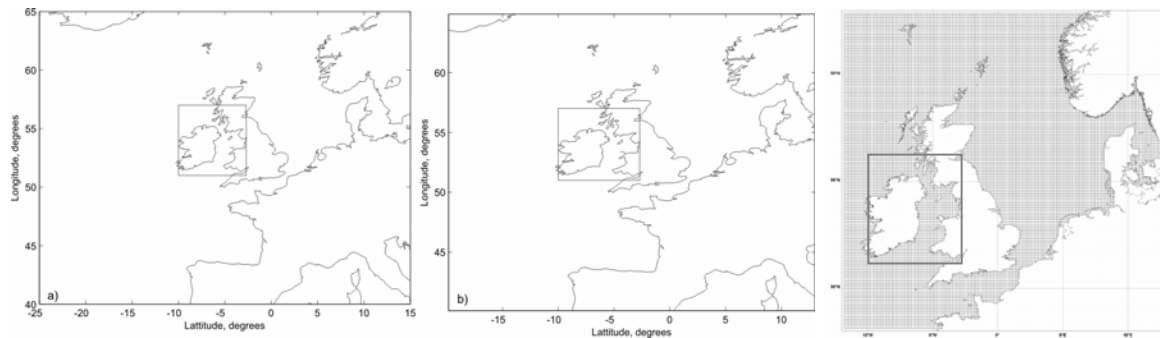
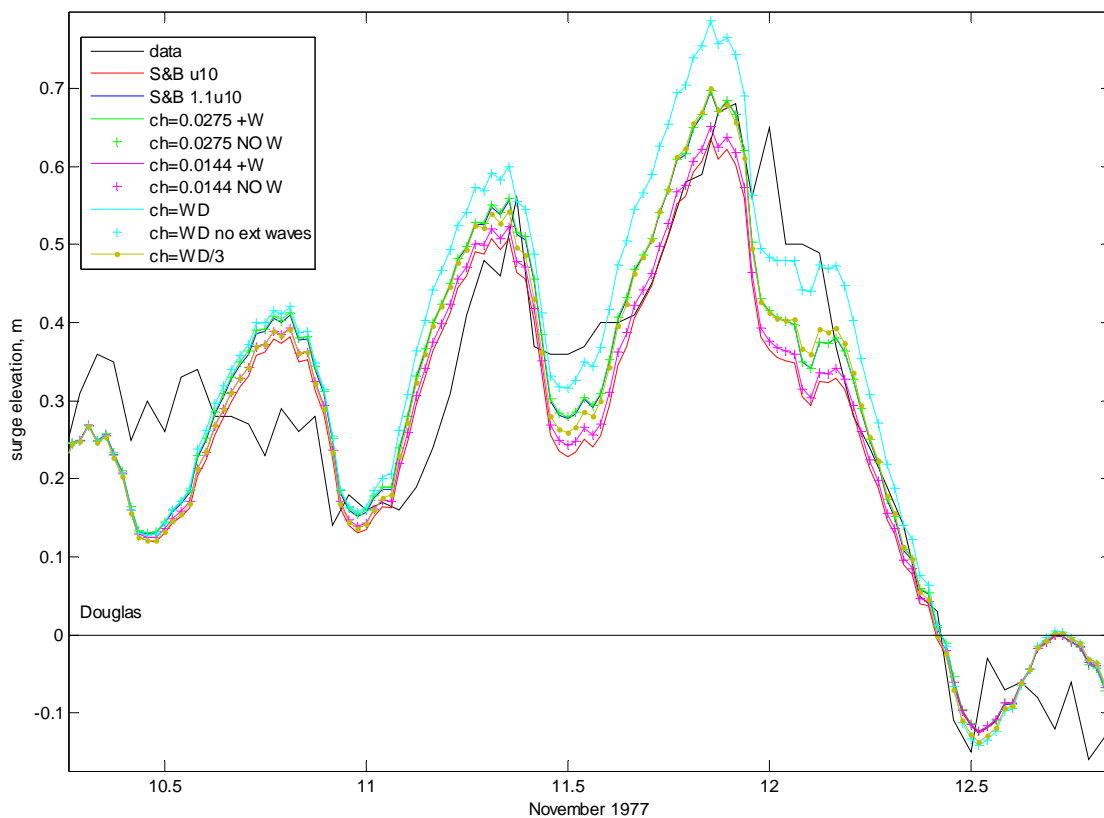


Figure 1. a) The model nesting for the wave simulation from the NE Atlantic model to the Irish Sea model and the current model nesting using b) POLCOMS and c) CS3.

The coarse grid models for POLCOMS and WAM were driven by 1° resolution ECMWF (ERA-40) data provided every six hours. The CS3 model was driven by Met Office mesoscale winds, with resolution of approximately 12 km, at hourly intervals. For the medium resolution Irish Sea model high resolution (both spatially, ½° by ½°, and temporally, 3-hourly) wind and pressure data (Jones and Davies, 1998) were used to drive the model to accurately simulate the wave and surge conditions in 1977, while the mesoscale wind data were used for the 2007 event.

Results

Comparison of the surge elevation at ports across in the eastern Irish Sea (Figure 2) has shown that to correctly simulate the surge elevation it is important to include the external surge and locally generated wave effects. The external swell effect was found to have little impact on the predictions in this location. Local wave effects were required to capture the wave age dependence in the surface drag, which varies in both time and space.



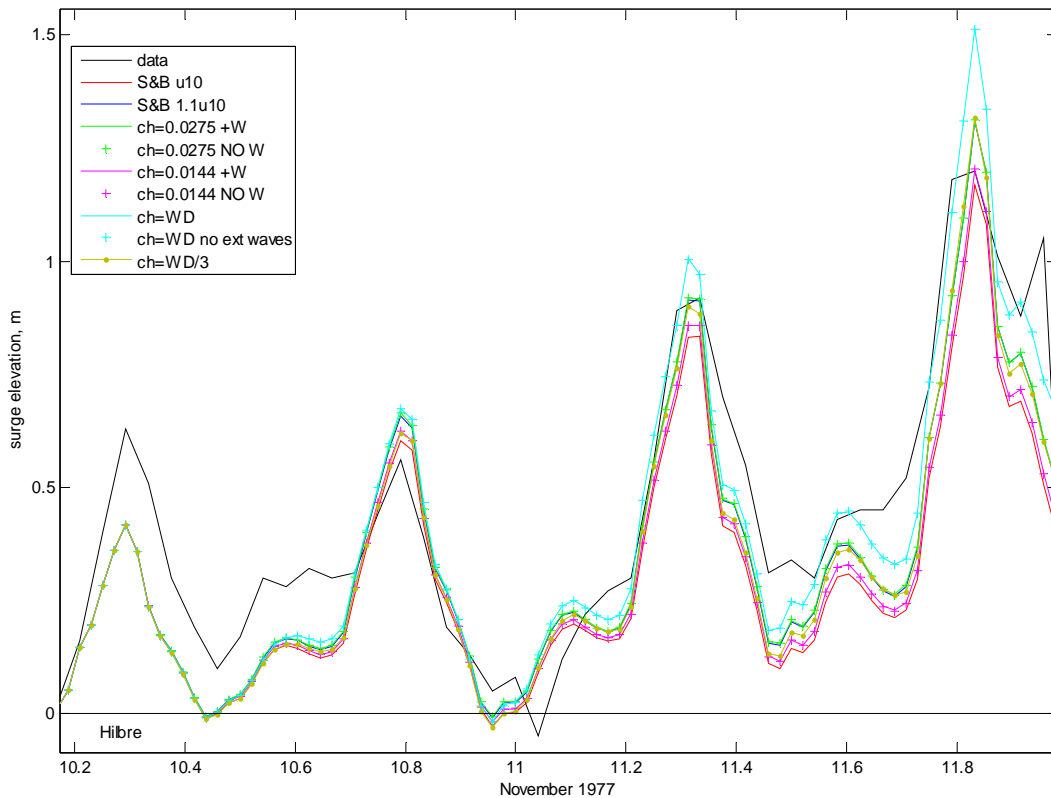


Figure 2. The predicted surge elevation ('S&B' or 'ch' in legend) and observed surge elevation ('data' in legend) at Douglas (a deep offshore location) and Hilbre (a shallow coastal location) in the eastern Irish Sea during November 1977. In the legend 'S&B' means the Smith and Banke method, 'ch' means the Charnock method where the value represents the value of the Charnock parameter, 'WD' means wave dependent Charnock parameter, '+w' means waves are included, 'No W' means no waves are included and 'no ext waves' means no external swell wave conditions (coarse model boundary conditions) were included in the model simulation.

To model the surface drag to accurately predict the surge events both the methods of Smith and Banke (1975) (S&B) and Charnock (1955) were investigated. We found that in shallow locations S&B performed well and could be represented by a Charnock value of 0.0144. For deep locations S&B under predicted the surge and required an enhancement factor of 1.1 to be applied to the winds, this could be represented by a Charnock value of 0.0275. Over a region of varying water depth the S&B and Charnock method with a fixed value are inadequate. Using a wave-dependent Charnock parameter as described by Janssen (2004), but scaling this by $\frac{1}{3}$, captured both time and spatial variation in the representation of the surface drag coefficient, providing much better prediction over this region.

Conclusions

The November 1977 and January 2007 storm surge events have been used to tune and validate the surge conditions in the eastern Irish Sea, using the coupled POLCOMS-WAM nested model. We have shown that although the Smith and Banke formula and the Charnock method for representing the surface drag can be tuned to accurately predict a surge event at a given location, it does not capture the surge events across a region. It was found that to accurately predict the peaks in the surge events a scaled wave-dependent Charnock parameter must be adopted. This accounts for both temporal and spatial changes in the wave age, producing the best surge prediction across a region.

This model setup will now be applied to perform long-term (10-yr) wave, tide and surge simulations to provide boundary conditions for the Liverpool Bay model. This will then enable the investigation into the potential of coastal flooding by waves in Liverpool Bay and also assess the importance of swell. At the finest resolution Liverpool Bay model, we will assess the shallow water capability of both WAM and SWAN compared with available data and, using a POLCOMS-WAM coupled model, examine the effects of wave-current interaction on the prediction of surges and waves at the coast.

References

- Charnock, H. (1955), Wind stress on a water surface, *Quarterly Journal of the Royal Meteorological Society*, 81(350), 639–640.
- Janssen, P.A.E.M. (2004), *The Interaction of ocean waves and wind*. Cambridge University Press, Cambridge, 300pp.
- Jones, J.E., Davies, A.M. (1998), Storm surge computations for the Irish Sea using a three-dimensional numerical model including wave-current interaction, *Continental Shelf Research*, 18(2), 201–251.
- Smith, S.D., Banke, E.G. (1975), Variation of the surface drag coefficient with wind speed, *Quarterly Journal of the Royal Meteorology Society*, 101(429), 665–673.

Impact of winter storms on sediment dynamics in the East-Frisian Wadden Sea (southern North Sea)

KARSTEN LETTMANN, JÖRG-OLAF WOLFF

Institute for Chemistry and Biology of the Marine Environment,
Carl von Ossietzky University Oldenburg,
Carl-von-Ossietzky-Straße 9–11, 26111 Oldenburg, Germany
email: lettmann@icbm.de, wolff@icbm.de

Keywords: European winter wind-storms, sediment transport, observations and modeling; Wadden Sea

ABSTRACT

We have applied a coupled hydrodynamic model (GETM) with a sediment model to investigate a hypothesis stating that extreme wind events are responsible for the observed loss of fine sediments in the East-Frisian Wadden Sea. Using pile station observations to construct artificial winds and sea-level, we considered three scenarios with increasing complexity to test the hypothesis. Although wave effects were not considered it seems that the results support the hypothesis.

Introduction

The East Frisian Wadden Sea is characterized by a chain of barrier islands with associated inlets which connect the tidal basins with the North Sea. The major physical controls are provided by the tides and meteorological forces (e.g., wind, radiation and freshwater fluxes). Extreme events like storm surges or winter ice coverage episodically throw the system into disarray in terms of hydrodynamics, sediment redistribution, and benthic ecology (Flemming, 2002).

Sedimentological evidence indicates a net export of suspended fine sediments with the following chain of arguments: Since the import of sediment from remote sources is insufficient to compensate the deficit created by sea-level rise, the East Frisian Wadden Sea is a strongly transgressive depositional system. In the course of sea-level rise, sediment is thus eroded on the upper shoreface and transported into the backbarrier basins. As a result, the whole barrier island system slowly migrates landwards as it accretes vertically, the rate being dictated by the volume of the deficit created by sea-level rise (Flemming, 2002). The migration rate currently amounts to about 100 m per 10 cm sea-level rise.

Over the last millennium, this natural transgressive response of the system has been severely obstructed by man in the form of land reclamation and dike construction. As a result, the size of the original Wadden Sea has been reduced by as much as 50% in some places (Mai and Bartholomä, 2000). The physical obstruction imposed by the dikes has had two major effects. On the one hand, the areas of the tidal basins, and hence the volumes of the associated tidal prisms, have been greatly reduced. On the other hand, average energy levels along the shoreline have increased, thereby truncating the natural sedimentary facies succession, as a result of which the finer-grained end-members (mud flats, salt marshes) have been eliminated (Flemming and Nyandwi, 1994).

In the course of continued sea-level rise, increasingly coarser sediment facies will hence be squeezed out along the dike (Flemming and Bartholomä, 1997). Based on this conceptual geological model (see Figure 1), which is supported by numerous observations worldwide, it is postulated that most of the imported suspended particles must eventually be eliminated from the system, simply because the accommodation space is not available. The overall fluxes of suspended matter per unit time, the periods of predominant import and export, and the dynamic conditions controlling resuspension and net export are still poorly understood.

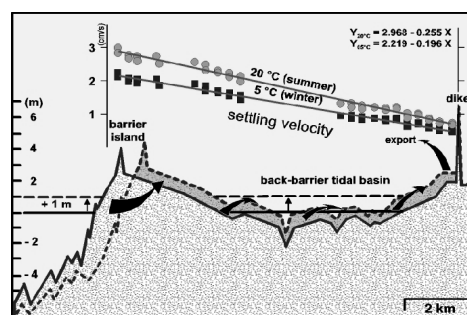


Figure 1. Reaction of a tidal system to sea level rise and cross shore distribution of sediment settling velocity (Flemming, pers. comm.).

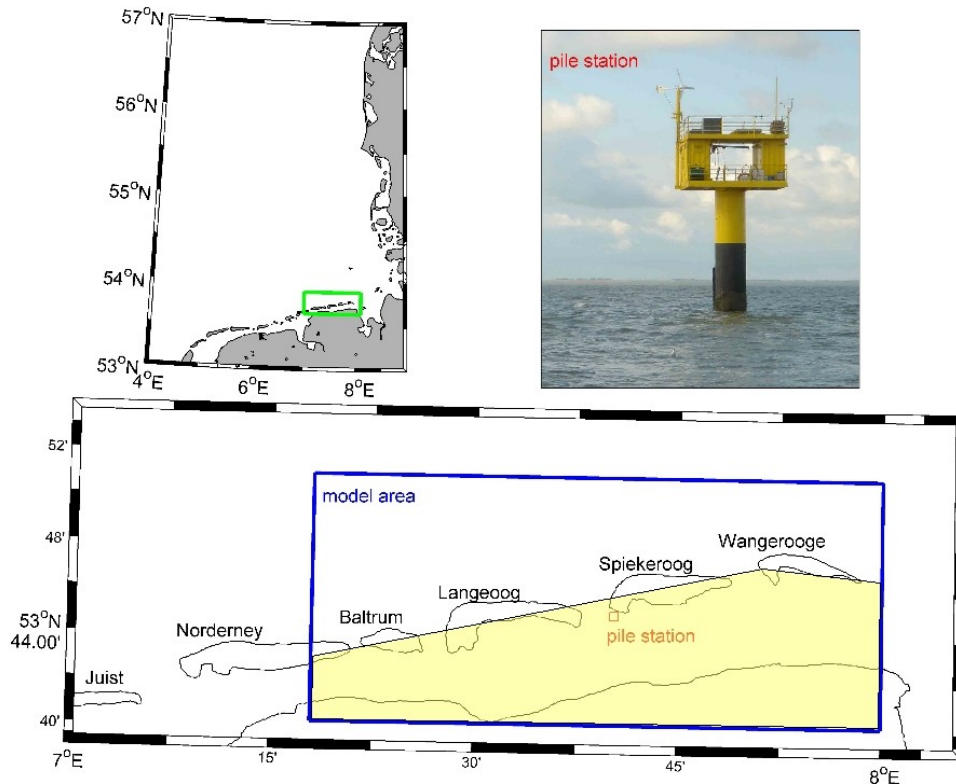


Figure 2. The considered model area as part of the southern North Sea. Furthermore, the pile station operated by the research group ‘BioGeoChemistry of Tidal Flats’ is shown on the figure top right. The sediment budgets are calculated for the yellow tidal basin area.

Considering this net export hypothesis for suspended matter outlined above, one must therefore assume that export conditions are created during stormy weather, although it is unclear whether this occurs regularly during the winter season, or only episodically during severe storm surges. Because ship-based observations are not possible during severe storms, this question was addressed by continuous measurements at a pile station (see Figure 2). From this pile station, we obtain important data like wind speed, water velocity, significant wave height or suspended sediment concentration during normal weather conditions and storm surges. In the winter season of 2006/2007 the southern North Sea endured three major storm surges (NLWKN, 2007). The storm surge on the 1 November 2006 ranges in amongst the class of the three highest sea levels ever recorded along the Lower-Saxonian coastline over the last 100 years (1906, 1962, 2006). Storm ‘Britta’ started to build up sea level from about midday of the 30 October to midnight when the strongest build-up occurred until about 06:00 with wind speeds measured at the pile station of up to 100 km h^{-1} and a local sea level of more than 2 m above mean high water at the pile station (see Figure 3). Maximum currents measured at the pile station were above 1.8 m s^{-1} .

Under normal weather conditions, there are some processes leading to an accumulation of (fine) sediment in the tidal basins. Here, Stokes drift due to wave effects and the effects of settling lag and scour lag could be mentioned (see e.g., Bartholdy, 2000). During extreme events like storm surges, we face conditions characterized by gale-force winds, much increased sea levels and associated swell. All these factors increase the erosion of sediments at the sea floor in the tidal inlets and on the tidal flats. Smaller sized particles, having also smaller sinking velocities, are therefore kept for a longer time in suspension. This situation potentially leads to an export of smaller sediment classes to the North Sea leaving behind sediments of larger size fractions behind the barrier islands in the East-Frisian Wadden Sea.

In detail, we want to test this hypothesis with our model by considering the effects of increased sea level and enhanced wind speeds. We explicitly mention that wave effects are not considered in this model study, although we believe in their great importance for sediment dynamics in tidal flat systems.

Model

For the high resolution numerical simulations of the hydrodynamics we have used the General Estuarine Transport Model (GETM, Burchard and Bolding, 2002).

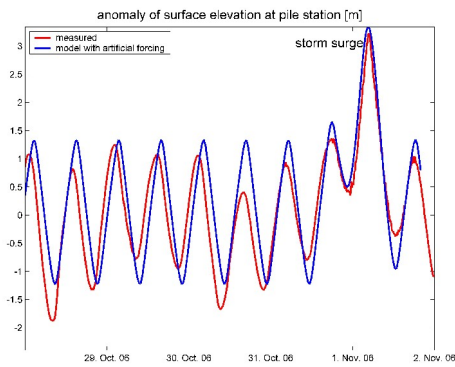


Figure 3. Surface elevation anomaly at the pile station. Red: measured elevation during the November 2006 storm surge. Blue: artificial elevation used in model with storm surge forcing (scenarios S2 and S3).

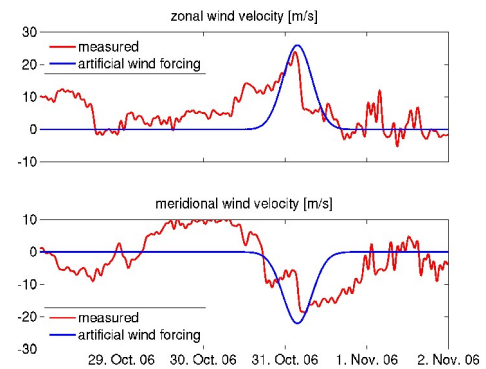


Figure 4. Zonal and meridional wind speed 10 m above sea level. Red: measured at pile station. Blue: artificial wind speeds used for model scenario S3.

GETM is a prognostic three-dimensional hydrodynamic model especially suited for shallow coastal regions under the influence of tidal currents where substantial areas are prone to drying and flooding during a normal tidal cycle. The model is based on the horizontal momentum equations and the continuity equation with two prognostic equations for the turbulent kinetic energy and its dissipation rate influencing the vertical eddy viscosity coefficient. These equations describe the purely dynamic situation. Coupled to GETM is a suspended particulate matter (SPM) model. The sediment module is based on a diffusion-advection equation with an additional sinking velocity, which is calculated using the formula of Soulsby (1997) with a fluid viscosity adopted for water at 4°C. We consider five non-cohesive sand fractions with diameters between 40 μm and 200 μm . Sediments are eroded from the bottom, if a critical bottom shear stress is exceeded. The sediment deposits, if the bottom stress of the fluid is below a critical value. As we consider non-cohesive sediments, these critical shear stresses increase with particle diameter and are calculated with the formula of Soulsby and Whitehouse (1997). The complete model setup (including forcing, boundary conditions and parameterizations) and comparisons with observations is described in more detail in Wolff et al. 2008 in preparation).

To investigate the response of the sediment system under normal and extreme weather situations we use an artificial surface elevation at the open boundaries (with the period of the M_2 -tide) and artificial wind speeds. These forcing functions have realistic magnitudes as can be seen from Figures 3 and 4. We simulate the water elevation of the storm surge by adding a Gaussian elevation peak at the end of the forcing period to the M_2 tidal signal. We consider three different model scenarios by starting with M_2 tidal forcing only and then adding first the artificial sea-level and then wind forcing (see Table 1).

Results and conclusions

In Figure 5, we show that our model captures the right order of magnitude and dynamic of suspended sediment concentration in the water column during the storm surge even with these simplified forcing functions (scenario S3).

For normal conditions (no storm surge, scenario S1) there is a slight accumulation of all sediment fractions in the tidal basin area (yellow area in Figure 2), which is demonstrated in Figure 6. It is also evident from Figure 6 that the increase of the water level leads to loss of sediment during storm surges (scenario S2). This loss is even higher when the wind is switched on (scenario S3). For scenario S3, the loss is highest for the smallest sediment fraction (see Figure 7).

The estimated loss of total sediment during a storm surge in the considered area is of the order 10^{-7} – 10^{-8} kg. Our model results seem to confirm the above

Table 1. Summary of different model scenarios.

scenario	boundary forcing	wind forcing
S1	M_2 -tide	no
S2	M_2 -tide + storm surge	no
S3	M_2 -tide + storm surge	yes

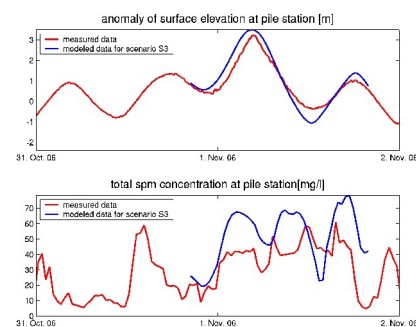


Figure 5. Data (red) and model results (blue) at the pile station. Top: surface elevation anomaly. Bottom: total suspended sediment 9 m above bed.

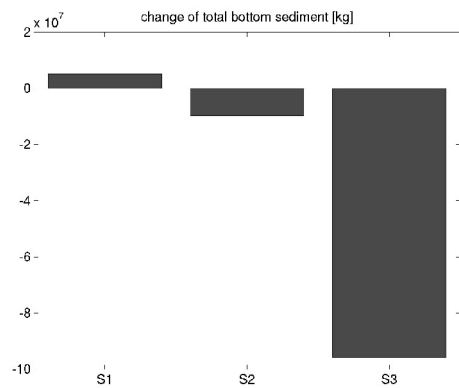


Figure 6. Change of total bottom sediment during the storm surge period in the tidal basin area for the different model scenarios. A positive change means accumulation of sediment.

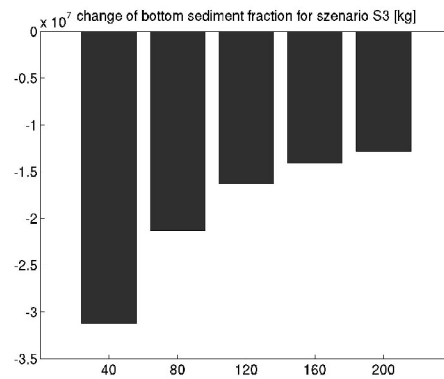


Figure 7. Change of bottom sediment fractions in the tidal basin area during the storm surge period for scenario S3.

mentioned hypothesis of increased loss of the fine sediment fraction during storm surges.

After all, we would like to point out again that these results are obtained without the consideration of wave effects, which might be very important for sediment dynamics in tidal flat systems. This is planned for future work.

Acknowledgements

We thank Joanna Staneva and Ulf Gräwe for helpful discussions concerning the numerical simulations with GETM. Thomas Badewien provided us with the data from the pile station and helped us with the evaluation of the model results. Furthermore, we thank the Bundesamt für Seeschifffahrt und Hydrographie (Federal Maritime and Hydrographic Agency, BSH) for providing topography data.

References

- Bartholdy, J. (2000), *Processes controlling import of fine-grained sediment to tidal areas: a simulation model*. Geological Society, London, Special Publications, Vol. 175, pp13–29.
- Burchard, H., Bolding, K (2002), *GETM – a general estuarine transport model*. *Scientific Documentation*, No EUR 20253 EN, European Commission, printed in Italy, 157pp.
- Flemming, B.W. (2002), *Effects of climate and human interventions on the evolution of the Wadden Sea depositional system (southern North Sea)*. In: Climate development and history of the North Atlantic realm, Wefer, G., Berger, W., Behre, K.E., Jansen, E. (Eds.), SpringerVerlag, Berlin, pp399–413.
- Flemming, B.W., Bartholomä, A. (1997), Response of the Wadden Sea to a rising sea level: a predictive empirical model, *German Journal of Hydrography*, 49, 343–353.
- Flemming, B.W., Nyandwi, N. (1994), Land reclamation as a cause of fine-grained sediment depletion in backbarrier tidal flats (southern North Sea), *Netherlands Journal of Aquatic Ecology*, 28, 299–307.
- Mai, S., Bartholomä, A. (2000), *The missing mud flats of the Wadden Sea: a reconstruction of sediments and accommodation space lost in the wake of land reclamation*. In: Muddy coast dynamics and resource management, Flemming, B.W., Delafontaine, M.T., Liebezeit, G. (Eds.), Elsevier Science, Amsterdam, pp257–272.
- Niedersächsischer Landesbetrieb für Wasserwirtschaft, Küsten und Naturschutz (NLWKN) (2007), *Jahresbericht 2006*. Am Sportplatz 23, 26506 Norden, Germany
- Soulsby, R.L. (1997), *Dynamics of marine sands. A manual for practical applications*. Thomas Telford, London.
- Soulsby, R.L., Whitehouse, R.J.S. (1997), *Threshold of sediment motion in coastal environments*. In: Proceedings of the Pacific Coasts and Ports '97 Conference, Christchurch, University of Canterbury, New Zealand. Vol. 1, pp149–154.
- Wolff, J.O., Stanev, E.V., Staneva, J.V., Lettmann, K., Flemming, B.W., Bartholomä, A., Reuter, R., Badewien, T.H. (2008), High resolution modelling of hydro- and sediment-dynamics in the East Frisian Wadden Sea (southern North Sea), *Ocean Dynamics*, Special Issue Wadden Sea. (In preparation.)

Forecasting methods for sustainable harbor development – Rio Grande Harbor, Brazil

ELISA H.L. FERNANDES¹, RAFAEL C. GONÇALVES¹, WILIAN C. MARQUES¹,
NICOLLE DEUSSFELD², ANDREAS MALCHEREK²

1. Laboratório de Oceanografia Física, Fundação Universidade Federal do Rio Grande, Caixa Postal 474, CEP 96201-900 Rio Grande-RS, Brazil
email: e.fernandes@furg.br, rafegoncalves@yahoo.com.br,
wilian_marques@yahoo.com.br
2. Hydromechanik und Wasserbau, Universität der Bundeswehr München, 85577 Neubiberg, Germany
email: nicolle.deussfeld@unibw.de, a61aamal@unibw.de

Keywords: numerical model, harbor development, hydrodynamics, sediment transport

ABSTRACT

Understanding the morphological evolution of coastal areas is of utmost importance for their management. This paper addresses the numerical modeling of the morphodynamic evolution of the Patos Lagoon under the main physical forcing (wind, tides and freshwater discharge). The lagoon is located at the southernmost part of Brazil, and its estuary shelters one of the most important harbors in the country. The modeling structure is composed by the hydrodynamic module Telemac-3D and by the morphological module SediMorph. Results from the modeling experiments indicate the main sedimentary dynamic processes responsible for the siltation and erosion of both cohesive and non-cohesive sediments in critical areas of the harbor, providing guidelines to minimize the volume and frequency of the dredging operations. Furthermore, it is possible to evaluate the morphodynamic processes responsible for the origin of large scale bottom features in the harbor main channel, particularly the evolution of dunes, responsible for rapid bathymetric changes in the navigation channels.

Introduction

The importance of estuarine systems and coastal zones has long been recognized not only by the scientific community, but also by people leaving nearby these areas. These ecosystems act as the interface between the oceans and the continents, having an essential role in regulating the exchanges between these compartments. They are highly variable and rich, supporting important economic activities. Thus, the management of these areas is normally related to difficult decisions and the necessity of compromising.

An increasing global interest in improving the understanding of the processes controlling the transport of sediments in coastal areas emerged in the last few years. This is related to the increasing necessity of dredging in ports and their access channels, in order to improve their commercial capacity, of monitoring environmental pollution, of understanding the interaction between contaminants and sediments, of understanding the dynamics of commercially important species, and of establishing management rules in these areas. The use of in situ measurements to study the processes involved in the water quality and transport of sediment in estuarine areas, however, have severe temporal and spatial limitations, which can be overcome by numerical modeling techniques.

The Patos Lagoon is the main hydrological resource in the South of Brazil, representing the most important nursery ground for commercially relevant species of fish and crustaceans. Several economic and leisure activities take place around the Lagoon, exposing the environment to a high number of impacts which can affect its hydrology. Such alteration can result in modifications in the transport pattern of sediment, organisms and nutrients, in the distribution of salinity and temperature, and in the exchanges between the estuarine and the adjacent coastal zone.

Harboring, fishing and tourism are the main economical activities in the area. Between the three ports located in the South of Brazil, Rio Grande Harbor is the most important, being considered the biggest in the

MERCOSUL area. Apart from being the only maritime harbor in the South of Brazil, Rio Grande Harbor is located in the deepest area of the South Atlantic Ocean, being connected to the whole country and to the main MERCOSUL partners. The high concentration of suspended matter coming from the riverine system located in the northern part of the lagoon, however, promotes the siltation of the access channels. Recently, the combination between the environmental and commercial demands and the necessity of maintenance and expansion of the actual capacity of Rio Grande Harbor generated the necessity of further improvements and significant dredging operations in the port access channel.

However, the high spatial and temporal variability of the Patos Lagoon, its estuarine area and the adjacent coastal zone indicate that studies about the processes controlling the dynamics of the system cannot be carried out based on field data alone. This limitation can be overcome by applying numerical models as sophisticated predictive tools for the interpolation/extrapolation of field data. Thus, the proposed approach for this study is to apply simultaneous and complementary hydrodynamic (TELEMAC System) and sediment transport (SediMorph Model) models to: 1) identify sedimentary dynamic processes which are responsible for the siltation and erosion of both cohesive and non-cohesive sediments in critical areas (harbor basins and navigation channels) in order to propose solutions that can minimize the volume and frequency of the dredging operations; 2) evaluate the morphodynamic processes responsible for the origin of large scale bottom features in the harbor main channel; 3) understand the effects of changes in the configuration of the access channel to the harbor.

Methods

The TELEMAC3D model was used to carry out three-dimensional simulations of the hydrodynamic of the study area. TELEMAC is a finite element flow model developed by ©EDF – *Laboratoire National d'Hydraulique et Environnement* of the company *Electricité de France (EDF)* to simulate the flow in estuaries and coastal zones (Hervouet, 2007). The morphodynamic simulation was carried out based on the coupling between the hydrodynamic model TELEMAC2D and the morphological and sediment transport model SediMorph. The SediMorph model computes the sedimentological processes at the alluvial bed of a free surface flow. These processes include the roughness of the bed resulting from the grain and from roughness, the bottom shear stress as a result of roughness and flow, the bed load transport rates, the erosion rates and the bed evolution itself. The deposition rates and the transport of the suspended load are calculated by TELEMAC2D. The morphodynamic simulation was performed during one year (2002).

The hydrodynamic model was forced with wind, tide and river discharge. The wind data was obtained from the Reanalysis web site (www.cdc.noaa.gov/cdc/reanalysis) and prescribed as surface boundary condition. River discharge from the main rivers (Camaquã, Taquari and Jacuí) were obtained from the Brazilian National Water Agency web site (www.ana.gov.br), and used at the continental liquid boundaries (Figure 1). At the oceanic liquid boundary, the 6 most significant tidal components in the study area were prescribed as free surface elevation. These data were collected from the Grenoble Model (Fes95.2). The morphological simulation was set with three classes of sediment: coarse sand (1 mm), fine sand (0.25 mm) and silt (0.02 mm). The first two were prescribed as bed load material while the last one was prescribed as suspended load. The initial conditions of sediment distribution at the bed were set according to Calliari (1980) and Toldo Jr. (1994). Both the hydrodynamic and the morphodynamic simulations were carried out for the study area defined between 28°S and 34°S, and the oceanic boundary was located at the 3600 m isobath (Figure 1). The response of the system was evaluated for three scenarios (Figure 2): 1) original configuration, 2) deepening in the New Harbor area, 3) deepening in the access channel.

Results

Results from the 3-D hydrodynamic simulations indicate that in the New Harbor area (Figure 3A) the new configuration (scenario 2) would induce an increase in the flood flows. A reduction in the ebb flows would occur in some events. Moving down the main access channel, a reduction in the ebb and flood flows is expected (Figure 3B), while closer to the mouth (Figure 3C) ebb flows are enhanced. Similar results were obtained for the comparison between scenarios 1 and 3.

Results from a six-month long morphodynamic simulation indicate alterations in the erosion/deposition patterns for the simulated scenarios. The main affected areas are highlighted in Figure 4. Table 1 presents quantitative results for selected points in each of the simulated scenarios. These results indicate that the dynamics of the points located in the upper part of the main access channel (points 1 and 2) will change from erosion to deposition tendency. The magnitude of this alteration is enhanced for scenario 2 in the New

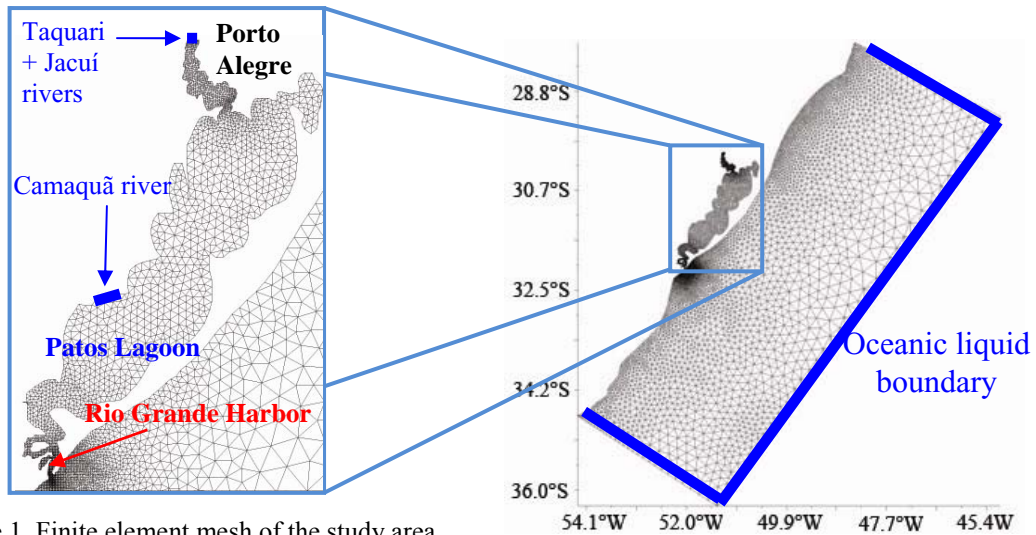


Figure 1. Finite element mesh of the study area.

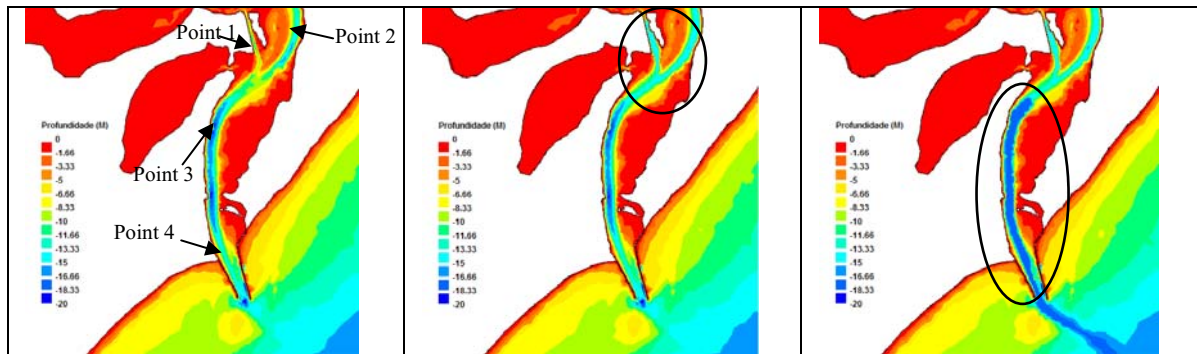


Figure 2. Simulated scenarios for the harbor expansion. A) original, B) deepening in the New Harbor area, C) deepening in all the access channel. (A) shows the location of the points where were analyzed time series of currents (Figure 3) and bottom evolution (Table 1)

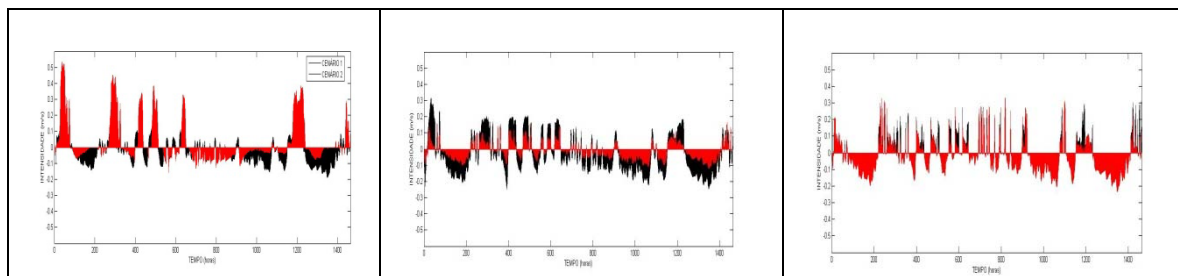


Figure 3. Comparison of calculated currents at the bottom between scenarios 1 (black) and 2 (red). A) Point 1 (New Harbor), B) Point 3, C) Point 4. Negative values indicate ebb flow.

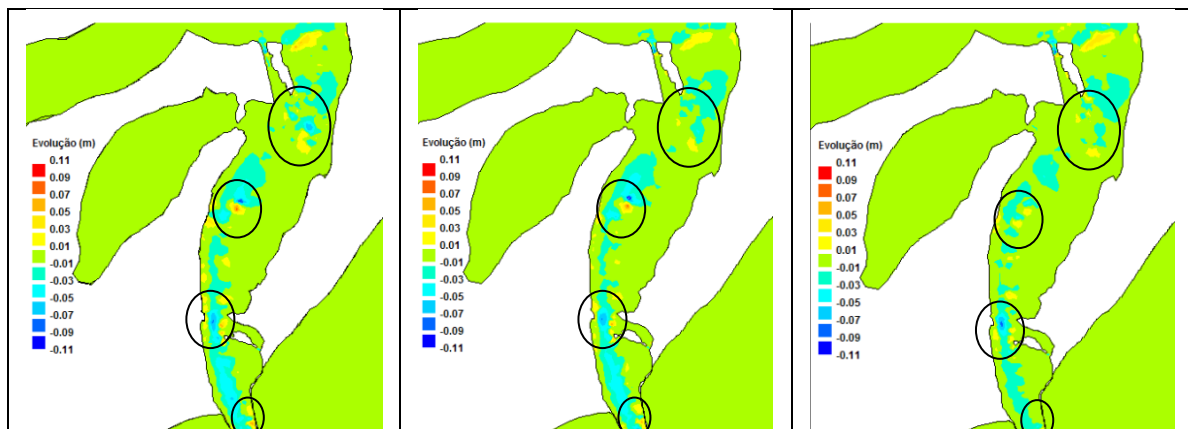


Figure 4. Bottom evolution after 6 months of morphodynamic simulation. Scenarios 1 (A), 2 (B), and 3 (C).

Table 1. Bottom evolution for scenarios 1, 2 and 3 after six months of simulation. Positive (negative) values indicate deposition (erosion).

Point	Scenario 1	Scenario 2	Scenario 3
1	-1.3 mm	2.6 mm	2.7 mm
2	-1.2 mm	2.0 mm	0.5 mm
3	-13.7 mm	-16.2 mm	-6.4 mm
4	-48.4 mm	-39.9 mm	-24.2 mm

Table 2. Integrated volume of sediment accumulated along each sector for the three scenarios.

Sectors	Scenario 1	Scenario 2	Scenario 3
Sector 1	3006 m ³	10398 m ³	4680 m ³
Sector 2	42889 m ³	0 m ³	198 m ³
Sector 3	2151 m ³	1579 m ³	20204 m ³
Total	48064 m³	11977 m³	25082 m³

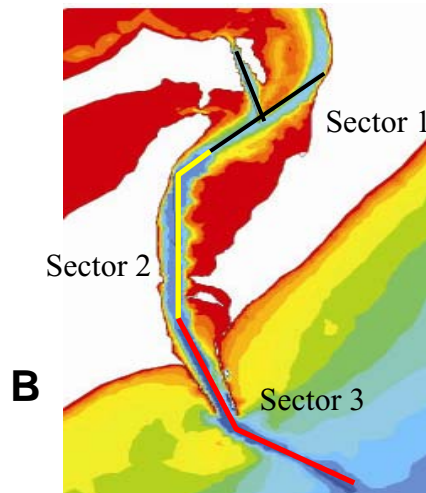


Figure 5. Sectors of the navigation channel where the accumulated volume of sediment was calculated.

Harbor area (point 2). Moving seawards (points 3 and 4), the proposed alterations will reduce the tendency of erosion observed at the moment.

In order to compare the volume of sediment deposited along the harbor area for the different scenarios, the channel was divided into three sectors (Figure 5). Table 2 presents the integrated volume at the end of the simulation along each sector, for the three scenarios. The first scenario presented a higher accumulation of sediment on sector 2, where the volume reached 42889 m³. Scenario 2 presented higher accumulation on sector 1, with a total volume of 10398 m³. Scenario 3 presented a smaller accumulation of sediment in sector 1 than in scenario 2, but it is still higher than the original configuration. Sector 3 showed the highest volume of sediment accumulation in this scenario, reaching 20204 m³. Between the three scenarios, scenario 1 presented the highest total sediment accumulation while scenario 2 presented the lowest total sediment accumulation. These results indicate that the proposed alterations for the harbor area will reduce the accumulation of sediment in the system.

Conclusions

Modeling results suggest that the proposed alterations for Rio Grande Harbor configuration will promote changes in the salinity excursion, stratification, and erosion and deposition patterns inside the estuarine system. The most significant alterations in these parameters were observed for Scenario 2, which enhances the salinity excursion and vertical stratification, and reduces the required volume of dredging.

References

- Calliari, L.J. (1980), *Aspectos sedimentológicos e ambientais na região estuarial da Lagoa dos Patos*. Dissertação de Mestrado, UFRGS.
- Hervouet, J.M. (2007), *Hydrodynamics of free surface flows – Modelling with the finite element method*. John Wiley & Sons.
- Toldo Jr., E.E. (1994), *Sedimentação, Predição do Padrão de Ondas e Dinâmica Sedimentar da Antepraia e Zona de Surfe dos Sistema Lagunar da Lagoa dos Patos*. Tese de Doutorado, UFRGS.

Quantitative analysis of numerically induced mixing in a coastal model application

HANNES RENNAU, HANS BURCHARD

Baltic Sea Research Institute Warnemünde, Seestraße 15,
18119 Rostock-Warnemünde, Germany
email: hannes.rennau@io-warnemuende.de, hans.burchard@io-warnemuende.de

Keywords: numerical mixing, advection schemes, variance decay

ABSTRACT

For an existing high-resolution coastal model simulation of the western Baltic Sea (Burchard et al., 2007a) using the numerical model GETM (Burchard and Bolding, 2002), an easy to implement diagnostic method for obtaining the spurious mixing is applied (Burchard and Rennau, 2007b). In the recent years various attempts have been made to estimate the amount of numerical mixing in numerical ocean models due to discretization errors of advection schemes. Many different suggestions have been made with various different approaches.

With the new diagnostic method the physical mixing is defined as the turbulent mean tracer variance decay rate. The numerical mixing due to discretization errors of tracer advection schemes is defined as the decay rate between the advected square of the tracer variance and the square of the advected tracer which can directly be compared to the physical variance decay. The source and location of numerical mixing is further investigated by comparing different advection schemes and analyzing the amount of numerical diffusion in each spatial dimension during the advection time step.

The results have shown that numerically and physically induced mixing are of the same orders of magnitude but with different vertical and horizontal distributions. The reasons of high numerical diffusion are being identified as a problem with bottom following coordinates when density gradients especially in regions of steep slopes are being advected in a direction normal to the isolines of depth. Due to the restrictions of the bottom following coordinates the density interfaces can only be reproduced by a spurious sawtooth-like profile. Hence strong dynamics induce an increased advection through but less along the vertical coordinate levels which produces the locally increased numerical mixing. A suggestion on how to decrease the amount of numerical mixing is the use of adaptive vertical coordinates.

Introduction

The Baltic Sea (Figure 1) is a semi-enclosed estuarine system on the European shelf with only shallow and narrow connections to the North Sea. Due to river runoff and precipitation the water exchange between North Sea and Baltic Sea is driven by a net outflow consisting of a permanent outflow of fresh surface water and sporadic so called inflow events of dense Kattegat water into the Baltic Sea. As this salty bottom water is carrying much oxygen to ventilate the deeper basins of the Baltic Sea, this process is the only way to supply the deeper basins of the Baltic Sea with oxygen and is hence a very important process for the whole ecosystem.

An existing high-resolution coastal model study of the western Baltic Sea has been used to quantify and qualify the amount of natural mixing of these dense gravity currents on their way through the western Baltic Sea (Burchard et al., 2007a). A realistic reproduction of dense bottom plumes requires reliable numerical schemes as there are sharp gradients to be advected over long distances without much physical mixing activity. To investigate the reliability of the physical mixing parameterization of the model, the additional numerical diffusion is qualified and quantified with this work using the method developed by Burchard and Rennau (2007b).

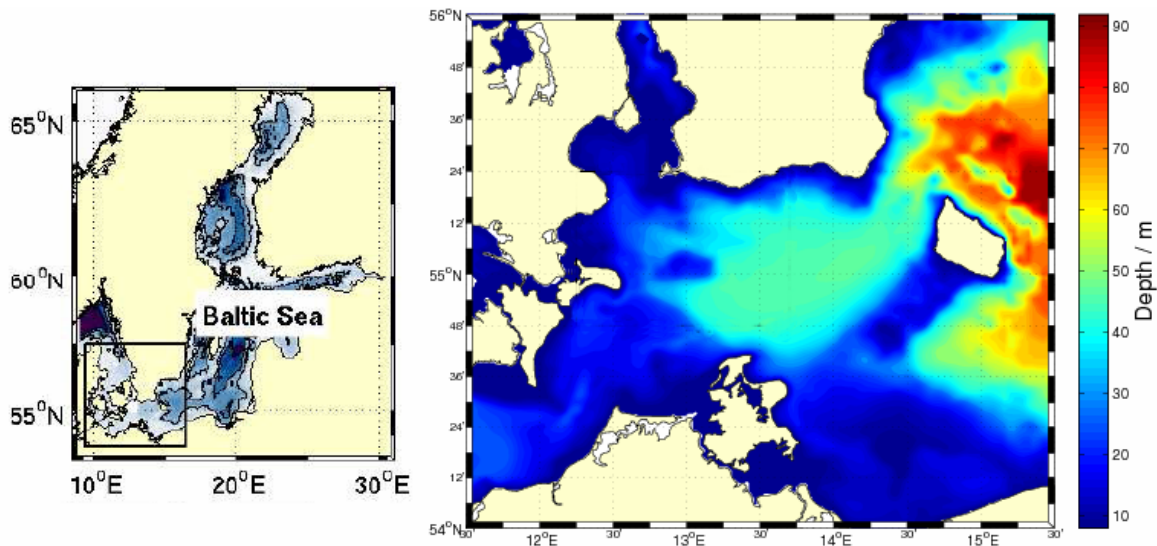


Figure 1. The left panel shows a map of the Baltic Sea where as the black box indicates the region where the coastal model simulation runs. The right panel shows a bathymetrical map of the Arkona Basin where most of the water mass transformation takes place.

Methods

To obtain a measure of how strong numerical diffusion is compared to the physical mixing in the model, two different approaches were taken. The first is to define the physical mixing as the turbulent mean tracer variance decay rate (Burchard et al., 2007a). The second approach is defined as the decay rate between the advected square of the tracer variance and the square of the advected tracer which can directly be compared to the physical variance decay. Both measures have been implemented into the numerical model GETM (Burchard and Bolding, 2002; www.getm.eu) which is a fully baroclinic, hydrostatic ocean model using general vertical coordinates. The model uses an Arakawa C-grid. The characteristic numerical features of GETM are the mode splitting between the fast barotropic and the much slower baroclinic mode, the high-order advection schemes for tracer and momentum-advection (Pietrzak, 1998) and the possibility in applying various different turbulence closure models due to the implementation of the well-tested state-of-the-art turbulence model GOTM (Burchard et al., 1999; Umlauf et al., 2005). For the calculation of the internal pressure gradient the scheme developed by Shchepetkin and McWilliams (2003) is used.

Results

To improve the model results concerning the simulation of dense bottom currents, bottom following coordinates with a non-linear zooming to the sea bed have been chosen. The strength of the vertical mixing parameterization is here being investigated relative to the additional numerical mixing. The numerical mixing has been found out to be significantly higher than the physical mixing in widespread areas of the simulated region. This can be seen in Figure 2 where the amount of physical mixing is plotted together with the numerical diffusion. Here a temporal averaging over the nine months simulation period and a spatial integration in vertical z -direction shows high numerical diffusion and high physical mixing especially in the regions of the Darss Sill and Drodgen Sill. The high physical mixing in this area is because these two sills can be regarded as the last barriers for dense bottom currents to propagate into the Baltic Sea. This area is one of the hot-spots of water mass transformation in the Baltic Sea because salt fronts are always present. Figure 2 also shows the different horizontal distribution of physical and numerical mixing for the whole model domain.

The highest numerical mixing generally occurs at moving fronts (Burchard and Rennau, 2007b). This can also be seen in Figure 2 where high numerical mixing filaments are correlated to the bathymetry (Figure 1) which can be seen for the region around the Darss Sill. Here the highest numerical mixing can be found at the lateral boundaries of the plume, exactly there where the lateral propagation of the plume is restricted by steep slopes. A good example for this is the horizontal distribution of the numerical mixing north of Kriegers Shoal shown in Figure 2 (marked by the white circle). Here, frequently occurring currents of dense water with a thickness of around 10–15 m propagate along a small channel of 35 m depth from west to east. The reason

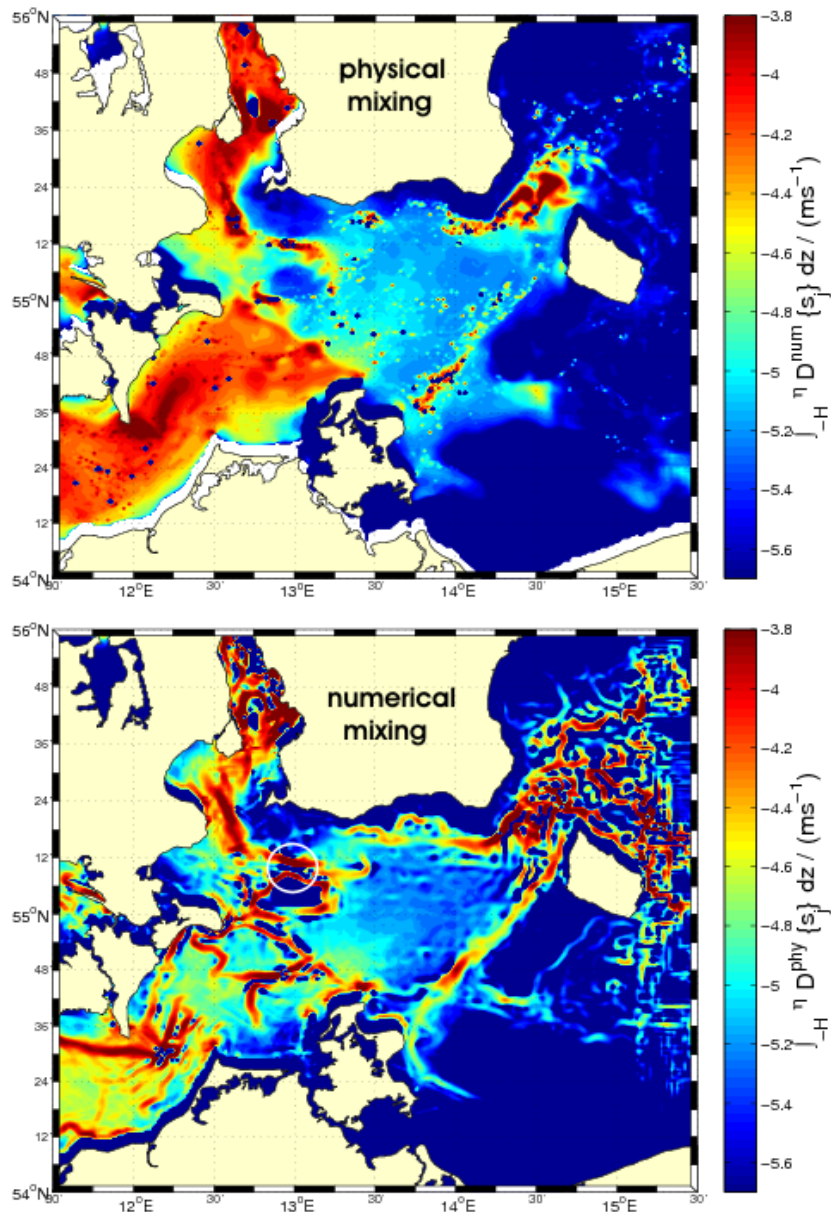


Figure 2. Upper panel showing the salinity variance decay which can be regarded as the measure for the amount of physical mixing in this region. The lower panel shows the values of numerical mixing for the same simulation area.

for increased numerical diffusion in these regions is mainly due to the strong vertical advection of density gradients through but not along the vertical coordinates, for example, due to the transversal physical dynamics of the plume. But the main reason for high numerical diffusion is the sawtooth-like horizontal density profile, especially at steep slopes. This is a known disadvantage of bottom following coordinates. But it is exactly this artificial profile that leads to a density exchange between the vertical layers, and therefore also to increased numerical diffusion.

A possible solution to decrease the numerical diffusion is to use adaptive vertical coordinates, which can adapt the vertical coordinates to the instantaneous density profile at a certain time. This will decrease the intensity of the sawtooth-like density profile of the plume at steep slopes, and hence reduce the numerical diffusion.

Conclusions

The numerical mixing due to discretization errors of the advection schemes is much higher than expected. It was shown that the numerical mixing shows a different horizontal distribution than the physical mixing and is the same order of magnitude as the physical mixing or even larger.

It has been shown that highest numerical mixing occurs mainly in regions of steep slopes where the plume density is advected between the vertical coordinates. The physical mixing in the model at the lateral boundaries of a plume is strongly influenced by the numerical diffusion, whereas the physical mixing is mainly in the center of the plume. Away from the plume edges the density is mainly advected along the vertical coordinates and not across the vertical coordinates and is much less influenced by numerical diffusion. In contrast, significant numerical mixing in z -level models is expected to be found not only at the lateral boundaries of the plume but also in the center of the plume. This is due to the fact that gravity currents in z -level models are necessarily advected through vertical coordinates whenever depth variations occur. Here, bottom following coordinates are consequently better suited to model the advection of dense bottom currents.

It has been found that the numerical diffusion is lower compared to the physical mixing in areas of active physical mixing. Here a good example is the region around the Darss Sill.

The main reason for high numerical mixing is the advection of density gradients through the vertical coordinates at steep slopes due to the sawtooth-type density interface. As a possible solution of this numerical disadvantage of sigma-coordinate models, adaptive vertical coordinates could lead to further improvements concerning numerical diffusion.

References

- Burchard, H., Bolding, K., Villarreal, M.R. (1999), *GOTM – a general ocean turbulence model. Theory, applications and test cases*. Tech. Rep. EUR 18745 EN, European Commission.
- Burchard, H., Bolding, K. (2002), *GETM – a general estuarine transport model. Scientific documentation*. Tech. Rep. EUR 20253 EN, European Commission.
- Burchard, H., Janssen, F., Bolding, K., Umlauf, L., Rennau, H. (2007a), Model simulations of dense bottom currents in the Western Baltic Sea, *Continental Shelf Research*. In press.
- Burchard, H., Rennau, H., (2007b), Comparative quantification of physically and numerically induced mixing in ocean models, *Ocean Modelling*. (In press.)
- Pietrzak, J. (1998), The use of TVD limiters for forward-in-time upstream-biased advection schemes in ocean modeling, *Monthly Weather Review*, 126, 812–830.
- Shchepetkin, A.F., McWilliams, J.C. (2003), A method for computing horizontal pressure-gradient force in an oceanic model with a nonaligned vertical coordinate, *Journal of Geophysical Research*, 108(C3), 3090, doi:10.1029/2001JC001047.
- Umlauf, L., Burchard, H., Bolding, K. (2005), *General Ocean Turbulence Model. Source code documentation*. Tech. Rep. 63, Baltic Sea Research Institute Warnemünde, Germany.

An efficient unstructured mesh finite volume model for coastal and estuarine hydrodynamics

JULIE D. PIETRZAK, GUUS STELLING, OLGA KLEPTSOVA

Environmental Fluid Mechanics Section,
Faculty of Civil Engineering and Geosciences, Delft University of Technology,
P.O. Box 5048, 2600 GA Delft, Netherlands
email: j.d.pietrzak@tudelft.nl, g.s.stelling@tudelft.nl, o.kleptsova@tudelft.nl

Keywords: C-grid, tangential velocities, stable Coriolis, unstructured grid model

ABSTRACT

Coastal and estuarine models based on unstructured meshes have distinct advantages over traditional Cartesian based models, Casulli and Walters (2000), Walters and Casulli (1998). For example, coastal flows are dominated by cross-shore flows in approximate geostrophic balance. For such flows it is important to ensure that the cross-shore region, within a Rossby radius of the coast, is well resolved. At the same time it is important to resolve the details of the coastline variability and bathymetry, since these too have an important influence on coastal dynamics and wave propagation. Consequently the last few years have seen the development of a large number of unstructured mesh models, Walters et al. (2008). Here a new unstructured mesh semi-implicit finite volume coastal ocean model is presented. The staggered C-grid (Mesinger and Arakawa, 1976), was adopted by many structured grid models, as the grid best suited to resolve coastal physics. The main drawback with this grid is a Coriolis mode that can be excited when the Rossby Radius is not well resolved (Arakawa and Lamb, 1977; Walters and Carey, 1984). There is however, another issue that affects both structured and unstructured C-grid models. It arises from the spatial interpolation required to calculate the tangential velocity components (Espelid et al., 2000; Ham et al., 2007).

Methods

We present a spatial interpolation for the reconstruction of the tangential velocity component on C-grids that is not only skew-symmetric, but also more accurate than previously published methods. We show that it is an improvement for both structured and unstructured grid models (Kleptsova et al., 2008). We also briefly discuss time integration methods and show how an efficient unstructured C-grid method can be developed. We demonstrate the advantages of such an approach using a circular basin test case dominated by flooding and drying, and geostrophy. We then apply the model to the Dutch coastal zone and show the advantages of an unstructured grid approach when solving flow problems, in this complex network of harbors and channels. Furthermore we show how the correct geometric representation impacts flow simulations in the coastal zone.

Conclusions

We present a model based on an unstructured C-grid and show how the correct choice of spatial and temporal discretization can lead to a stable, accurate and efficient unstructured mesh model.

References

- Arakawa, A., Lamb, V.R. (1977), Computational design of the basic dynamical processes of the UCLA general circulation model, *Methods in Computational Physics*, 17, 173–265.
- Casulli, V., Walters, R. (2000), An unstructured grid, three-dimensional model based on the shallow water equations, *International Journal for Numerical Methods in Fluids*, 32(3), 331–348.
- Espelid, T., Berntsen, J., Barthel, K. (2000), Conservation of energy for schemes applied to the propagation of shallow-water inertia-gravity waves in regions with varying depth, *International Journal for Numerical Methods in Engineering*, 49(12), 1521–1545.
- Ham, D., Kramer, S., Stelling, G., Pietrzak, J. (2007), The symmetry and stability of unstructured mesh C-grid shallow water models under the influence of Coriolis, *Ocean Modelling*, 16(1–2), 47–60.

- Ham, D., Pietrzak, J., Stelling, G. (2005), A scalable unstructured grid three-dimensional finite volume model for the shallow water equations, *Ocean Modelling* 10, 153–169.
- Kleptsova, O., Pietrzak, J., Stelling, G.S., (2008), On the accurate and stable reconstruction of tangential velocities in C-grid ocean models, *Ocean Modelling*. (Submitted.)
- Mesinger, F., Arakawa, A. (1976), *Numerical Methods Used in Atmospheric Models*, Vol. 1, GARP Publication Series No. 17. Joint Organizing Committee.
- Walters, R. and Carey, G. (1984), Numerical noise in ocean and estuarine models, *Advances in Water Resources*, 7, 15–20.
- Walters, V., Casulli, R. (1998), A robust, finite element model for hydrostatic surface water flows, *Communications in Numerical Methods in Engineering*, 14(10), 931–940.
- Walters, R.A., Hanert, E., Pietrzak, J., Le Roux, D.Y. (2008), Solution of the shallow water equations using unstructured, staggered grids, *Ocean Modelling*. (Submitted.)

On the parameterization of biological influences on offshore sand wave dynamics

BAS W. BORSJE^{1,2}, SUZANNE J.M.H. HULSCHER¹,
PETER M.J. HERMAN³, MINDERT B. DE VRIES^{1,2}

1. Water Engineering and Management, University of Twente, P.O. Box 217, 7500 AE Enschede, Netherlands
email: b.w.borsje@utwente.nl, s.j.m.h.hulscher@utwente.nl
2. Deltares, Rotterdamseweg 185, P.O. Box 177, 2600 MH Delft, Netherlands
email: mindert.devries@deltares.nl
3. Centre for Estuarine and Marine Ecology, Netherlands Institute of Ecology (NIOOKNAW), P.O. Box 140, 4400 AC Yerseke, Netherlands
email: p.herman@nioo.knaw.nl

Keywords: benthos, sediment dynamics, bedforms, modeling; North Sea

ABSTRACT

On the bed of the North Sea sand waves are present, which grow up to 25% of the water depth and migrate with a speed of tens of meters per year. These sand waves can pose a hazard to offshore constructions, navigation, pipelines and telecommunication cables.

The bed of the North Sea is also covered by a great number of organisms, living in and on the bed of the sea, which are known to have significant influence on the stability of the bed. This paper proposes a parameterization of these bio-geomorphological interactions, in order to model the inherent dynamics in offshore seabed patterns.

Three species are included in the parameterization, which influence the stability of the bed in opposite modes. First, the bivalve *Tellina fabula* is known for its destabilizing effect on the bed during its burrowing and feeding activities. On the other hand, the tube building worm *Lanice conchilega* reduces the near-bottom flow around and across the tube fields. Finally, the sea urchin *Echinocardium cordatum* influences the vertical sediment distribution by filtering the finer particles from the sediment surface to the deeper sediment.

T. fabula is found to be responsible for a reduction of the critical bed shear stress up to a factor 0.6, while *L. conchilega* reduces the ripple height with a factor 0.5, due to the deceleration of the near bottom flow. These ripples are present on top of the sand waves, and are the main origin of the bottom roughness. Finally, *E. cordatum* is able to increase the medium grain size at the bed-water interface with a factor 2. Given the measured biomass of *T. fabula*, *L. conchilega* and *E. cordatum* on the Dutch Continental Shelf, the predicted occurrence of sand waves, in which the parameterization is included, shows significantly better results, compared to the prediction for the default case. This means that inclusion of biological activity is important to predict the occurrence of sand waves.

Introduction

The interaction between benthos and sediment dynamics in the intertidal area has been exhaustively documented (e.g., Widdows and Brinsley, 2002, and references therein). They show that benthos are able to influence the strength of the bed by several orders of magnitude, and thereby have a significant influence on the sediment dynamics on a large spatial and temporal scale (Borsje et al., in press). However, benthos are also present in shallow self sea, for which the North Sea is an example. At the bed of these shallow seas, sand waves are present, which can grow up to 25% of the water depth and migrate with a speed of a couple of meters per year.

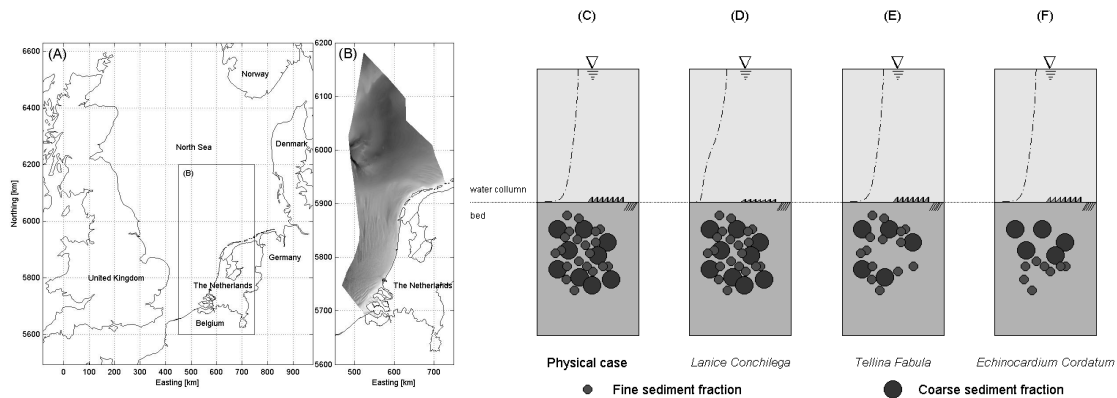


Figure 1. Overview of bedforms in the Dutch part of the North Sea (A-B) and a schematization of the biological influences on the fluid and sediment dynamics (D-F) compared to the physical case (C).

Given the large biological influences in the intertidal area, strong interactions are also expected in the North Sea area (Borsje et al., 2008), although the biomass in the North Sea area is much smaller compared to the intertidal area. In order to predict the bio-geomorphological interaction in offshore seabed patterns, this paper proposes a parameterization in which biological activity is expressed in physical parameters.

Three benthic species are included in this parameterization on the basis of (i) their abundance in the North Sea, (ii) their strong modification of the environment they are living in, and (iii) their contrasting type of feeding and burrowing, and thereby contrasting influence on the sediment and fluid dynamics. The three species selected are *Lanice conchilega*, *Tellina fabula* and *Echinocardium cordatum*.

The interaction between the selected benthos and the environment is schematized in Figure 1. The tube building worm *L. conchilega* protrudes several centimeters from the sediment in the water column, and thereby influences the near-bottom flow. For dense tube assemblages the near-bottom flow reduces, and consequently lower ripples are present (Figure 1d). Due to the digging and feeding activities of the bivalve *T. fabula* up to 10 cm deep in the sediment, the properties of the surficial sediment are modified and the sediment is more prone to erosion (Figure 1e). Finally, the sea urchin *E. cordatum* lives in the top 20 centimeters of the bed and mixes sediment in vertical direction (Figure 1f), resulting in relatively coarser sediment in the top layer of the bed, compared to the physical case (Figure 1c).

Parameterization of biological activity

While *L. conchilega* reduces the near bottom flow, the ripples on the top of the sand waves will become smaller, as observed in the field by Featherstone and Risk (1977). These ripples are the main origin of bottom roughness. To model the influence of *L. conchilega* on the near bottom flow, a vegetation model (Uittenbogaard, 2003) is adopted with the inclusion of the relevant dimension of *L. conchilega* in the field. The comparison between the model result and flume experiments executed by (Friedrichs et al., 2002) is shown in Figure 2a, for different densities of artificial tube building entities. Given the reduction of the near bottom flow by a factor 0.5, the ripple height will reduce by a factor 0.6, following the empirical relations derived by O'Donoghue et al. (2006).

To parameterize the transport of particles from the sediment surface deeper into the sediment by *E. cordatum*, we adopt an active layer concept. In this concept, the probability of entrainment of a particle is defined in a step function, for which the probability of entrainment of a particle has a constant value in an active layer of thickness I_{bio} near the bed surface, and vanishes below this layer (Hirano, 1971). The layer underneath the active layer is called the substrate, which is physically covered by the active layer. As a result, the grain size distribution in both layers can be assigned differently. By adopting an active layer thickness which is equal to the area of influence by *E. cordatum* the top layer can be modeled as a bioturbated layer, while the substrate can be modeled as a non bio-turbated layer. Based on an experimental study for *E. cordatum* in New Zealand, Lohrer et al., (2005) found that *E. cordatum* displaces up to $20,000 \text{ cm}^3 \text{ m}^{-2} \text{ d}^{-1}$, suggesting that surface sediment is reworked about every 3 days at site where *E. cordatum* is abundant.

E. cordatum is regarded as a non-selective deposit feeder (Lohrer et al., 2005). However, due to two reasons, *E. cordatum* will cause a heterogeneous sediment distribution in the top centimeters of the bed.

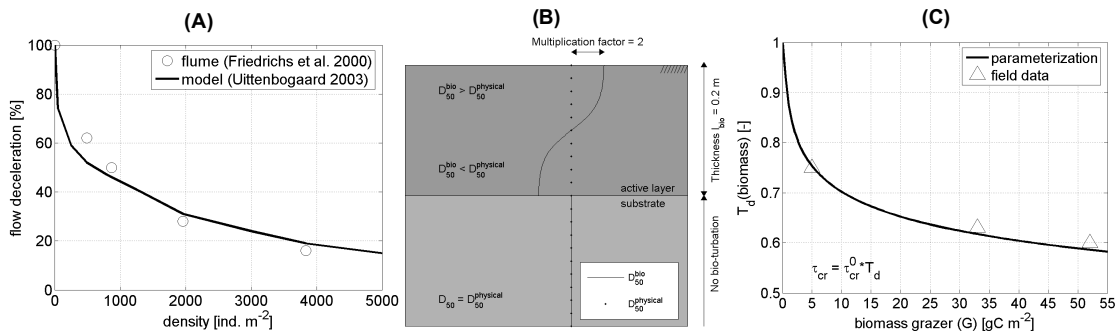


Figure 2. Parameterization for the relation between (A) density *L. conchilega* and reduction of the near bottom flow, (B) *E. cordatum* and increase in medium grain size at the sediment water interface and (C) biomass *T. fabula* and the multiplication-factor for the critical bed shear stress.

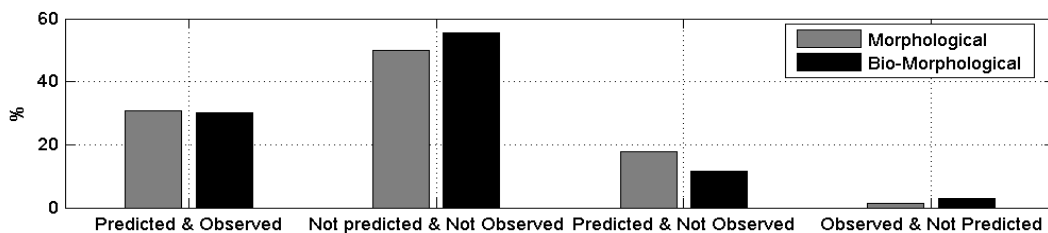


Figure 3. Results for the Morphological (default) and Bio-Morphological model, evaluated against observed sandwave occurrence in the Dutch part of the North Sea. The overall correct prediction increases with almost 4000 km² by including the proposed parameterization in the model (van der Veen et al., 2006).

Firstly, because finer particles have a relative larger surface area and have therefore a larger chance to get ingested and brought downward. Secondly, fine sediment is richer in organic matter compared to coarse sediment, and therefore *E. cordatum* moves to another spot, while relative larger particles are not ingested and are still at their original position. The heterogeneous vertical sediment distribution is shown in Figure 2b, in which the thickness of the bio-turbated layer (l_{bio}) and the multiplication factor for the medium grain size needs to be imposed. Based on measurements of *Arenicola marina* (Baumfalk, 1979), which is a comparable non-selective deposit feeders, the multiplication factor could reach values up to 2, meaning a medium grain size twice as large, compared to the default case. The thickness of the bio-turbated layer could reach values up to 0.2 m (Holtmann et al., 1996)

Data on the bio-engineer capacity of the bivalve *T. fabula* are scarce, but the sediment modification by the bivalve *Macoma balthica* is much better known. Both bivalves have comparable feeding strategies (selective deposit as well suspension feeding). However, *M. balthica* is mostly found in muddy sediments, while *T. fabula* prefers fine sediments. Therefore, the distribution of *M. balthica* is much more bordered close to the coast, in contrast to *T. fabula* which can be found in all other parts of the North Sea. Nevertheless, the relation used for *M. balthica* is a good alternative to model the bio-sediment interactions for *T. fabula*. The biomass of the bivalve is related to the critical bed shear stress by a destabilizing factor (T_d), as shown in Figure 2c, where τ_{cr} is the critical bed shear stress for erosion. The superscript '0' for the critical shear stress represents the values without the influence of biological activity. The destabilizing factor is defined by Borsje et al. (in press) and quantitatively shown in Figure 2c.

Model results

In order to show the significance of bio-geomorphological interactions in the occurrence of sandwaves, the proposed parameterization is included in a idealized sand wave occurrence model (van der Veen et al., 2006). In this model, sand waves are seen as free instabilities of the bed, which are preserved by the tidal current, and own their dimensions to the strength of the tidal current, the grain size of the bed material and the local water depth. This type of model is shown to fairly predict the occurrence of sandwaves for the North Sea in both a qualitative (Hulscher and van den Brink, 2001) and quantitative way (Cherlet et al., 2007). The interested reader is referred to Dodd et al. (2003) for more details on the theoretical approach in idealized sand wave models and to van der Veen et al. (2006) for the specific model set-up. The spatial distribution of the three benthic species and their biomass or density is based on data provided by Holtmann et al. (1996).

The case in which both sandwaves are predicted by the model and observed in the field, is not much influenced by the included biological activity. However, the quite large over-prediction (column predicted and not observed) in the model of van der Veen et al. (2006) is partly restricted by *L. conchilega* and *E. cordatum*. Both species are able to preserve a flat bed for almost 4,000 km² in the Dutch part of the North, while the physical parameters suggest sand waves.

Conclusions

This paper proposes a parameterization on the interaction between three subtidal benthic species and sediment dynamics. By including this parameterization in an idealized sand-wave model, the occurrence of sand waves is significantly better predicted, compared to the default case. In summary, biota is able to preserve a stable flat bed, while the physical conditions suggest bed patterns. Likewise the opposite effect is induced by destabilizing benthos. In reality, much more benthos are present in the North Sea, with a much stronger spatial distribution than modeled in this paper, moreover the temporal variation needs to be accounted for by extending the models to predict seabed dynamics. However, the inclusion of the three most relevant bio-engineers in the North Sea already shows the necessity to account for bio-geomorphological interactions in predicting sand wave occurrence in shallow shelf seas.

Acknowledgements

This research is supported by the Dutch Technology Foundation STW, applied science division of NWO and the Technology Program of the Dutch Ministry of Economic Affairs.

References

- Baumfalk, Y.A. (1979), On the pumping activity of Arenicola Marina. *Netherlands Journal of Sea Research*, 13, 422–427.
- Borsje, B.W., de Vries, M.B., Hulscher, S.J.M.H., de Boer, G.J. (2008), Modeling large-scale cohesive sediment transport affected by small-scale biological activity, *Estuarine, Coastal and Shelf Science*. (In press.)
- Borsje, B.W., de Vries, M.B., Bouma, T.J., Hulscher, S.J.M.H., Herman, P.M.J. (2008), *Biogeomorphological interactions in offshore seabed patterns*. In: Proceedings of the 31st International Conference on Coastal Engineering, Hamburg, Germany.
- Cherlet, J., Besio, G., Blondeaux, P., van Lancker, V., Verfaillie, E., Vittori, G. (2007), Modeling sand wave characteristics on the Belgian Continental Shelf and in the Calais-Dover Strait, *Journal of Geophysical Research*, 112, C06002, doi:10.1029/2007/JC004089.
- Dodd, N., Blondeaux, P., Calvete, D., de Swart, H., Falques, A., Hulscher, S.J.M.H., Rozynski, G., Vittori, G. (2003), The use of stability methods for understanding the morphodynamical behaviour of coastal systems, *Journal of Coastal Research*, 19, 849–865.
- Featherstone, R.P., Risk, M.J. (1977), Effect of tube-building polychaetes on intertidal sediments of the Minas Basin, Bay of Fundy, *Journal of Sedimentary Petrology*, 47, 446–450.
- Friedrichs, M., Graf, G., Spring, B. (2000), Skimming flow induced over a simulated polychaete tube lawn at low population densities, *Marine Ecology Progress Series*, 192, 219–228.
- Lohrer, A.M., Thrush, S.F., Hunt L., Hancock, N., Lundquist, C. (2005), Rapid reworking of subtidal sediments by burrowing spatangoid urchins, *Journal of Experimental Marine Biology and Ecology*, 321, 155–169.
- Hirano M. (1971), River bed degradation with armouring, *Proceedings of the Japanese Society of Civil Engineering*, 195, 55–65.
- Holtmann, S.E., Groenewold, A., Schrader, K.H.M., Asjes, J., Craeymeersch, J.A., Duineveld, G.C.A., van Bostelen, A.J., van der Meer, J. (1996), *Atlas of the Zoobenthos of the Dutch Continental Shelf*. Ministry of Transport, Public Works and Water Management, North Sea Directorate, Rijswijk. 1–244pp.
- Hulscher, S.J.M.H., van den Brink, G.M. (2001), Comparison between predicted and observed sand waves and sand banks in the North Sea, *Journal of Geophysical Research*, C5, 106, 9327–9338.
- O'Donoghue, T., Doucette, J.S., van der Werf, J.J., Ribberink, J.S. (2006), The dimensions of sand ripples in full-scale oscillatory flows, *Coastal Engineering*, 53, 997–1012.
- Uittenbogaard, R. (2003), *Modelling turbulence in vegetated aquatic flows*. Riparian Forest Vegetated Channels Workshop, Trento (Italy).
- van der Veen, H.H., Hulscher, S.J.M.H., Knaapen, M.A.F. (2006), Grain size dependency in the occurrence of sand waves, *Ocean Dynamics*, 56, 228–234.
- Widdows, J., Brinsley, M.D. (2002), Impact of biotic and abiotic processes on sediment dynamics and the consequences to the structure and functioning of the intertidal zone, *Journal of Sea Research*, 48, 143–156.

Relating river plume structure to vertical mixing using potential energy anomaly budgets and salinity coordinates

GERBEN J. DE BOER^{1,2}, JULIE D. PIETRZAK¹

1. Environmental Fluid Mechanics Section,
Faculty of Civil Engineering and Geosciences, Delft University of Technology,
P.O. Box 5048, 2600 GA Delft, Netherlands
email: g.j.deboer@tudelft.nl, j.d.pietrzak@tudelft.nl
2. Deltares, Rotterdamseweg 185, P.O. Box 177, 2600 MH Delft, Netherlands
email: gerben.deboer@deltares.nl

Keywords: ROFI, tidal straining, numerical model, potential energy anomaly; Rhine river plume

ABSTRACT

River plumes are complex 3D structures of low-salinity water in the coastal marine environment that dominate transport pathways of fine sediments, nutrients and pollutants. They exhibit significant spatial and temporal variability due to wind and river discharge variations, as well as due to the tide. Due to the high spatial and temporal variability, at many coastal locations the plume is only present for a fraction of the time. The behavior of river plumes under the effect of tidal advection, tidal straining and tidal mixing is the focus of this paper. The large effect of the tide on the position of a characteristic isohaline is illustrated in Figures 1 and 2.

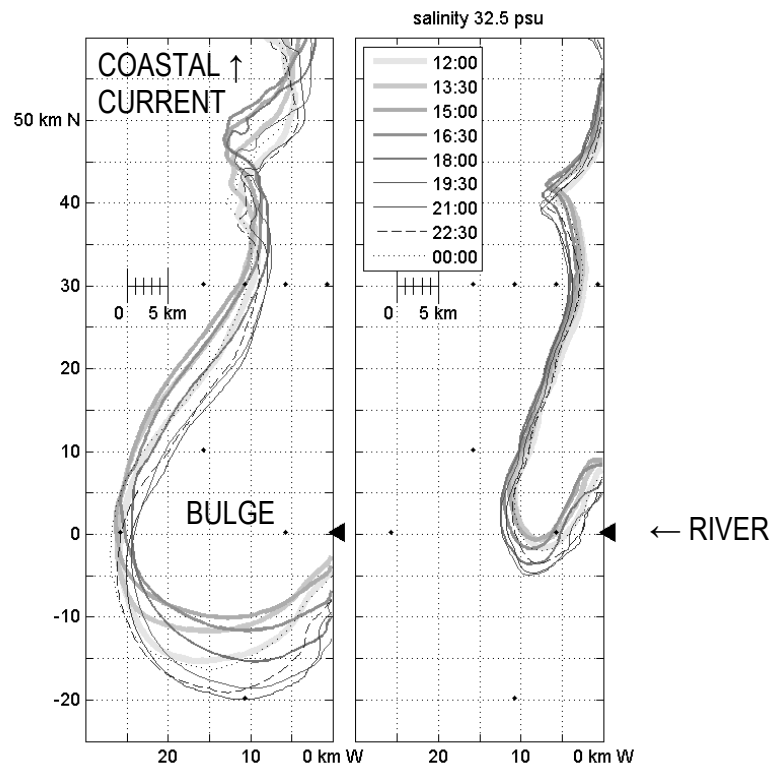


Figure 1. Plan view of the time-varying position of a characteristic isohaline (32.5 psu) in a 3-D river plume simulation under the influence of an S_2 neap tide performed by de Boer et al. (2006). The left panel shows the surface layer, the right panel the bottom layer. The black triangle indicates the position of the river that debouches into the coastal sea. The times agree with those in Figure 2.

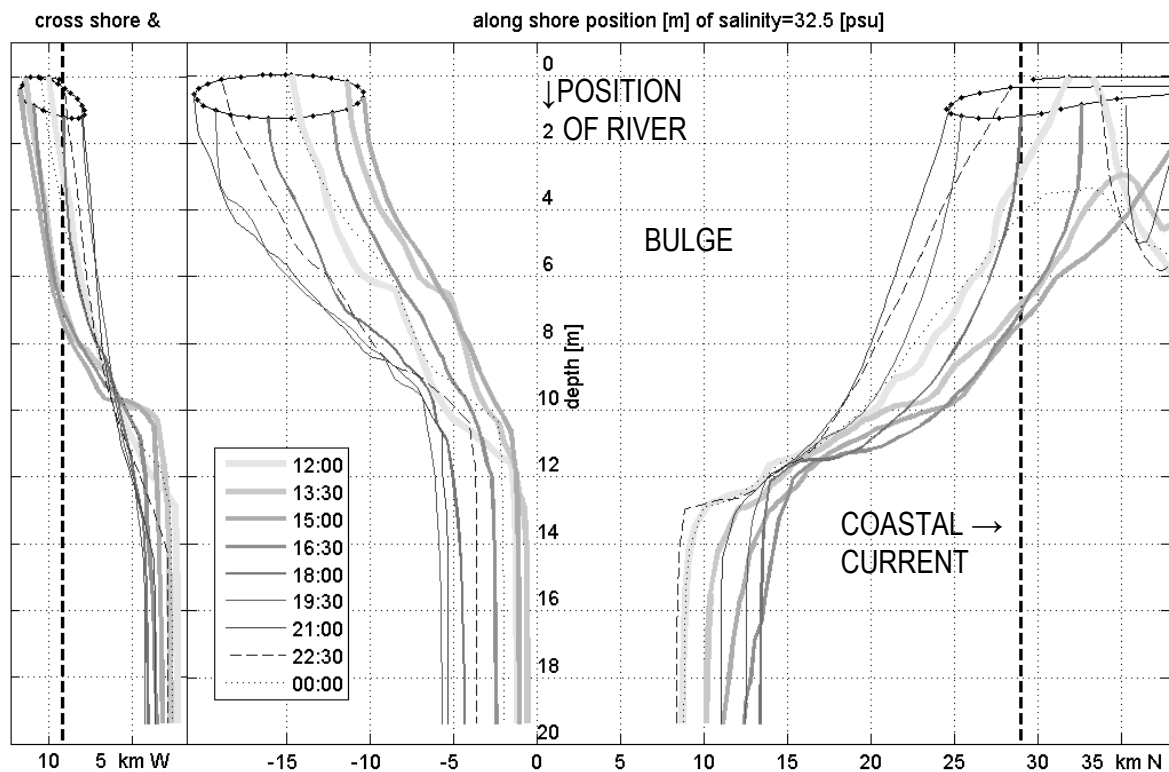


Figure 2. Cross section views of the time-varying position of a characteristic isohaline (32.5 psu) in a 3-D river plume simulation under the influence of an S_2 neap tide performed by de Boer et al. (2006). The thick vertical dotted line indicates where the cross shore (left) and the alongshore (right) cross-sectional planes intersect. The times agree with those in Figure 1.

Objective

In addition to the spatial and temporal variability imposed by tidal advection and tidal straining, the river plume can exhibit various regimes due to changes in wind and tidal mixing. The Rhine ROFI, for example, has been observed to switch from a well-mixed bottom advected plume to a stratified surface trapped plume over the course of a spring-neap cycle (Simpson et al., 1993). Due to these aspects 3-D river plume structures are considered difficult to analyze as a single body. “Many of these difficulties stem from a Cartesian, or Eulerian, view of the plume” (Hetland, 2005). Therefore Hetland (2005) adopted salinity coordinates as a means to overcome this difficulty. Another powerful diagnostic tool for this issue is provided by the potential energy anomaly (ϕ) budgets as introduced by Simpson and co-workers. They defined ϕ as the work required to bring about complete vertical mixing per unit of volume. Recently more complete formulations of the ϕ equation have been derived by de Boer et al. (2008) and Burchard and Hofmeister (2008); they include all horizontal advection, straining and dispersion terms. These formulations are suitable for direct analysis of the numerical model results. In this paper we compare the two methods by applying them to the numerical simulations of an idealized tidally dominated river plume as shown in Figure 1 and 2. We analyze the intratidal plume movements as well as the net mixing over the tidal cycle for both well-mixed spring and stratified neap tide cases.

References

- de Boer, G.J., Pietrzak, J.D., Winterwerp, J.C. (2006), On the vertical structure of the Rhine region of freshwater influence, *Ocean Dynamics*, 56(3–4), 198–216.
- de Boer, G.J., Pietrzak, J.D., Winterwerp, J.C. (2007), Using the potential energy anomaly equation to investigate tidal straining and advection of stratification in a region of freshwater influence, *Ocean Modelling*, 22(1–2), 1–11.
- Burchard, H., Hofmeister, R. (2007), A dynamic equation for the potential energy anomaly for analyzing mixing and stratification in estuaries and coastal seas, *Estuarine Coastal and Shelf Science*, 77(4), 679–687.
- Hetland, R.D. (2005), Relating river plume structure to vertical mixing, *Journal of Physical Oceanography*, 35, 1667–1688.
- Simpson, J.H., Bos, W.G., Schirmer, F., Souza, A.J., Rippeth, T.P., Jones, S.E., Hydes, D. (1993), Periodic stratification in the Rhine ROFI in the North Sea, *Oceanologica Acta*, 16(1), 23–32.

Turbulent kinetic energy dissipation in the Rhine ROFI

ELISABETH FISCHER¹, HANS BURCHARD¹, ROBERT D. HETLAND²

1. Baltic Sea Research Institute Warnemünde, Seestraße 15,
18119 Rostock-Warnemünde, Germany
email: elisabeth.fischer@io-warnemuende.de, hans.burchard@io-warnemuende.de
2. Department of Oceanography, Texas A&M University,
College Station TX 77843-3146, USA
email: hetland@tamu.edu

Keywords: dissipation maximum, 3-D numerical modeling; Rhine ROFI

ABSTRACT

In coastal regions with tides that are similar to a Kelvin wave, turbulent kinetic energy dissipation is maximum at the bottom at high and at low water, when alongshore currents are strongest. Dissipation measurements in the Rhine ROFI described by Fisher et al. (2002) revealed a local maximum 5 m below the surface at high water, which could not yet be explained. By means of a three-dimensional simulation, the tidal cycle of dissipation is investigated, together with relevant physical properties. The maximum turns out to be due to a strong alongshore shear.

Introduction

The Rhine region of freshwater influence (ROFI, Simpson et al. 1993), an approximately 20 km wide and 100 km long strip of the North Sea in front of the Dutch coast, is characterized by a semi-diurnal cycle of stratification due to tidal straining (strain induced periodic stratification, SIPS, Fisher et al., 2002). The tides are similar to an M_2 Kelvin wave traveling northeastward parallel to the coastline, resulting in the alongshore velocity component being in phase with the surface elevation. Tidal ellipses are near-degenerate outside the plume area and are directed parallel to the coast; within the stratified region they have a pronounced clockwise rotation at the surface and counterclockwise at the bottom. The arising strong cross-shore shear interacts with the density gradients normal to the coast and forces fresher over more saline water during flooding, and vice versa. Maximum stratification thus coincides with high water, when tidal stirring is maximum itself.

The tidal shear due to bottom friction acting on the alongshore velocity component is two times as high as for the cross-shore tide, which has its strongest bottom shear during flooding and ebbing. Consequently, turbulent kinetic energy dissipation ε has maxima at the bottom at high and at low water. However, shear is approximately constant throughout the water column, but has maxima between the surface and 5 m below.

The turbulent kinetic energy budget is given by Equation (1), whereas k denotes the kinetic energy, t the time, P the shear production, B the buoyancy production, Tr transport terms, and ε the turbulent kinetic energy dissipation.

$$\frac{Dk}{Dt} = P + B + Tr - \varepsilon \quad (1)$$

Observations

Approximately 11 km offshore and 41 km northeast of the Rhine estuary (52°18'N, 04°18'E; position B in Figure 1a), ε was measured by means of a free-fall microstructure profiler over four periods of 15 h between 29 March and 21 May 1999 (Fisher et al., 2002). Figure 1b shows the first two sequences, which were obtained during low wind stress (<0.07 Pa). At the bottom, ε has maxima at high and at low water, the first of which are extending upwards with a phase delay increasing and values decreasing with height. This is caused by tidal shear production in the bottom boundary layer, which, however, does not explain the mid-depth maxima.

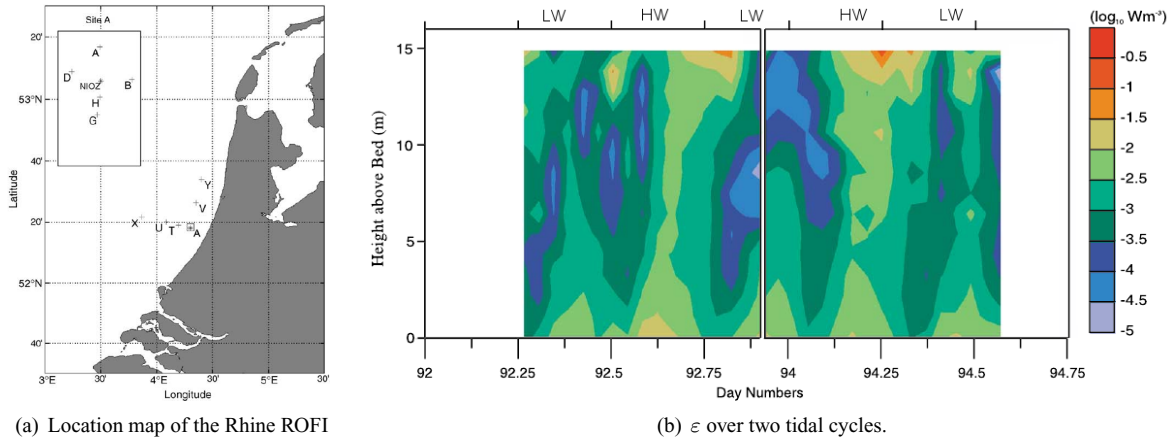


Figure 1. Measurement site and results (adapted from Fisher et al., 2002, Figure 1, 6a).

Model set-up

By means of a three-dimensional simulation using the General Estuarine Transport Model (GETM, www.getm.eu), the temporal and spatial evolution of ε and relevant physical properties is investigated. We use the same model grid as de Boer et al. (2006), that is a rectilinear grid with grid cells of $500 \text{ m} \times 500 \text{ m}$ close to the plume region (up to 65 km from coast, between 30 km southwest and 75 km northeast of the river mouth) and exponentially increasing size outside (zooming-out at the northwest (left) and -east (top) boundary). The x -axis is situated perpendicular to the coast, the y -axis parallel. The Rhine is 500 m wide (one grid cell) and 75 km long, its depth decreases linearly from 20 m at the mouth to 5 m at the freshwater source. In order to save storage and simulation time, the river is angled and lies parallel to the coastline.

An idealized configuration is used, i.e., a flat bottom (water depth 20 m), a straight coastline, and zero wind. The only forcings are a surface elevation according to a Kelvin wave solution at the three open boundaries and a constant river runoff of $1500 \text{ m}^3 \text{ s}^{-1}$. Simulations with a higher river discharge or rather light wind conditions show comparable results.

Model results and discussion

The observed dissipation maxima could be reproduced by our simulation and are shown in Figure 2. The highest values occur half an hour before local high water in the upper 5 m of water columns located in the offshore part of the plume, e.g., 14 km offshore and 8 km northeast of the river mouth. A second patch of high dissipation extends from mid-depth to the surface one and a half hours later. Around low water, a similar, though much less distinct spreading is visible.

There are no convective instabilities, which could have caused vertical mixing and thus the enhanced ε . As visible in Figure 3, the upper half of the water column is stably stratified at high water, when the highest dissipation occurs, and, though well mixed, not unstable at any other time. Only at flooding instabilities develop at the bottom, noticeable from the white gaps in Figure 4 (right panel) where the buoyancy production is positive.

The dissipation maximum below the surface is not related to mixing at the plume front; the spreading of ε does not coincide with the plume front. It is due to strong mid-depth shears (see shear production in Figure 4, left panel). The cross-shore shear shifts from strongly negative (offshore displacement) to positive (onshore displacement) at the moment of the dissipation maximum. At the same time the alongshore shear has its maximum (down-coast displacement in the sense of Kelvin wave propagation). The horizontal velocities are shown in Figure 5.

Conclusions

The cross-shore shear is negative during flooding and positive during ebbing due to tidal ellipses changing at about 5 m below the surface from clockwise above to counterclockwise below. At high water, the maximum alongshore shear below the surface causes a maximum of turbulent kinetic energy and its dissipation.

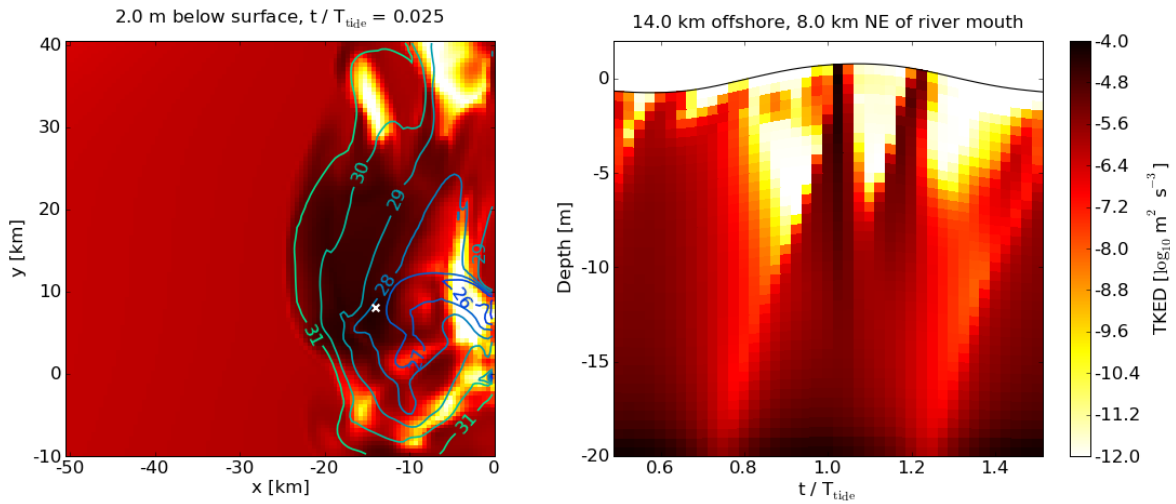


Figure 2. Turbulent kinetic energy dissipation ε . The contours in the left panel represent the salinity [g kg^{-1}], the white cross marks the position of the water column shown in the right panel. The legend on the right-hand side applies for both plots.

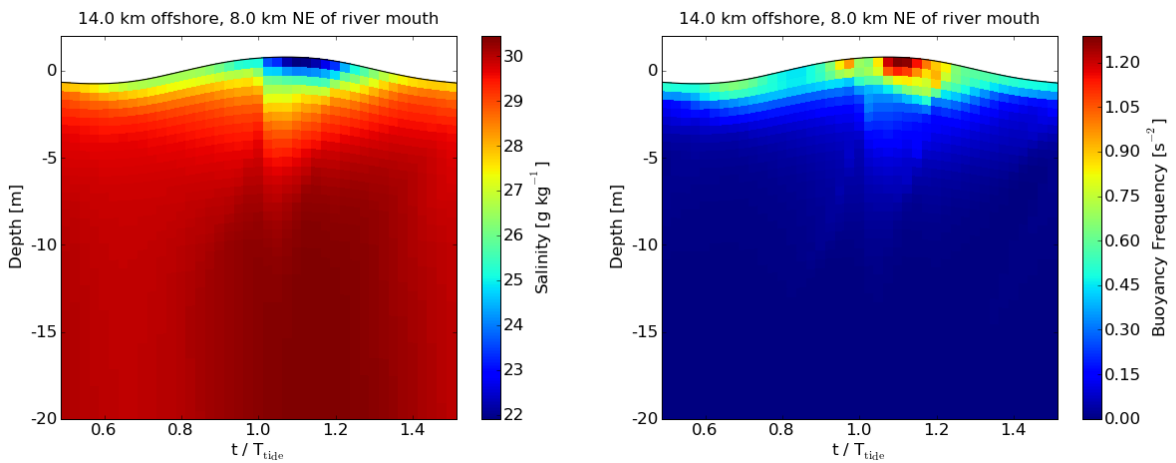


Figure 3. Salinity and buoyancy frequency. The upper half of the water column is stable at any time.

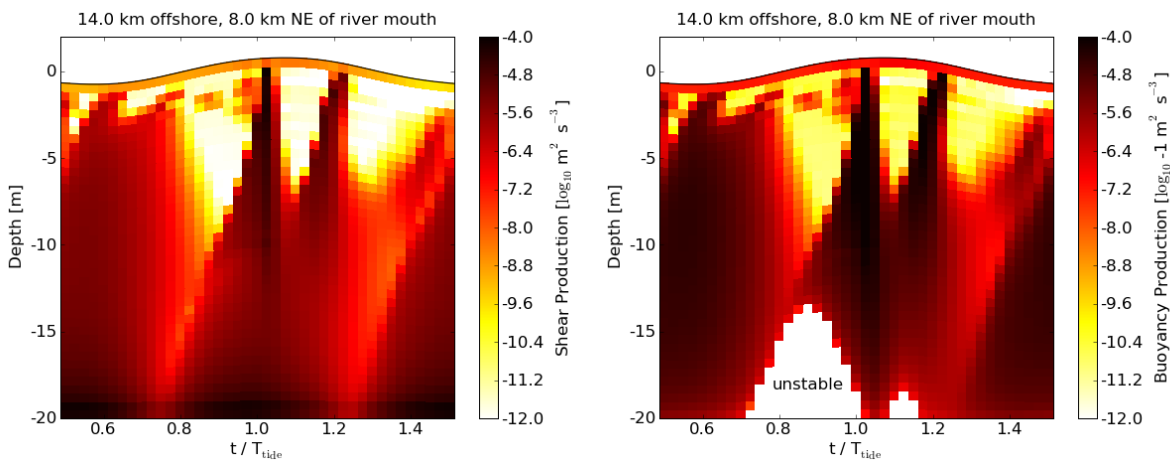


Figure 4. Shear (P) and buoyancy production (B).

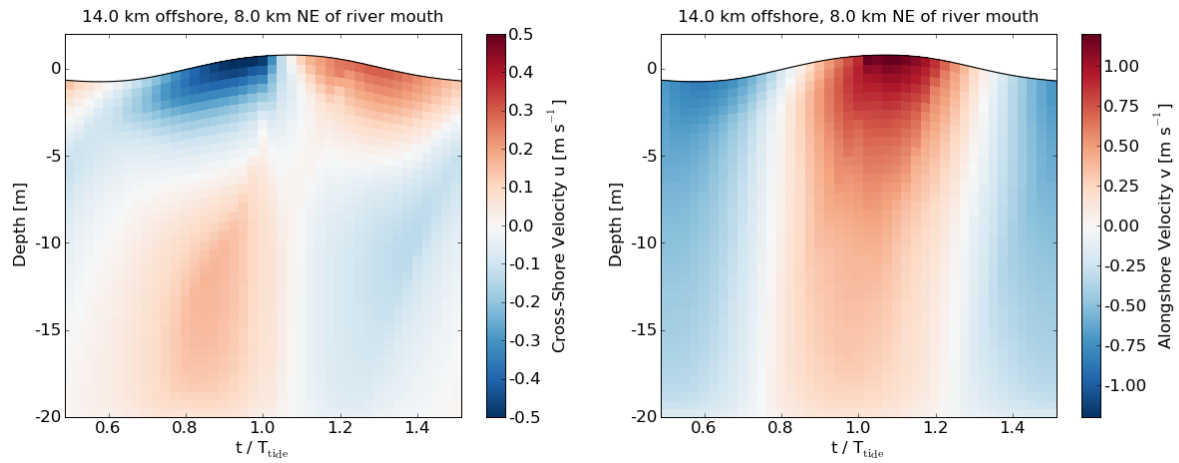


Figure 5. Cross-shore (u) and alongshore velocity (v).

References

- de Boer, G.J., Pietrzak, J.D., Winterwerp, J.C. (2006), On the vertical structure of the Rhine region of freshwater influence, *Ocean Dynamics*, 56, 198–216.
- Fisher, N.R., Simpson, J.H., Howarth, M.J. (2002), Turbulent dissipation in the Rhine ROFI forced by tidal flow and wind stress, *Journal of Sea Research*, 48, 249–258.
- Simpson, J. H., Bos, W.G., Schirmer, F., Souza, A.J., Rippeth, T.P., Jones, S.E., Hydes, D. (1993), Periodic stratification in the Rhine ROFI in the North Sea, *Oceanologica Acta*, 16, 23–32.

Liverpool Bay: a coastal sea's responses to winds, waves, tides and freshwater

ELEANOR R. HOWLETT¹, M. JOHN HOWARTH¹, TOM P. RIPPETH²

1. Proudman Oceanographic Laboratory, 6 Brownlow Street, Liverpool L3 5DA UK
email: elow@pol.ac.uk, mjh@pol.ac.uk
2. School of Ocean Sciences, College of Natural Science, Bangor University,
Menai Bridge, Anglesey LL59 5AB UK
email: t.p.rippeth@bangor.ac.uk

Keywords: stratification, potential energy anomaly, mixing, Coastal Observatory

ABSTRACT

Liverpool Bay, in the eastern Irish Sea, is a shallow shelf sea heavily impacted by humans. As a Region of Freshwater Influence (ROFI), fed by a number of rivers, including the Dee, Mersey and Ribble, each with flows up to $600 \text{ m}^3 \text{ s}^{-1}$, Liverpool Bay is host to large horizontal and vertical gradients. Although this region has been studied intensively by a number of groups, gaps in the understanding of the dynamics remain, which is evident in the accuracy of numerical models. Using data from the Proudman Oceanographic Laboratory Coastal Observatory (Figure 1), the structure of Liverpool Bay is examined. Just over two years worth of moorings data, CTD transects, wind and wave measurements, river flows from the Centre for Ecology and Hydrology, and Met Office model predictions are used to test current theories and locate deficiencies.

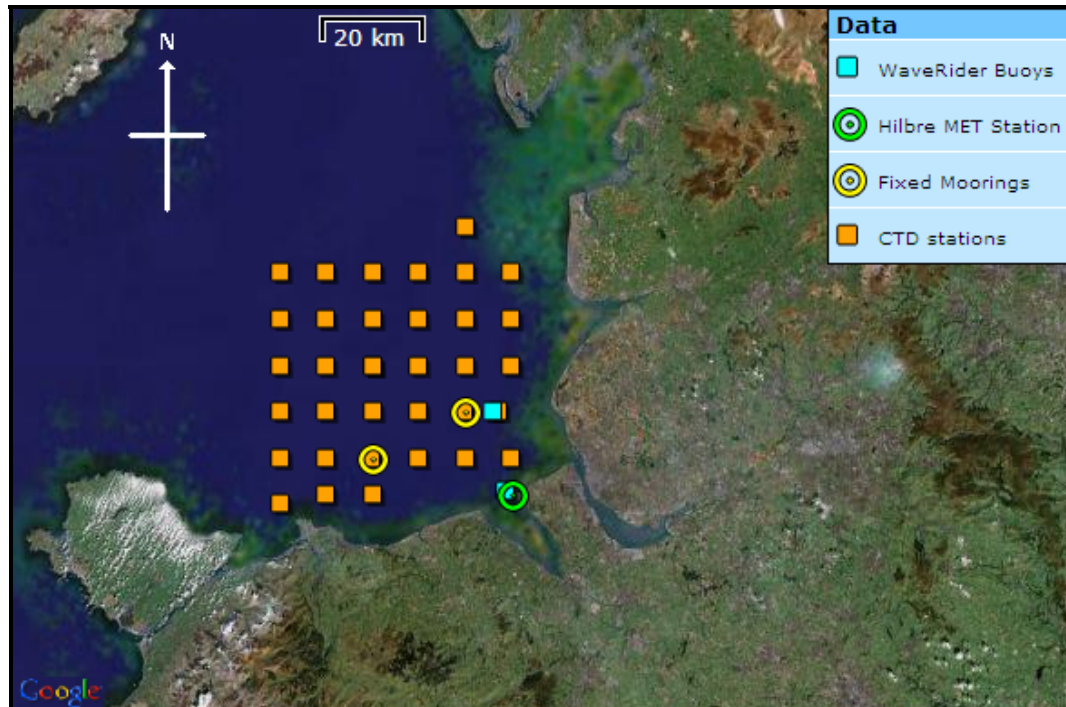


Figure 1. Location of measurements from the Proudman Oceanographic Laboratory Coastal Observatory used for this project. There are also many river flow gauging stations in North Wales and North-west England, operated by the Environment Agency, which have not been shown here. Meteorological data are also available from the Met Office model. Map © 2008 TerraMetrics Powered by Google, taken from the Coastal Observatory website <http://coastobs.pol.ac.uk/gmapper/>.

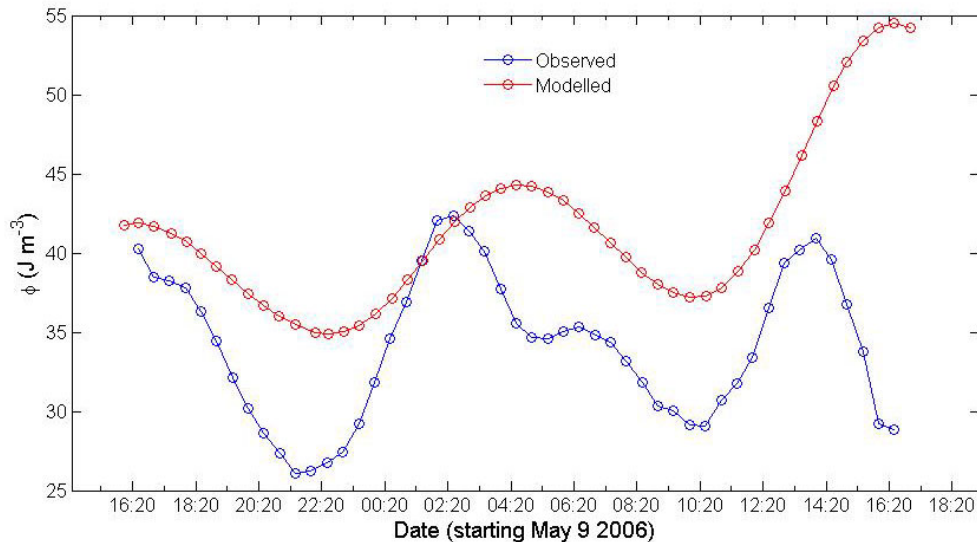


Figure 2. The potential energy anomaly (ϕ) during a 25-hour station at site A in May 2006. The blue line represents the potential energy anomaly calculated from CTD casts at site A. The red line indicates the results of the potential energy model.

Method and results

Previous theories regarding the vertical structure of Liverpool Bay predominantly looked at the effects of tides on stratification. SIPS (Strain Induced Periodic Stratification; Simpson et al., 1990) theory explains the semi-diurnal cycle of stratification formation and destruction as a result of the interaction between the horizontal density gradients and the tidal shear. Sharples and Simpson (1995) postulated the existence of post-neap enduring stratification occurring at an N_2 modulation, a product of the intensity of tidal mixing. Whilst these theories do occasionally explain the vertical structure of Liverpool Bay, there are many occurrences when they do not. For example, there are periods when enduring stratification occurs at spring, not neap tides. It is the effect of wind, wave and river flow events that causes the disparity between theory and reality.

The degree of stratification at a point in time is the result of the buoyancy-mixing competition. Buoyancy in Liverpool Bay originates from freshwater inputs from rivers and rainfall and from surface heating, which acts to stratify the region. Winds, waves and tides act to destratify the region, by mixing the water column. To examine the influences of these different buoyancy and mixing processes, a very simple potential energy model has been created following the methods of Simpson and Bowers (1981), Rippeth et al. (2001) and Wiles et al. (2006). The potential energy anomaly (Simpson and Bowers, 1981) defines the amount of energy required to overturn a water column. Changes to the amount of energy in the water column are either caused by buoyancy inputs or mixing processes, which can be defined by a series of equations. These equations are used in the potential energy model in conjunction with data from the Coastal Observatory, to predict the state of the stratification at a point in time. The model can also determine the importance of individual processes at specific times.

To test the potential energy model, a 25-hour station from May 2006 was examined. This period was subject to low wind and wave forcing and occurred when the tidal range was ~ 4.5 m, following a neap tide. River flow was less than $50 \text{ m}^3 \text{ s}^{-1}$ and rainfall was insignificant. The potential energy anomaly was calculated from CTD casts during the 25-hour station and was also predicted using the potential energy model. The results are shown in Figure 2. During this period in May 2006, the model recreates the potential energy anomaly fairly well, although it is clear that there is too much of a buoyancy input. Assuming this model is correct, it was the tidal straining term that caused most of the change to the stratification during the 25-hour station in 2006. The next challenge is to determine how successful the model is during a period of elevated wind and wave mixing, and to separate periods when winds are from the Southeast or when they are from the West. Mixing efficiencies for both wind and wave mixing must also be determined.

Errors in predictions arise principally from the calculations of horizontal gradients. There are two methods for calculating these at present: using the two moorings which unfortunately are not located directly parallel to the horizontal gradient; using a tidal excursion technique which assumes no mixing will take place within

a parcel of water over a 6 hour period. There are also possibilities of using the CTD transects to calculate the horizontal gradients, but again these are subject to the tidal excursion problem and are only available every 4–6 weeks.

Conclusions

The two year time-series from Coastal Observatory moorings have shown that current theories do not always correctly predict stratification. The potential energy model, following the route taken by Simpson and Bowers (1981), Rippeth et al. (2001) and Wiles et al. (2006), indicates that recreating the level of stratification in Liverpool Bay is an immensely complex problem, caused by the numerous factors affecting water column stability.

References

- Rippeth, T.P., Fisher, N.R., Simpson, J.H. (2001), The cycle of turbulent dissipation in the presence of tidal straining, *Journal of Physical Oceanography*, 31, 2458–2471.
- Sharples, J., Simpson, J.H. (1995), Semi-diurnal and longer period stability cycles in the Liverpool Bay area of fresh water influence, *Continental Shelf Research*, 15(2–3), 295–313.
- Simpson, J.H., Bowers, D.G. (1981), Models of stratification and frontal movement in shelf seas, *Deep-Sea Research*, 28(7A), 727–738.
- Simpson, J.H., Brown, J., Matthews, J., Allen, G. (1990), Tidal straining, density currents, and stirring in the control of estuarine stratification, *Estuaries*, 13, 125–132.
- Wiles, P.J., van Duren, L.A., Hase, C., Larsen, J., Simpson, J.H. (2006), Stratification and mixing in the Limfjorden in relation to mussel culture, *Journal of Marine Systems*, 60(1–2), 129–143.

Residual circulation and horizontal density gradients in the Liverpool Bay region of freshwater influence

FLORENCE I. VERSPECHT¹, TOM P. RIPPETH¹, ALEJANDRO J. SOUZA², HANS BURCHARD³,
M. JOHN HOWARTH², JOHN H. SIMPSON¹

1. School of Ocean Sciences, College of Natural Science, Bangor University, Menai Bridge, Anglesey LL59 5AB UK
email: f.verspecht@bangor.ac.uk, t.p.rippeth@bangor.ac.uk,
j.h.simpson@bangor.ac.uk
2. Proudman Oceanographic Laboratory, 6 Brownlow Street, Liverpool L3 5DA UK
email: ajso@pol.ac.uk, mjh@pol.ac.uk
3. Baltic Sea Research Institute Warnemünde, Seestraße 15, 18119 Rostock-Warnemünde, Germany
email: hans.burchard@io-warnemuende.de

Keywords: residual currents, tidal mixing, strain induced periodic stratification

ABSTRACT

Tidal straining is proposed as a key mechanism influencing the magnitude and timing of the horizontal mass flux of nutrients, terrestrial carbon and anthropogenic contaminants across Regions of Freshwater Influence (ROFIs), the critical interface between estuaries and continental shelf seas. Evidence for this hypothesis is presented in estimates of the long-term residual current profile, obtained from five years of continuous ADCP measurements, taken at the Proudman Oceanographic Laboratory Coastal Observatory mooring in Liverpool Bay. The observed mean residual velocities are found to be three times larger than those predicted by Heaps' (1972) 'classical' solution. The strongest residual currents from the coastal observatory mooring are shown to occur when the water column periodically alternates between a well mixed and stratified state, a consequence of tidal straining, rather than simply related to the density gradient. These results are used for the further development of the POLCOMS 3D numerical model to improve the simulation of physical processes that drive the off-shore flux of freshwater.

Introduction

Regions of freshwater influence (ROFIs) provide the critical interface between estuaries and continental shelf seas, across which freshwater and suspended particulate matter, and consequently terrestrial carbon, nutrients and anthropogenic contaminants, are exchanged. On a local scale, the water quality in, and the flux of terrestrial carbon through, coastal and estuarine waters is fundamentally dependent on the mixing of water masses, residence times and particulate matter which mediate primary productivity, biogeochemical cycling, pollutant dispersal and ecosystem sustainability (Tett et al., 1993).

On a global scale the discharge of freshwater into the ocean plays a role in climate dynamics which is out of all proportion to its total volume flux. Although global freshwater discharge (~ 0.6 Sv; $1 \text{ Sv} = 10^6 \text{ m}^3 \text{ s}^{-1}$) is dwarfed by deep ocean fluxes (for example, the North Atlantic subtropical gyre horizontal plane transport is ~ 120 Sv) it plays a major role in determining climate through its influence on ocean stratification. Rahmstorf (1995) showed that an increase in total freshwater flux to the ocean of just 10% could substantially reduce or shut down the North Atlantic 'thermohaline' circulation with a potentially severe impact on the climate of the North Atlantic and Western Europe.

Within ROFIs the physical processes characteristic of both estuaries and continental shelf seas overlap to create a particularly subtle and complex regime. An understanding of the complex range of processes and their interactions, which drive and control the freshwater flux across these critical interfaces, is thus a vital prerequisite to the development of management tools for ROFIs.

ROFIs tend to be characterized by strong lateral salinity (cf. density) gradients. Whilst tidal currents dominate, it is the normally much weaker, residual circulation which determines the fate of freshwater. The classical view of residual circulation in ROFIs is an estuarine circulation forced by a lateral density gradient, under the influence of the Earth's rotation (Heaps, 1972). The strength of the resultant horizontal mass flux is strongly linked to the level of friction opposing the flow, which is in turn influenced by the degree of stratification in the system. Both the level of friction encountered and level of stratification are determined by the competition between the various stratifying influences and the mixing processes. The paradox is that interfacial stresses promote mixing, yet are a consequence of minimal mixing, hence the critical link between dynamics and mixing.

Recent theoretical work has identified tidal straining as contributing substantially to the horizontal mass flux in partially stratified estuaries (Prandle, 2004). The aim of this investigation is to test the hypothesis that the magnitude and timing of the offshore flux of freshwater in tidally stirred shelf seas is largely determined by tidal straining. An integrated analysis of coastal observatory observations and numerical model predictions are used to identify and quantify the physical processes which determine the offshore freshwater flux in regions of tidally energetic continental shelf seas influenced by freshwater inflow.

Tidal straining

Tidal straining results from the differential advection of the offshore salinity gradient by the sheared tidal flow. In regions where the tide is a standing wave, it results in the formation and intensification of stratification on the ebb phase of the tide, and the removal of stratification on the flood (Simpson et al., 1990). Strain induced periodic stratification (SIPS) with a semi-diurnal and semi-monthly switching between a stratified and mixed water column has been observed in Liverpool Bay (Simpson et al., 1991) and in many other freshwater influenced regions of tidally stirred continental shelf seas.

Two processes are responsible for the horizontal mass flux resulting from SIPS: on an ebb tide in creasing stratification suppresses turbulence and on a flood tide increased vertical mixing results from convection, producing a tidal mixing asymmetry. Although the pulsed residual creation resulting from mixing asymmetries is qualitatively equivalent to gravitational circulation, the magnitude of the exchange flow will not – as is the case with gravitation circulation – be dependent on the average magnitude of vertical mixing, but rather on the tidal asymmetry of the vertical mixing. At a specific location, a consequence of the straining of the density field by the tide is thus asymmetry in water column structure, vertical mixing and residual creation. The asymmetry between the flood and ebb tides poses a great challenge to numerical models, as the timing and magnitude of stratification and shear must be correctly simulated on an intra-tidal time scale in order to reproduce the asymmetry, and thus correctly predict the mass flux.

Data sampling and analysis

An integrated analysis of coastal observatory data and numerical model predictions are used to identify and quantify the physical processes responsible for the cross shelf transport of freshwater. A unique 5-year time series of state variables was collected by the POL coastal observatory at the two main mooring sites and a CTD survey grid (Figure 1). This time series includes mooring data from ADCPs and CTDs and is used together with meteorological data from the Hilbre Island and Bidston weather stations, freshwater outflow from the Dee, Mersey and Ribble estuaries, and predictions from the POLCOMS 3D numerical model.

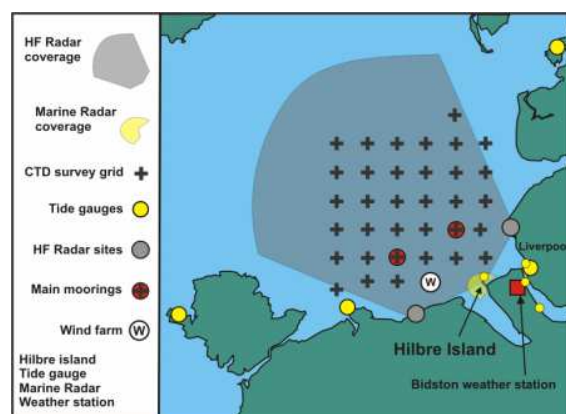


Figure 1. Coastal Observatory in Liverpool Bay.

The horizontal density gradient ($\delta\rho/\delta x$) was estimated using the tidal excursion method, and used to calculate the horizontal Richardson number (1), where g is the gravitational acceleration, h is the mean depth of the water column, and u_T is the tidal amplitude. A version of the horizontal Richardson number (Ri) was used by Simpson et al. (1990) to determine the conditions for the maintenance of stratification (2.06×10^{-3}) and SIPS

(1.96×10^{-4}). This was useful for determining whether Ri predicted periods of stratification, mixing and SIPS accurately when compared to the calculated stratification parameter (Φ).

$$Ri = \frac{g}{\rho} \frac{\delta\rho}{\delta x} \left(\frac{h}{u_T} \right)^2 \quad (1)$$

Time series data

As an example, a one month subset of the 5-year time series is presented below (Figure 2). The stratification parameter (Φ), calculated using ρ_{surface} and ρ_{bed} (Figure 2e), revealed periods of stratification (Figure 2f: 1–5 March and 24–29 March), vertical mixing (Figure 2f: 19–24 March) and SIPS (Figure 2f: 8–14 March). The horizontal density gradient ($\delta\rho/\delta x$) fluctuated most significantly during SIPS periods (Figure 2g) and had an long-term mean of $5.9 \times 10^{-5} \text{ m}^{-1}$. For most of the time series the Ri model predicted the state of the water column accurately (Figure 2h). There were discrepancies (e.g., 19–24 March), when the Ri predicted SIPS but the water column was closer to a vertically mixed state, likely due to the increased wind power during this time (Figure 2a). This highlights the complexity of the system and the absence of additional physics, such as wind, in the Ri model.

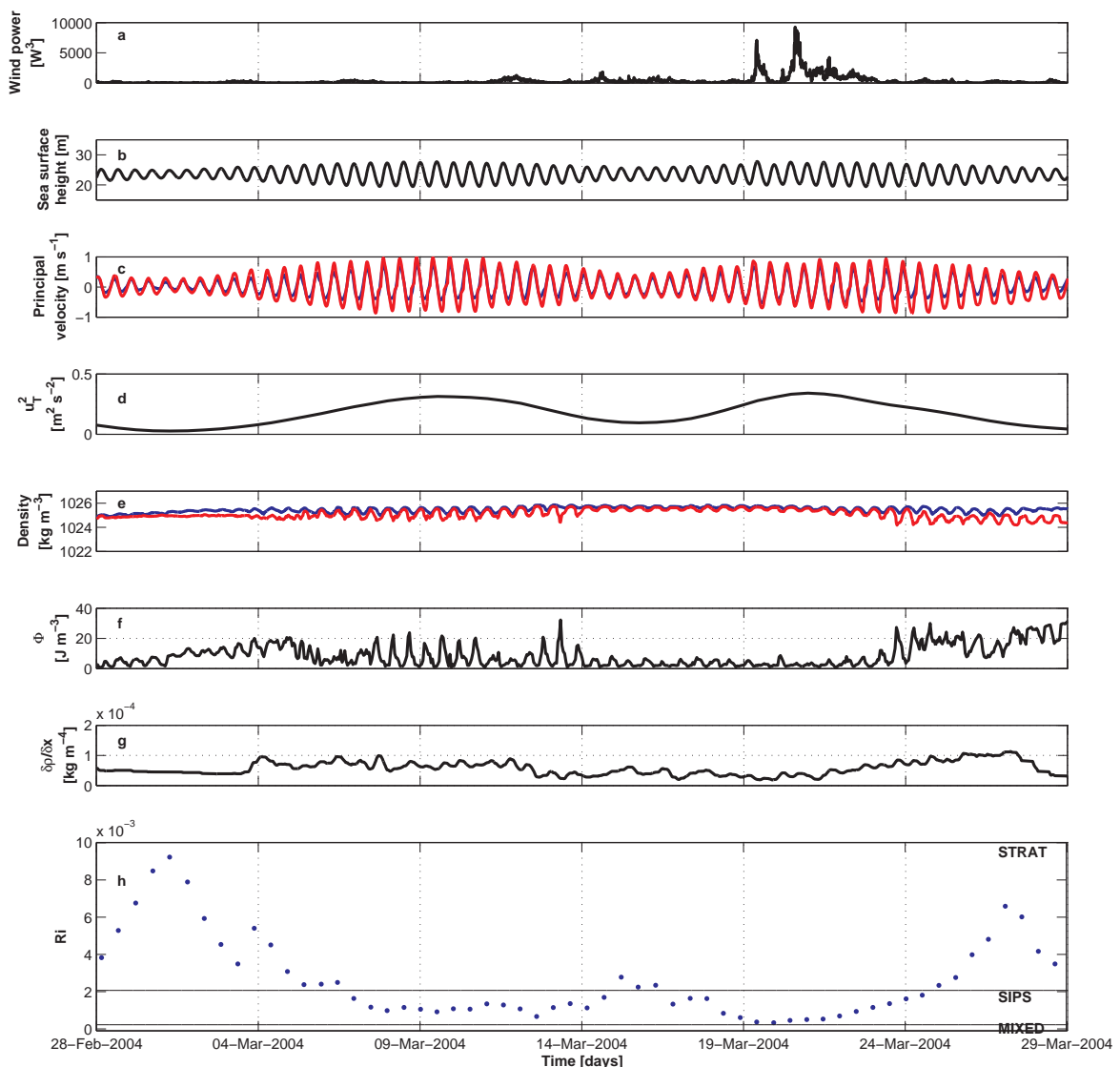


Figure 2. One month time series from Coastal Observatory mooring A. Red lines are from surface, blue lines are from near bed. (a) Wind power (W^3) from Bidston weather station, (b) Sea surface height (m), (c) Principal current velocity (m^{-1}), (d) Tidal amplitude ($\text{m}^2 \text{s}^{-2}$), (e) Density (kg m^{-3}), (f) Φ (J m^{-3}), (g) $\delta\rho/\delta x$ (kg m^{-4}), and (h) Ri with critical values for the maintenance of SIPS and stratification.

Residual velocities

The observed mean residual velocity profile was calculated from two years of ADCP data collected at the COBS mooring A. The results of this were compared to the Heaps (1972) solution (Figure 3). The horizontal density gradient is used to calculate the Heaps (1972) solution, and the resulting residual velocity profile was highly sensitive to this variable. When the observed horizontal density gradient ($5.9 \times 10^{-5} \text{ m}^{-1}$), calculated through the tidal excursion method, was used to obtain the profile the residual velocities were severely underestimated. Variation of the horizontal density gradient through a range of values resulted in a best-fit $\delta\rho/\delta x$ of $2 \times 10^{-4} \text{ m}^{-1}$ that approximated the measured residual profile more closely.

It is suggested that the discrepancy between the residual profiles obtained using Heaps' (1972) model and those calculated from the measured ADCP current time series arises due to the tidal mixing asymmetry resulting from tidal straining.

Conclusions

These preliminary results suggest the importance of the influence of tidal straining on the horizontal density gradient in determining the magnitude and timing of the horizontal mass flux. Continuing work will investigate the relationship between the horizontal density gradient and the horizontal mass flux through understanding of the asymmetric cycle of vertical mixing. The results of this will be used to test the predictive capacity of the POLCOMS 3D numerical model, identifying potential areas of improvement.

References

- Heaps, N.S. (1972), Estimation of density currents in the Liverpool Bay Area of the Irish Sea, *Geophysical Journal of the Royal Astronomical Society*, 30, 415–432.
- Prandle, D. (2004), Saline intrusion in partially-mixed estuaries, *Estuarine, Coastal and Shelf Science*, 59, 1597–1630.
- Rahmstorf, S. (1995), Bifurcations of the Atlantic thermohaline circulation in response to changes in the hydrological cycle, *Nature*, 378, 145–149.
- Simpson, J.H., Brown, J., Matthews, J., Allen, G. (1990), Tidal straining, density currents, and stirring in the control of estuarine stratification, *Estuaries*, 13, 125–132.
- Simpson, J.H., Sharples, J., Rippeth, T.P. (1991), A prescriptive model of stratification induced by freshwater runoff, *Estuarine, Coastal and Shelf Science*, 33, 23–35.
- Tett, P.B., Joint, I.R., Purdie, D.A., Baars, M., Oosterhuis, S., Daneri, G., Hannah, F., Mills, D.K., Plummer, D., Pomroy, A.J., Walne, A.W., Witte, H.J. (1993), Biological consequences of tidal stirring gradients in the North Sea, *Philosophical Transactions of the Royal Society of London A343*, 494–508.

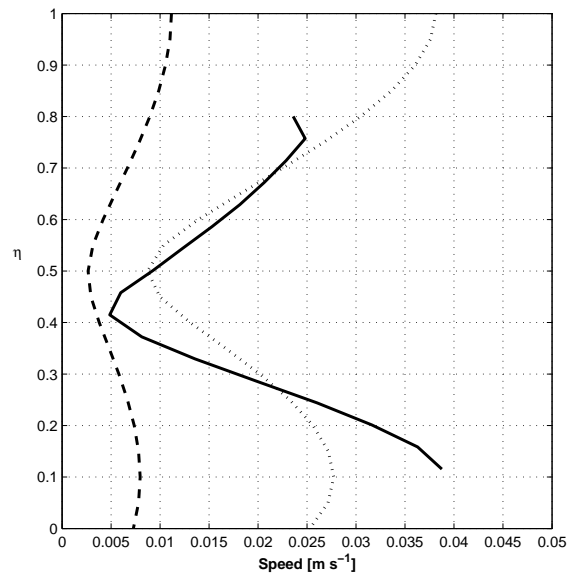


Figure 3. Residual velocity profile. η is a non-dimensional function of the height above sea bed. Solid line is observed mean residual profile from ADCP data, dashed line is Heaps' (1972) solution using observed $\delta\rho/\delta x$ ($5.9 \times 10^{-5} \text{ m}^{-1}$), and dotted line is best-fit Heaps' (1972) solution, using $\delta\rho/\delta x$ of $2 \times 10^{-4} \text{ m}^{-1}$.

Surface currents and bottom dissolved oxygen in Long Island Sound

JAMES O'DONNELL, ADAM HOUK, FRANK BOHLEN

Department of Marine Sciences, University of Connecticut, 1080 Shennecossett Road,
Groton CT 06340-6048, USA

email: james.odonnell@uconn.edu, adam@servo.dms.uconn.edu, bohlen@uconn.edu

Keywords: currents, dissolved oxygen; Long Island Sound

ABSTRACT

Western Long Island Sound is connected to the New York Harbor and the Hudson River through the East River, a tidal canal. Though the time mean, cross-sectional average flow is thought to be westward into the Harbor, there is near-surface layer which transports fresh water into the Sound. This has a buoyancy flux has a significant influence on the vertical stratification. The structure and variability of the shallow near surface motion has not been resolved with moored current meters. We report the results of simultaneous observation of the vertical structure of the hydrography using a moored array of CTDs and dissolved oxygen sensors, and the circulation using both bottom mounted ADCPs and HF-Radar systems. We find that the magnitude of the long term mean flow is consistent with previous inferences but that there substantial variation associated with the direction of the wind. Correlation of the axial wind component, the magnitude of the surface current and the rate of change of bottom dissolved oxygen concentration suggest that the modulation by wind of the rate of generation of the vertical stratification has a major influence on the vertical flux of oxygen to the hypoxic zone of Long Island Sound.

Impact of density gradients on net sediment transport into the Wadden Sea

HANS BURCHARD¹, GÖTZ FLÖSER², JOANNA V. STANEVA^{3,2},
THOMAS H. BADEWIEN⁴, ROLF RIETHMÜLLER²

1. Baltic Sea Research Institute Warnemünde, Seestraße 15,
18119 Rostock-Warnemünde, Germany
email: hans.burchard@io-warnemuende.de
2. Institute for Coastal Research, GKSS Research Centre, Max-Planck-Straße 1,
21502 Geesthacht, Germany
email: goetz.floeser@gkss.de , rolf.reithmueller@gkss.de
3. Institute for Chemistry and Biology of the Marine Environment,
Carl von Ossietzky University Oldenburg,
Carl-von-Ossietzky-Straße 9–11, 26111 Oldenburg, Germany
email: joanna.staneva@gkss.de
4. Institute of Physics, Carl von Ossietzky University Oldenburg,
Carl-von-Ossietzky-Straße 9–11, 26111 Oldenburg, Germany
email: thomas.badewien@uni-oldenburg.de

Keywords: horizontal density gradients, tides, SPM transport; Wadden Sea

ABSTRACT

In this presentation, the hypothesis is tested whether horizontal density gradients have the potential to significantly contribute to the accumulation of suspended particulate matter (SPM) in the Wadden Sea. It is shown by means of long-term observations at five different positions in the Wadden Sea of the German Bight that the water in the inner regions of the Wadden Sea is typically about $0.5\text{--}1.0\text{ kg m}^{-3}$ less dense than the North Sea water, see Figure 1. During winter this occurs mostly due to freshwater run-off and net precipitation, during summer mostly due to differential heating. It is demonstrated with idealized one-dimensional water column model simulations, using a constant in space and time horizontal salinity gradient (resulting in a high water to low water salinity difference of 2 g kg^{-1}), that the interaction of such small horizontal density gradients with tidal currents do generate net onshore SPM fluxes. Major mechanisms for this are tidal straining (Simpson et al., 1990; Jay and Musiak, 1994), estuarine circulation and tidal mixing asymmetries (Geyer 1993; for a comparative discussion of these mechanisms, see also Burchard and Baumert, 1998). The magnitude of these does strongly depend on the settling velocity, with particles settling too slowly resulting in almost vertically homogeneous distributions and thus small residual fluxes.

Three-dimensional model simulations with GETM (www.getm.eu, see Burchard and Bolding, 2002) in a semi-enclosed Wadden Sea embayment (see Figure 2 for the model bathymetry) with periodic tidal forcing have been carried out. Comparison of surface and bottom salinities in the deeper tidal channels shows that tidal asymmetries should compare in strength with the one-dimensional model simulations, see Figure 3. When the settling velocity is sufficiently high ($w_s = 10^{-3}\text{ m s}^{-1}$) SPM is accumulating in the Wadden Sea bight due to density gradients. This is proven through a comparative model simulation in which the dynamic effects of the density gradients are switched off, with the consequence of no SPM accumulation, see Figure 4.

These numerical model results motivate future targeted field studies in different Wadden Sea regions with the aim to further support the hypothesis. A full version of this paper has been published by the same authors (see Burchard et al., 2008).

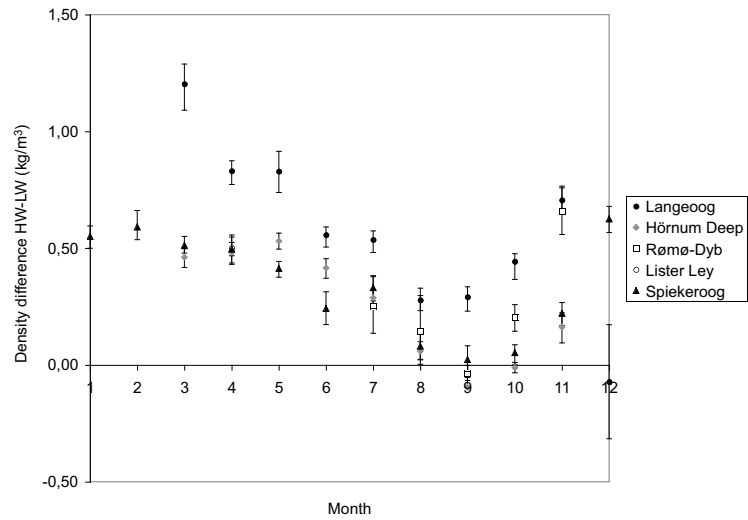


Figure 1. Monthly averaged density differences between high water and low for five pile positions in the Wadden Sea of the German Bight.

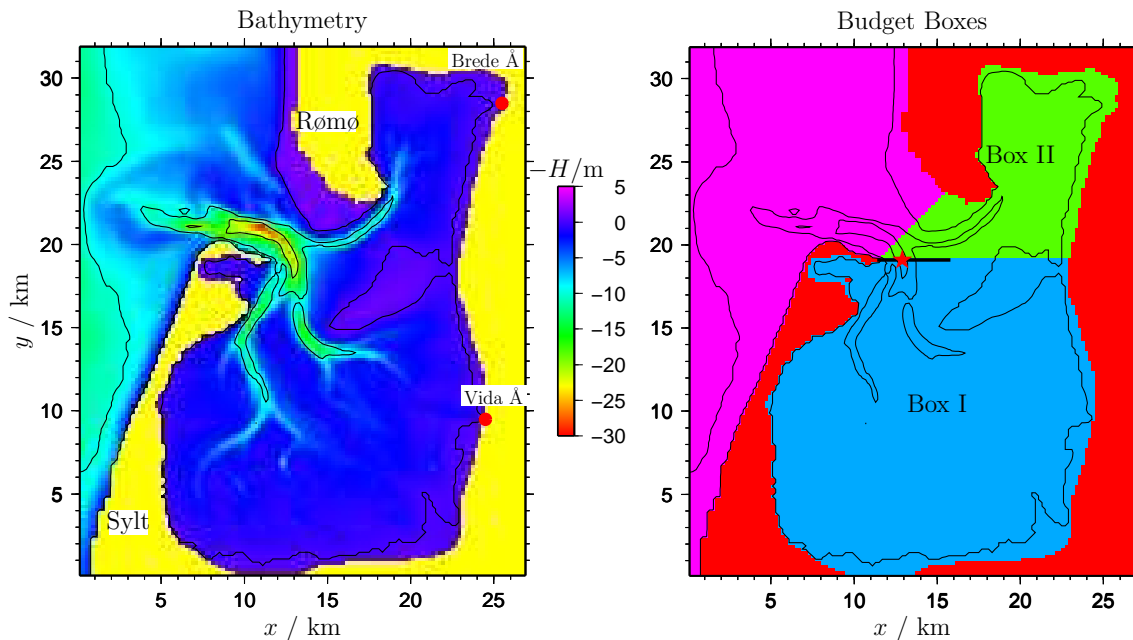


Figure 2. Left panel: Model topography, Sylt-Rømø Bight. Red dots show the locations for the Brede Å and the Vida Å river run-off. Right panel: Areas covered by the budget boxes I and II. The red star indicates the location of the salinity time series (position P, see Figure 3). In both panels, the 0 m, 10 m and 20 m isobaths are drawn.

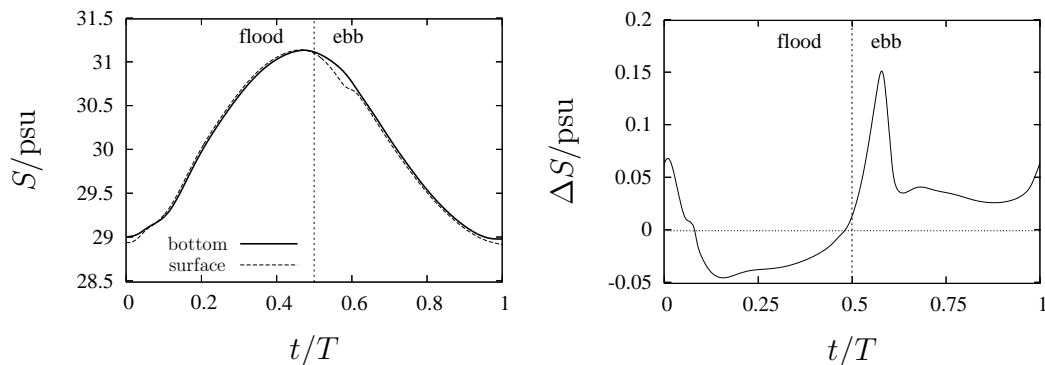


Figure 3. Time series of salinity at position P (see Figure 2) during the 55th tidal cycle, simulated with the three-dimensional model under consideration of density differences.

Left: Bottom and surface salinity; right: Bottom-surface salinity difference.

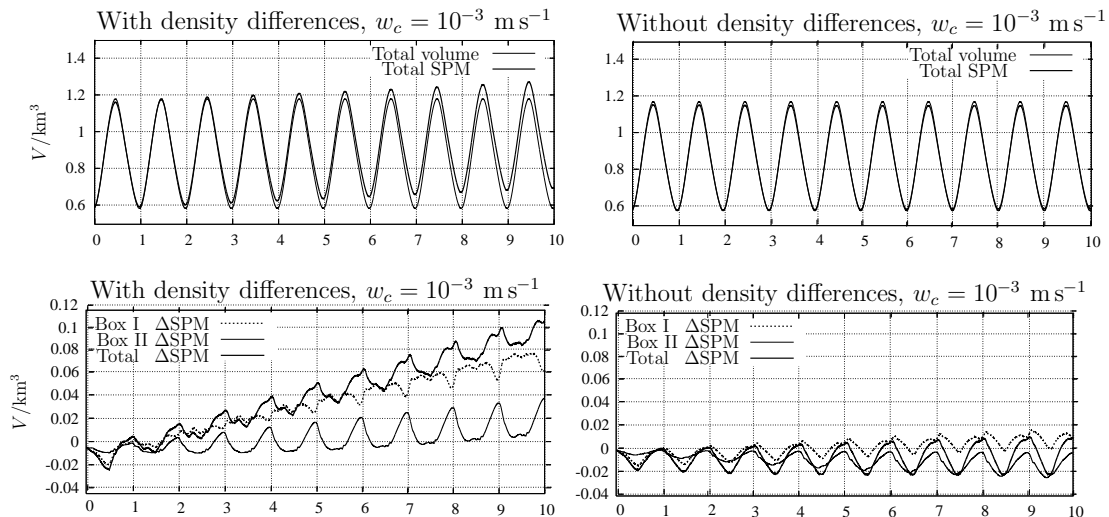


Figure 4. Time series of total water volume and SPM content integrated over budget boxes I and II for $w_c = 10^{-3} \text{ m s}^{-1}$ (upper panels) and SPM flux into budget boxes I and II and their sum for $w_c = 10^{-3} \text{ m s}^{-1}$ (lower panels) for the simulation with density differences (left panels) and without density differences (right panels). The simulations show the tidal periods 46–55, where the SPM concentration has been initialized to unity after tidal period 45.

References

- Burchard, H., Baumert, H. (1998), The formation of estuarine turbidity maxima due to density effects in the salt wedge. A hydrodynamic process study, *Journal of Physical Oceanography*, 28, 309–321.
- Burchard, H., Bolding, K. (2002), *GETM – a general estuarine transport model*. Scientific documentation, Tech. Rep. EUR 20253 EN, European Commission.
- Burchard, H., Flöser, G., Staneva, J.V., Riethmüller, R., Badewien, T. (2008), Impact of density gradients on net sediment transport into the Wadden Sea, *Journal of Physical Oceanography*, 38, 566–587.
- Geyer, W.R., The importance of suppression of turbulence by stratification on the estuarine turbidity maximum, *Estuaries*, 16, 113–125.
- Jay, D.A., Musiak, J.D. (1994), Particle trapping in estuarine tidal flows, *Journal of Geophysical Research*, 99, 445–461.
- Simpson, J.H., Brown, J., Matthews, J., Allen, G. (1990), Tidal straining, density currents, and stirring in the control of estuarine stratification, *Estuaries*, 26, 1579–1590.

A dynamic equation for the potential energy anomaly for analyzing mixing and stratification in estuaries and coastal seas

RICHARD HOFMEISTER, HANS BURCHARD

Baltic Sea Research Institute Warnemünde, Seestraße 15,
18119 Rostock-Warnemünde, Germany
email: richard.hofmeister@io-warnemuende.de, hans.burchard@io-warnemuende.de

Keywords: potential energy anomaly, stratification, mixing, differential advection

ABSTRACT

We present a time-dependent dynamic equation for the potential energy anomaly (PEA), which has been defined by Simpson (1981):

$$\phi = \frac{1}{D} \int_{-H}^{\eta} gz(\bar{\rho} - \rho) dz = -\frac{1}{D} \int_{-H}^{\eta} gz\tilde{\rho} dz \quad (1)$$

with the sea surface elevation η , the mean water depth H , the actual water depth $D = H + \eta$, the gravitational acceleration g , the density ρ and the depth-mean density

$$\bar{\rho} = \frac{1}{D} \int_{-H}^{\eta} \rho dz \quad (2)$$

The time-dependent dynamic equation is rigorously derived from dynamic equations for potential temperature and salinity, the continuity equation and the equation of state for sea water. The terms locally changing PEA are each related to a physical process: (A) the PEA advection, (B) the depth-mean straining, (C) the non-mean straining, (D) the vertical advection, (E) the vertical mixing, (F) surface and bottom density fluxes, (G) inner sources of density, e.g., due to absorption of solar radiation and the nonlinearity of the equation of state and (H) horizontal divergence of horizontal turbulent density fluxes. The evaluation of the terms in the PEA equation is then carried out for three different model setups:

1. A one-dimensional tidal straining study, with idealized sinusoidal forcing of the mean current and a prescribed constant horizontal density gradient. Comparison to empirical estimates for some terms in the PEA equation are made for the one-dimensional study.
2. A two-dimensional estuarine circulation study (see Figure 1 for an overview over the setup) which shows contributions of all the kinematic terms and very different regimes, depending on the location in the estuary.
3. The application of the dynamic equation in a realistic, three-dimensional hindcast study in the Limfjord, Denmark (Figure 2 shows the location and the bathymetry of the estuary). Changes in stratification in the realistic regime cannot be clearly related to one or two major processes but are a result of several different contributions in the dynamic equation of PEA.

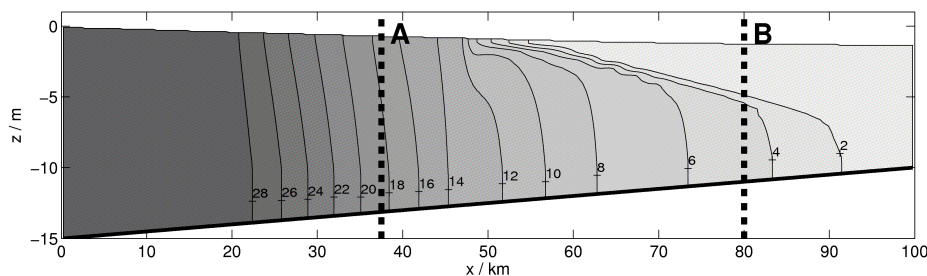


Figure 1. The salinity distribution in the idealized estuary. The dynamic equation of the PEA is evaluated at locations A and B. The contour lines show salinities in g kg^{-1} .

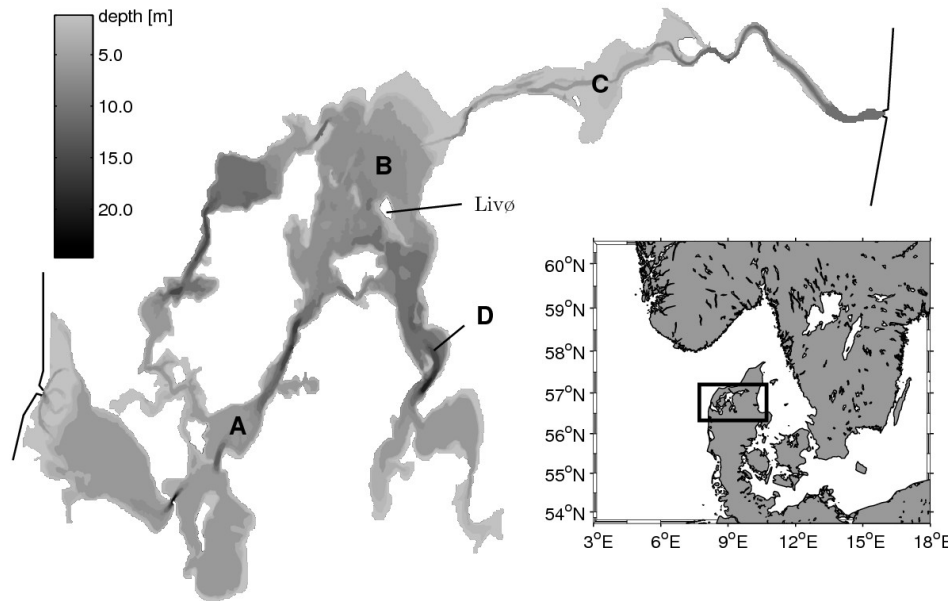


Figure 2. Bathymetry and location of the Limfjord, Denmark. There is a mean salinity difference between western and eastern opening of about 10 g kg^{-1} . The terms of the dynamic equation of the PEA are evaluated at location B.

The PEA equation provides a general reference for empirical bulk parameterizations of stratification and mixing processes in estuaries and coastal seas and it is a tool for complete analysis of the relevant physical processes from high-resolution field measurements and numerical models.

References

- Burchard H., Hofmeister, R. (2008), A dynamic equation for the potential energy anomaly for analyzing stratification and mixing in estuaries and coastal seas, *Estuarine, Coastal and Shelf Science*, 77, 679–687.
- Simpson, J.H. (1981), The shelf-sea fronts: implications of their existence and behaviour, *Philosophical Transactions of the Royal Society of London, Series A*, 302, 531–546

Instabilities and thermohaline stratification at a tidal mixing front: A case study for the German Bight

JOANNA V. STANEVA

Institute for Coastal Research, GKSS Research Centre, Max-Planck-Straße 1,
21502 Geesthacht, Germany
email: joanna.staneva@gkss.de

Keywords: stratification, fronts, tidal mixing; German Bight

ABSTRACT

In this study we present the results from a nested-grid three-dimensional numerical model for the German Bight and the North Sea. The annual cycle and spatial variability of the vertical stratification and mixing is simulated using the General Estuarine Transport Model (GETM). Atmospheric forcing and tides play an essential part for the synoptic and neap-spring variations of sea surface temperature, stratification and tidal fronts. The processes that influence the mesoscale variability of the thermal stratification have been evaluated by means of model circulation. The response of model circulation and vertical stratification to the surface forcing is studied as well. The development of thermohaline stratification due to baroclinic instability is evaluated. The model results are further compared with data from observations. We demonstrate some of the model capabilities for a more realistic simulation of the frontal circulation of the shelf sea areas.

Shelf and slope processes offshore Fremantle, Western Australia

CHARITHA B. PATTIARATCHI

School of Environmental Systems Engineering, University of Western Australia,
MO15, 35 Stirling Highway, Crawley 6009, Western Australia, Australia
email: chari.pattiaratchi@uwa.edu.au

Keywords: observation system, shelf and slope processes

ABSTRACT

The continental shelf and slope region off Fremantle, Western Australia, is unique compared with other continental shelves. The anomalous Leeuwin current dominates the circulation at the shelf edge and offshore, and transports warm, nutrient-poor water poleward. On the continental shelf, the wind forces the circulation, with coastally trapped waves also contributing. The presence of offshore islands and a submarine canyon make the system more complex. Thus an ocean observation system to monitor this unique physical/biological oceanographic system would provide exciting opportunities for undertaking process studies. This observation system includes HF radar systems, autonomous ocean gliders and moored instruments.

In this presentation, integrated data from these systems will be used to examine the upwelling/downwelling processes in the presence of topography. The Leeuwin current creates a downwelling environment along the shelf break; however, the topography (Perth submarine canyon and Rottnest Island) and strong summer winds cause localized upwelling. In autumn and winter, higher density inner shelf waters, resulting from high evaporation during the summer and then cooling exit the shelf as higher density bottom plumes. A major feature revealed in the ocean glider data, and visible in satellite images, was the presence of vertically mixed water at the shelf edge, which increased the primary production. Thus the observation system ('pre-operational system') provides a great opportunity to gain a deeper understanding of the physical processes and their relationship to biological processes.

Observations of bottom stress in combined waves and currents

JUDITH WOLF, ALEJANDRO J. SOUZA, KYLE F.E. BETTERIDGE, RODOLFO BOLAÑOS SANCHEZ

Proudman Oceanographic Laboratory, 6 Brownlow Street, Liverpool L3 5DA UK
email: jaw@pol.ac.uk, ajso@pol.ac.uk, kefb@pol.ac.uk, rbol@pol.ac.uk

Keywords: currents, waves, bottom friction

ABSTRACT

Observations of currents, waves and sediment transport were made during the LEACOAST2 experiment. The objective is to understand the sediment transport in this energetic environment in combined waves and currents. For this it is necessary to calculate the bed shear stress. The use of observed data for Reynolds' stress calculations is problematical for combined waves and currents. Direct Reynolds' stress calculations in combined waves and currents are contaminated by waves even though the instrument should be outside the wave boundary layer (although within the tidal current boundary layer) even when the observations are corrected for tilt. In theory there should be no contribution from the irrotational wave motion in the covariance method of obtaining the bottom stress but in practice a very small error in tilt can produce an error contribution from the wave motion which can overwhelm the turbulent contribution. It is not straightforward to remove the effect of waves, since waves and turbulence co-exist at wave frequencies. Various methods for separation of waves and turbulence are examined.

Introduction

One method to remove the wave component is to remove the part of the near-bed current fluctuations correlated with bottom pressure in the frequency band 0.05–0.5 Hz (Wolf, 1999). The remainder of the signal is then identified as turbulence and the Reynolds' stress is then computed from this component. This method is compared with alternative methods of computing the bottom stress from the inertial dissipation method and the available empirical formulations. Other methods are discussed in Bricker and Monismith (2007), Feddersen and Williams (2007), Trowbridge (1998) and Shaw and Trowbridge (2001).

There is some evidence that wave-induced turbulence may in fact persist throughout the water column, e.g., Babanin (2005). There has been a persistent tendency for the observed drag coefficient to be about a factor of two less than that typically required in numerical circulation models which suggests that the processes of nearbed turbulence and bottom stress are not fully accounted for (Wolf, 1999). The wave boundary layer thickness variation in the direction of wave propagation results in an additional steady velocity known as wave streaming, which determines the direction of the net sediment transport. The effect of wave streaming just outside the wave boundary layer is taken into account in Nielsen and Callaghan (2003) and Myrhaug and Holmedal (2005). The importance of these processes is discussed.

Data

During the LEACOAST2 experiment data were collected from three instrumented tripods deployed near the shore parallel breakwaters at Sea Palling on the Norfolk coast (F1, F2, F3, see Figure 1), during two experiments: Experiment 1 (March–May 2006), Experiment 2.1 (October–December 2006) and 2.2 (December 2006–January 2007). The instrumentation included acoustic and optical instrumentation (ADCP, ADV, LISST and bedform scanners). One tripod (F2) was deployed in the intertidal zone. The others were deployed in water depths of 6–8 m. The tidal range is about 2 m with tidal currents reaching 0.7 m s^{-1} . The ADV data provides 3-axis high frequency observations of currents at a single point, near the bed. On F1 there were three instruments at three heights above the bed but only one with a pressure sensor and none with tilt sensors. F2 and F3 had combined pressure and tilt sensors. Detailed quality control including despiking was carried out. Vertical velocities are still prone to contamination by the wave component of current. The data from F3 for Experiment 2.1 was examined in some detail as this period included neap tides and spring tides with low wave heights and a large storm event at the beginning of November 2006 (Figure 2).

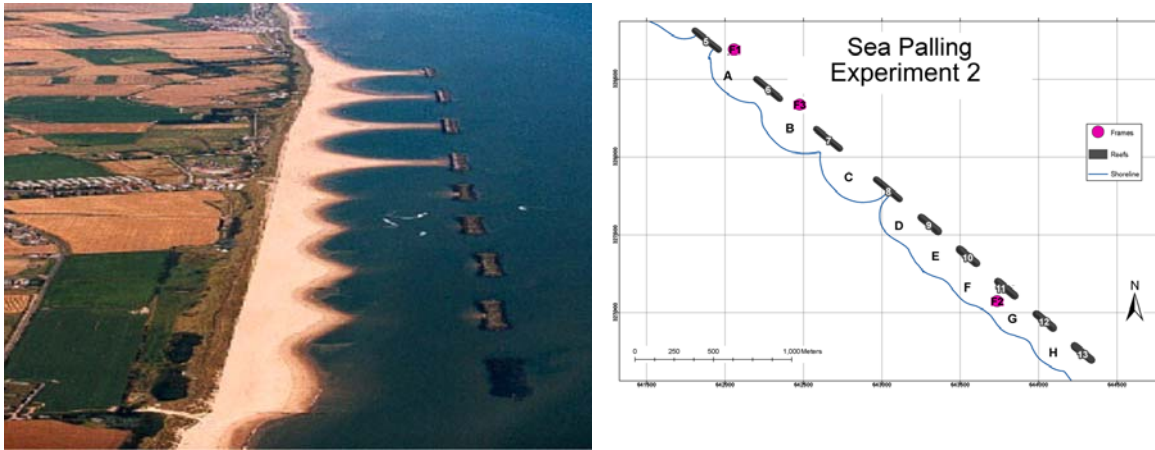


Figure 1. Shore parallel breakwaters and Experiment 2 locations of in situ tripods (purple circles)

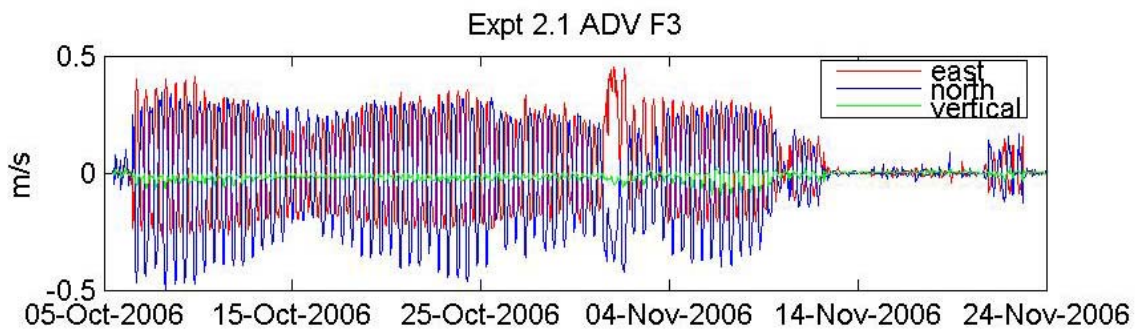


Figure 2. ADV time series for Experiment 2.1 at F3.

Bed shear stress

A first estimate of the bed stress has been made using the method of Soulsby and Clarke (2005), using observed wave height and period and depth-averaged current speed and direction from ADCP at F1 (Figure 3). This is compared with the critical shear stresses for bedload and suspended load using the median grain size of $300 \mu\text{m}$. The critical bed shear stress for various grain sizes from $200 \mu\text{m}$ (fine sand) to $400 \mu\text{m}$ (medium sand) is obtained from Soulsby (1997). A typical value for $300 \mu\text{m}$ is 0.2 Pa , there is little change over this size range, with a slight increase with increasing grain size. For suspended sediment we need friction velocity, $u^* > w_s$. For $300 \mu\text{m}$, this gives a critical stress of 1.5 Pa . These thresholds have been indicated by dashed lines in Figure 3.

The mean stress is close to the current-only stress while the maximum stress is close to the wave-only stress. In low wave conditions the current stress is mainly tidal. A tidal asymmetry can be seen with the flood tide (to SE) having higher stress although the stress exceeds the estimated critical stress for sand transport on both flood and ebb. The combined wave and current stress is larger than the sum of the current and wave stress as also observed by Souza et al. (2001).

Wave and turbulence separation

Further tests of the different methods will be carried out and the results presented in the oral presentation.

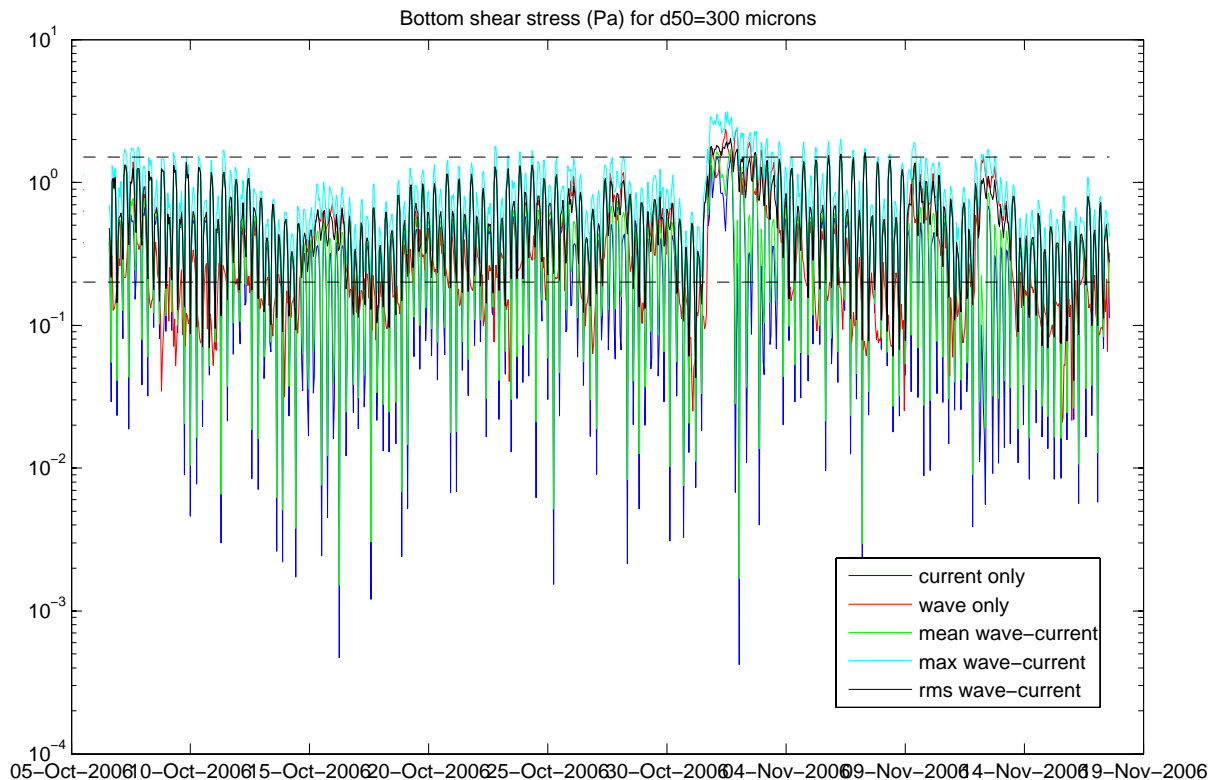


Figure 3: Bottom shear stress from Soulsby and Clarke (2005) for wave and current only and combined wave-current conditions

Summary

The flow in this area is influenced strongly by both tidal currents and waves and the bed is quite mobile, thus it is complex to understand and separate the different processes. It is expected that the critical stress may increase with increasing fraction of silt (Dong, 2007). A first look at the combined wave and current bed stress shows the bedload is mobile under most tidal conditions whereas the suspended load is mobilized in storm waves. The net transport is to the south.

References

- Babanin, A.V. (2006), On a wave-induced turbulence and a wave-mixed upper ocean layer, *Geophysical Research Letters*, 33, L20605, doi:10.1029/2006GL027308.
- Bricker, J.D., Monismith, S.G. (2007), Spectral wave-turbulence decomposition, *Journal of Atmospheric and Oceanic Technology*, 24, 1479–1487.
- Dong, P. (2007), A two-fraction formulation of critical shear stresses for sand and silt mixtures, *Journal of Coastal, Port, Harbour and Waterway Engineering*, 133, 238–241.
- Feddersen, F., Williams, A.J. (2007), Direct estimation of the Reynolds' stress vertical structure in the nearshore, *Journal of Atmospheric and Oceanic Technology*, 24, 102–116.
- Nielsen, P., Callaghan, D.P. (2003), Shear stress and sediment transport calculations for sheet flow under waves, *Coastal Engineering*, 47, 347–354.
- Myrhaug, D., Holmedal, L.E. (2005), Bottom friction caused by boundary layer streaming beneath random waves for laminar and smooth turbulent flow, *Ocean Engineering*, 32, 195–222.
- Shaw, W.J., Trowbridge, J.H. (2001), The direct estimation of near-bottom turbulent fluxes in the presence of energetic wave motions, *Journal of Atmospheric and Oceanic Technology*, 18, 1540–1556.
- Soulsby, R. (1997), *Dynamics of marine sands*, Thomas Telford, London.
- Soulsby, R.L., Clarke, S. (2005), *Bed shear-stresses under combined waves and currents on smooth and rough beds*. Hydraulics Research Report TR 137.
- Souza, A.J., Dickey, T.D., Chang, G.C. (2001), Modelling water column structure and suspended particulate matter in the Middle Atlantic continental shelf during the passage of Hurricanes Edouard and Hortense, *Journal of Marine Research*, 59(6), 1021–1045.

- Trowbridge, J.H. (1998), On a technique for measurement of turbulent shear stress in the presence of surface waves, *Journal of Atmospheric and Oceanic Technology*, 15, 290–298.
- Wolf, J. (1999), The estimation of shear stresses from near-bed turbulent velocities for combined wave-current flows, *Coastal Engineering*, 37(3–4), 529–543.
- Wolf, J., Osuna, P., Howarth, M.J., Souza, A.J. (2007), *Modelling and measuring waves in coastal waters*. In: Proceedings of International Conference on Coastal Engineering 2006, San Diego. American Society of Civil Engineers (ASCE). Vol. 1, 539–551.

Boils and turbulence in a weakly stratified shallow tidal sea

STEVE A. THORPE¹, J.A. MATTIAS GREEN¹, JOHN H. SIMPSON¹,
THOMAS R. OSBORN², W. ALEX M. NIMMO SMITH³

1. School of Ocean Sciences, College of Natural Science, Bangor University, Menai Bridge, Anglesey LL59 5AB UK
email: s.a.thorpe@bangor.ac.uk, m.green@bangor.ac.uk, j.h.simpson@bangor.ac.uk
2. Department of Earth and Planetary Science, Johns Hopkins University, 301 Olin Hall, 3400 N. Charles Street, Baltimore MD 21218-2608, USA
email: osborn@jhu.edu
3. School of Earth, Ocean and Environmental Sciences, University of Plymouth, Drake Circus, Plymouth PL4 8AA UK
email: alex.nimmo.smith@plymouth.ac.uk

Keywords: ocean turbulence, boils, tides; Irish Sea

ABSTRACT

Measurements of turbulence are made in a weakly, but variably, stratified region of tidal straining in the eastern Irish Sea using turbulence sensors profiling vertically through the water column on FLY and profiling horizontally on the AUV Autosub III. Boils on the sea surface are identified using the Autonomously Recording Inverted Echo Sounder (Mark 2), ARIES II, a two-beam upward-pointing sidescan sonar mounted on a rig resting on the seabed. The boils have mean horizontal dimensions of about 25 m and are continually present when turbulence within the water column near the surface is large, typically when $\varepsilon > 3 \times 10^{-6} \text{ W kg}^{-1}$, compared to the rates of about $1 \times 10^{-7} \text{ W kg}^{-1}$ near times of slack tide when no boils are observed. The top of a region with a relatively high ε gradually extends upwards from the seabed as the tidal flow increases and can, in stably stratified conditions, be detected in the ARIES II sonographs as it approaches the sea surface. Upward-moving bursts of enhanced turbulence, with horizontal dimensions of about 5–9 m in the direction of the tidal flow, are identified below the surface during periods of high tidal flows. These bursts result in slight upward displacements of the AUV from its set operational depth. Boils first appear at times before the region of generally enhanced turbulence reaches the surface: large localized upward-moving bursts appear to precede the main advancing region of small-scale turbulence.

Introduction

Sea-surface boils have been reported to occur in well-mixed water in the southern North Sea where the water depth is 45 m and the tidal flow is $\sim 1 \text{ m s}^{-1}$ (Nimmo Smith et al., 1999), although no accompanying measurements have been made of the rate of turbulent dissipation. The physical processes involved in the formation of surface boils in shallow, well-mixed, shelf seas remain uncertain, but they are thought to be associated with hairpin vortices (Theodorsen, 1952) and with bursts or ejections carrying a flux of momentum and small-scale turbulent motion upwards from the turbulent boundary layer adjoining the seabed. After moving upwards through the water column, these impinge on the water surface to produce the structures described as boils. An enhanced sediment concentration is observed in boils and on the surface (Nimmo Smith et al., 1999), providing evidence of a transport mechanism from the seabed to the surface. The aim of the present paper is to describe the physical properties of these rising bursts within the water column using an array of different sensors (for details see Thorpe et al., 2008).

Instruments and observations

The Autonomously Recording Inverted Echo Sounder, ARIES II (see Thorpe et al., 1998), was placed on the sea bed in the eastern Irish Sea (northeast of the Isle of Anglesey) in $\sim 43 \text{ m}$ water depth on 12 July 2006, and

was recovered after a continuous recording period of three days. The estuaries of the rivers Mersey and Dee were about 70 km to the east of the deployment site.

A series of repeated casts with the FLY-profiler was made about 1.8 km north of the ARIES II position for 25 hrs from midday on 13 July. Estimates are made of ε , the rate of loss of turbulent kinetic energy per unit mass, using the methods described by Simpson et al. (1996), between a depth of about 5 m and a height of 0.15 m from the seabed. Current data were obtained from a bottom mounted 600 kHz RDI ADCP sampling every second at a site about 0.4 km west of ARIES II. Vertical profiles of stratification were obtained from CTD casts made every 4 hrs during the FLY series.

The 7 m long AUV Autosub (Millard et al., 1998) was deployed at on 13 July and set to run 5 km legs at a constant height of 6 m above the seabed or at constant depths, across and along the tidal flows in a square around the ARIES II position. The AUV was unable to make progress over the bed when opposed by the tidal flows exceeding 1 m s^{-1} ; in consequence we only analyzed six hours of data from the 50-hour mission. The AUV carried a CTD, two ADCPs, and a turbulence package with two air-foil sensors and a fast-response thermistor. The CTD, ADCP, and the sub's internal navigation logged data every second, whereas the turbulence package sampled at a rate of 512 Hz (see Thorpe et al., 2003).

The tidal flow at the site was not symmetrical, with ebb currents weaker than those in floods. For much of the time the vertical density gradient was constant, but following the westward flow of the ebb tide the upper 20 m of the water column was $\sim 0.6^\circ\text{C}$ warmer than the water at depth. Stratification was reduced in periods of increased turbulence of the eastward-going flood tide and no subsequent stratification was re-established at the end of the flood flow. This is consistent with the effects of tidal straining of the horizontally varying density field (e.g., Rippeth et al., 2001). The shear in the westward-going ebb tide tilts isotherms, carrying the warmer and less saline water in the east over the cooler, more saline, offshore water. As the flood tide subsequently carries the stratified water eastwards, the vertical stratification is affected by turbulence at the seabed and by the effect of vertical shear acting on the horizontal density gradients.

The dissipation measurements show a high dissipation during periods of strong tidal flow (Figure 1), and the phase delay of the onset of high dissipation with distance from the seabed is clearly identified in the data (Simpson et al., 2000; see also Thorpe et al., 2008). Further, vertical displacements of the AUV of a meter or more occur during the periods of high dissipation. The observed rms variations in depth are typically 0.8 m with a negative skewness of about -1.0 , suggesting an advective effect of turbulence with relatively large *upward* motions and with a horizontal scale comparable to or greater than the AUV length (7 m).

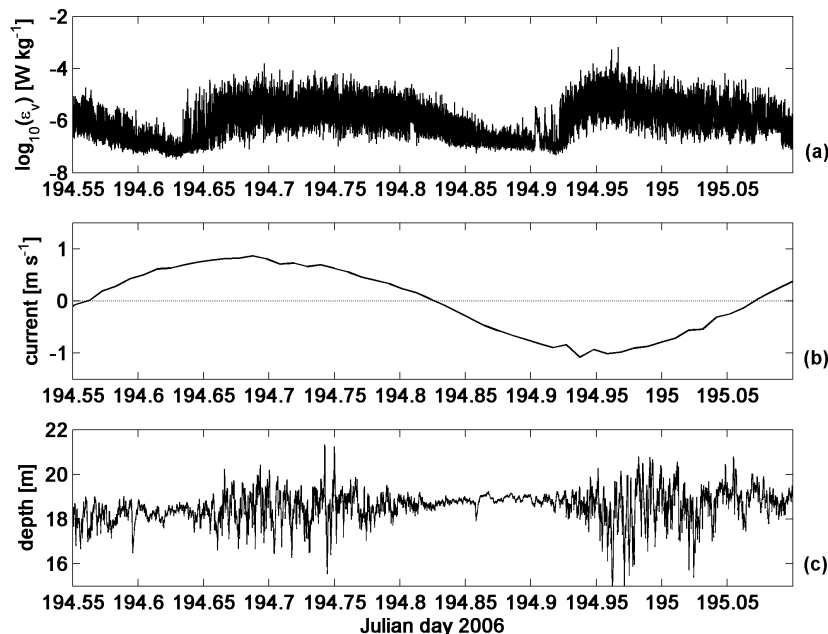


Figure 1. Turbulence measured by the AUV over a tidal cycle at a depth of about 18 m. (a) $\log[\varepsilon \text{ (W kg}^{-1}\text{)}]$; (b) east/west current velocity (direction 262°); (c) Autosub's depth of operation.

Conditional sampling

The Autosub data is ‘conditionally sampled’ by choosing a variable, say dT/dt (the conditional), and finding all the periods within a selected AUV leg in which the conditional exceeds some selected threshold value, e.g., the mean plus the standard deviation. The times, t , at the center of these periods are found. One second average values of similar or other recorded data, say of $\log \varepsilon$, lying to either side of these times (e.g., from $t - 15$ s to $t + 15$ s), are then averaged (according to the relative times at which they occur) to form a section of mean values of the data around the selected extreme values of the conditional variable (dT/dt). If the threshold of the conditional is not set too high, a substantial number of times are found. Averaging these together to form a single section allows coherent patterns or trends to be detected, even in the presence of turbulent fluctuations or wave-induced motions.

The mean width of regions of elevated $\log \varepsilon$ increases from 4.9 m at 6 mab to 9.0 m at a depth of 8.3 m (the latter section is shown in Figure 2). On average the AUV rises as, or shortly after, it passes through regions of enhanced ε , which is consistent with regions of large dissipation having vertical velocities transporting turbulent bursts upwards from the seabed. The temperature variation across the regions of relatively high dissipation is generally small, but the temperature minimum seen in Figure 2 is consistent with eddies carrying relatively cold water upwards. The distance between groups in which $\log \varepsilon$ exceeds two standard deviations is 43.4 m, whereas the distance is reduced to 19.9 m with a threshold of one standard deviation.

Sonographs

An example of a sonograph, obtained from ARIES II, is shown in Figure 3. The scattering layers are seen to rise at speeds of $\sim 1 \text{ cm s}^{-1}$, which are similar rates to the upward speeds of the spreading turbulence seen in the FLY data. The layers occur at times when the enhanced turbulence is approaching the surface and have a typical horizontal separation of about 4 m. A total of 870 clearly resolved surface boils were identified within 110 m from ARIES II in sonographs during periods of strong tidal flow. The mean along-tide dimension was 22.4 ± 9.8 m and the across-tide dimension was 25.4 ± 12.7 m (both dimensions equal to roughly half the water depth). The layers are thus larger than the upward moving bursts identified before ($L \sim 4.9\text{--}9$ m).

Discussion

The regions of enhanced dissipation have a horizontal scale of about 5–9 m and are consistent with blobs of turbulent water moving upwards at speeds sufficient to displace Autosub from its track. Their source is provisionally identified with the bursts, ejections and hairpin vortices known to occur in the bottom boundary

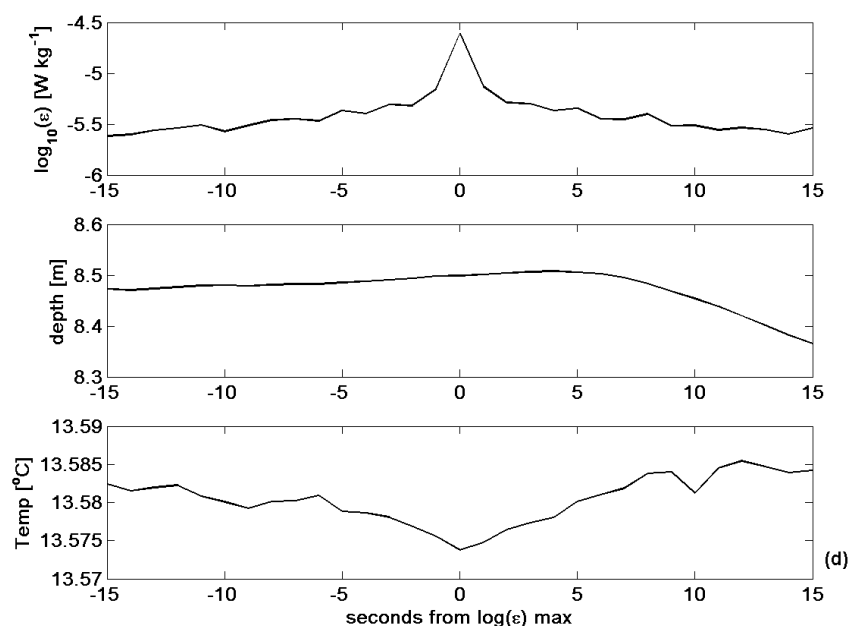


Figure 2. Conditional sampling plots (data from 8.3 m depth) for $\log \varepsilon > \mu(\log \varepsilon) + 1.5\sigma(\log \varepsilon)$. The sections shown are (a) $\log[\varepsilon \text{ (W kg}^{-1}\text{)}]$, (b) AUV depth, and (c) temperature. The number of samples was 138.

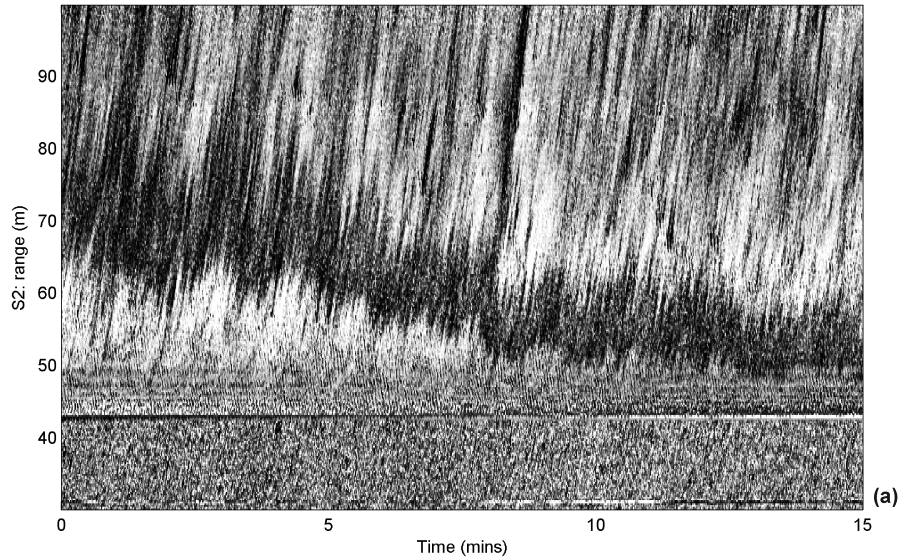


Figure 3. Sonograph showing the scattering in the along-tide beam from the rising region of enhanced turbulence during a period of increasing flood tide (the sea-surface is the line at 43 m). The scattering layer first appears at a range of between 70 and 80 m, falling to 50–60 m at the end of the sonograph. The boils are best seen by viewing the sonograph from below at a small angle to the plane of the figure, when their outlines appear as ghost-like crescent shaped regions of enhanced acoustic scatter.

layer. At the surface these features ‘spludge’, resulting in divergent motions which spread the bursts and their contents horizontally to form the 20 m scale features identified as boils. As suggested by Simpson et al. (2000), turbulence spreads upwards as it is generated at continually higher levels by an increase in the turbulent production term. The additional process described here is the upwards transport of small-scale turbulence from near the seabed by relatively large bursts or ejections. Where the upper levels are stratified, the upward moving bursts may have sufficient energy to pass through a weak thermocline to reach the surface, or it may be locally dissipated, contributing to the downward entrainment of water.

References

- Millard, N.W., Griffiths, G., Finnegan, G., McPhail, S.D., Meldrum, D.T., Peabody, M., Perrett, J.R., Stevenson, P., Webb, A.T. (1998), Versatile autonomous submersibles – the realization and testing of a practical vehicle, *Underwater Technology*, 23, 7–17.
- Nimmo Smith, W.A.M., Thorpe, S.A., Graham, A. (1999), Surface effects of bottom-generated turbulence in a shallow tidal sea, *Nature*, 400, 251–254.
- Rippeth, T.P., Fisher, N.P., Simpson, J.H. (2001), The cycle of turbulent dissipation in the presence of tidal straining, *Journal of Physical Oceanography*, 31, 2458–2471.
- Simpson, J.H., Crawford, W.R., Rippeth, T.P., Campbell, A.R., Choek, J.V.S (1996), The vertical structure of turbulent dissipation in shelf seas, *Journal of Physical Oceanography*, 26, 1580–1590.
- Simpson, J.H., Rippeth, T.P., Campbell, A.R. (2000), *The phase lag of turbulent dissipation in tidal flow*. In: Interactions between estuaries, coastal seas and shelf seas, Yanagi, T. (Ed.). Tokyo: Terr Scientific Pub. Co. (TERRAPUB), pp57–67.
- Theodorsen, T. (1952), *Mechanism of turbulence*. In: Proceedings of the Midwestern Conference on Fluid Mechanics. Columbus, Ohio, 2nd Edition, pp1–18.
- Thorpe, S.A., Ulloa, M.J., Baldwin, D., Hall, A.J. (1998), An Autonomously Recording Inverted Echo Sounder; ARIES II, *Journal of Atmospheric & Oceanic Technology*, 15, 1347–1361.
- Thorpe, S.A., Osborn, T., Jackson, J., Hall, A.J., Lueck, R.G. (2003), Measurements of turbulence in the upper ocean mixing layer using Autosub, *Journal of Physical Oceanography*, 33, 122–145.
- Thorpe, S.A., Green, J.A.M., Simpson, J.H., Osborn, T.R., Nimmo Smith, W.A.M. (2008), Boils and turbulence in a weakly stratified shallow tidal sea. *Journal of Physical Oceanography*. (In Press.)

Hydrodynamics of fringing reef systems: Ningaloo Reef, Western Australia

RYAN J. LOWE¹, SOHEILA TAEBI¹, GRAHAM SYMONDS², CHARITHA B. PATTIARATCHI¹,
GREG N. IVEY¹, RICHARD BRINKMAN³

1. School of Environmental Systems Engineering, University of Western Australia, M015, 35 Stirling Highway, Crawley 6009, Western Australia, Australia
email: ryan.lowe@uwa.edu.au, taebi@uwa.edu.au, chari.pattiaratchi@uwa.edu.au, greg.ivey@uwa.edu.au
2. CSIRO Marine and Atmospheric Research, Floreat 6014, Western Australia, Australia
email: graham.symonds@csiro.au
3. Australian Institute of Marine Science, Townsville 4810, Queensland, Australia
email: r.brinkman@aims.gov.au

Keywords: coral reefs, nearshore circulation, wave transformation; Ningaloo Reef

ABSTRACT

The response of the circulation of Ningaloo Reef (the largest fringing coral reef in Australia) to wave, wind and tidal forcing was investigated using field data and preliminary output from a numerical model. A 6-week field experiment measuring waves, currents, and water levels was conducted during April–May 2006, which focused on the dynamics of flow within a representative reef-channel circulation cell (one of hundreds that comprise the overall system). Results indicate wave-forcing as the dominant mechanism driving the circulation of Ningaloo Reef, with lagoonal flushing times of 5–8 hours under typical offshore wave conditions. Cross-reef wave-driven currents, however, were significantly weaker ($\sim 0.1\text{--}0.2\text{ m s}^{-1}$) than expected from the reef literature, likely due to the presence of considerable wave setup inside the shallow lagoon of this fringing reef. Preliminary results from a coupled wave-circulation numerical model, presently under development, are discussed.

Introduction

The Ningaloo Reef tract extends approximately 260 km along the North-West Cape of Western Australia (Figure 1a). Unlike the Great Barrier Reef, which is separated from shore by an expansive coastal lagoon, Ningaloo Reef lies adjacent to shore. It is therefore classified as a fringing reef, making it the largest fringing reef system in Australia (Taylor and Pearce, 1999). The reefs that comprise Ningaloo are located between a few hundred meters to a maximum of 7 km offshore, and are separated from shore by lagoons with 2–3 m mean depth (Taylor and Pearce, 1999). These reefs are broken every few kilometers by relatively deep channels through which a majority of the water exchanged between the lagoons and ocean is believed to occur.

Broadly speaking, the circulation of reefs can be driven by a number of forcing mechanisms including waves, tides, wind, and buoyancy effects (Monismith, 2007). The relative importance of each mechanism varies, and is a function of both a reef's geomorphology and the forcing conditions present at the site. Relatively few studies have focused on the physical oceanography of Ningaloo Reef, but have suggested that breaking waves drive the dominant circulation patterns throughout much of this system (e.g., Hearn et al., 1986; Brinkman, 1998). Conceptually, wave breaking near the reef crest increases the mean sea level in the surf zone (wave setup), establishing a pressure gradient that drives a cross-shore flow across a shallow reef flat and into a deeper lagoon (Figure 1b). On fringing reefs bounded by a shoreline, water entering the lagoon must return to the ocean through narrow gaps (channels) in the reef. Therefore, the circulation of Ningaloo Reef can be thought of as consisting of up to a hundred of these individual reef-lagoon-channel circulation cells. Although a number of analytical models have been developed to predict wave-driven flows on reefs (e.g., Symonds et al., 1995; Hearn, 1999; Gourlay and Colleter, 2005), such models have been derived by solving simplified forms of the 1-D cross-shore mass and momentum equations. While these 1-D approaches may be suitable for reefs that are not bounded by a coastline (e.g., atolls and barrier reefs), it is unclear (largely due to a lack of field data) whether these existing reef models can be utilized on fringing reefs such as Ningaloo where the flows are inherently 2-D.

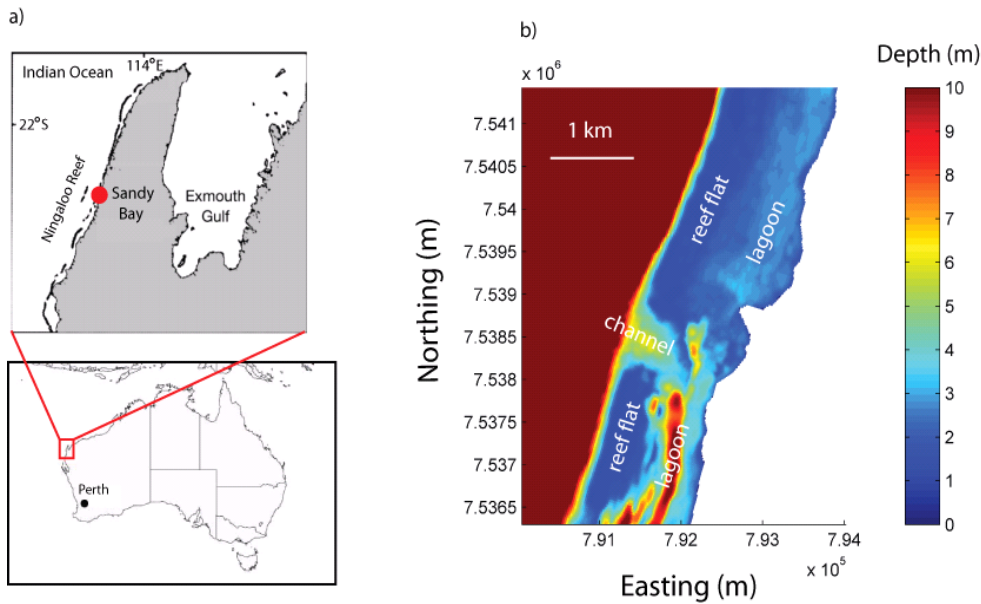


Figure 1. Ningaloo Reef, Western Australia. a) Field site (Sandy Bay) on the North West Cape. b) Bathymetry derived from hyperspectral imagery, highlighting the dominant morphological features (note that depths >10 m are not shown).

The goal of the present study was to conduct a detailed field study into the dynamics governing the circulation of a ~ 5 km section of Ningaloo Reef centered at Sandy Bay (Figure 1b). This site was chosen because the reef appeared, from aerial photographs, to have morphological characteristics fairly representative of Ningaloo as a whole. In particular, the field data collected will serve as the foundation for the development and validation of a coupled wave-circulation numerical model, initially focused on this section of Ningaloo. Future work will concentrate on upscaling the model to simulate the circulation over much larger sections of Ningaloo [$O(100$ km)]; such a model will ultimately help to improve predictions of the transport of material (e.g., nutrients, contaminants, larvae, waterborne pests, etc.) within Ningaloo Marine Park, predictions upon which a variety of regulatory and management decisions can eventually be made.

Field experiment and numerical model

An extensive field experiment was conducted at Sandy Bay from 10 April to 30 May 2006. A large array of instruments including 12 acoustic Doppler current profilers (ADCPs), nine single point current meters, and a series of wave and tide gauges, were deployed in the channel, along the reef crest north and south of the channel, within the lagoon and offshore (not shown). Significant wave heights H_s were computed by transforming the raw pressure data collected by both the current meters and wave gauges using linear wave theory. Hourly Eulerian current time-series U_E were obtained from each current meter by averaging all samples in a burst, and were then rotated onto the principal component axes of the velocity variance. Wave setup distributions η were computed from the raw pressure data following Raubenheimer et al. (2001), using a reference level site on the forereef prior to breaking where we assumed $\eta = 0$, i.e., wave setdown is estimated to be small here.

A preliminary 2D coupled wave-circulation numerical model was developed for the region surrounding Sandy Bay using Delft3D. Anticipating that the wave-driven flows in this system will be strongly dependent on the fine-scale [$O(10$ m)] spatial variations in reef bathymetry, for this modeling we incorporated high-resolution bathymetry derived from hyperspectral imagery (horizontal resolution = 3.5 m; depth rms error $\sim 10\%$). The model domain extended ~ 20 km alongshore by ~ 8 km in the cross-shore with a nominal ~ 20 m grid resolution. The wave model (SWAN) was forced at the offshore boundary using directional wave conditions during the experiment, measured by a Nortek AWAC deployed on the forereef. The iteratively-coupled Delft3D-FLOW module was forced at the open boundaries using measured tidal harmonics with wind-forcing applied using data obtained from a weather station operated by AIMS, located on the coast ~ 20 km north of the study site.

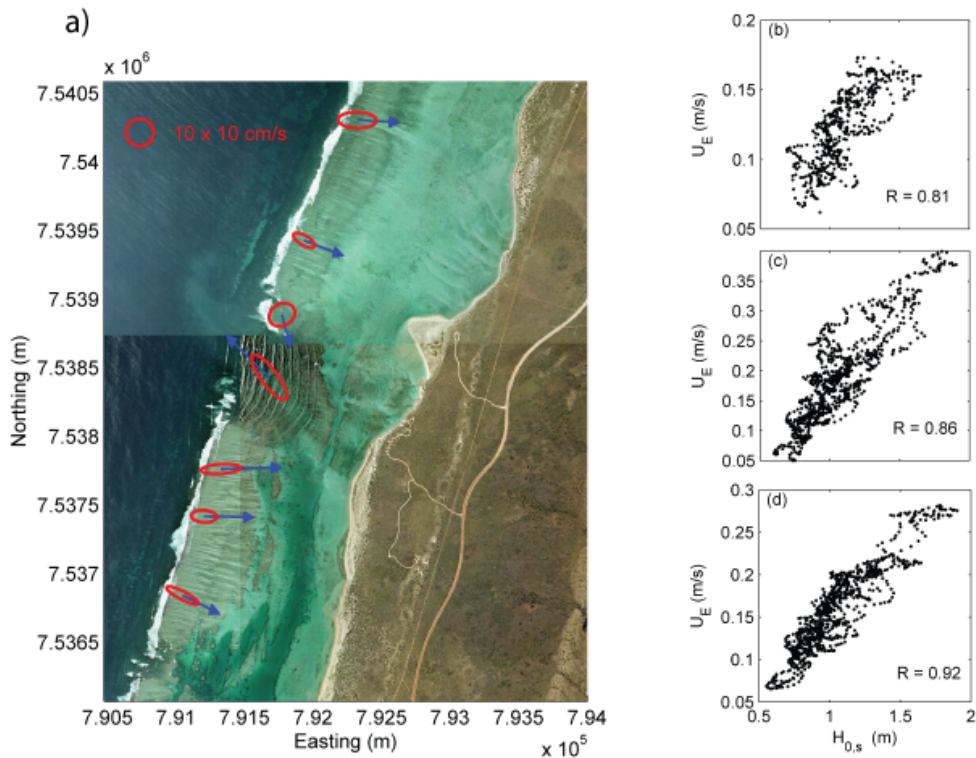


Figure 2. a) Experiment-averaged current vectors (blue) and velocity variance ellipses (radii represent one standard deviation). Depth-averaged current speed as a function of offshore significant wave height, measured on the b) north reef flat, c) channel, d) south reef flat.

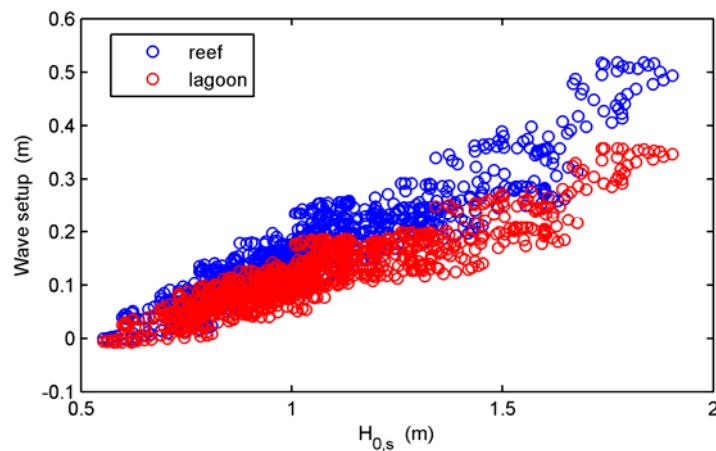


Figure 3. Wave setup as a function of offshore significant wave height, measured near the reef crest and within the lagoon for the northern reef section.

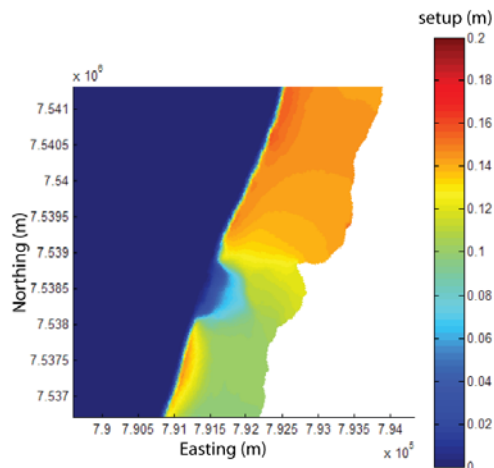


Figure 4. Modeled time-averaged wave setup field.

Preliminary results

During the experiment, the mean tidal amplitude was ~ 0.3 m, offshore significant wave heights ranged from 0.5 to 2.0 m, and winds varied between 2–6 m s^{-1} , coming mostly from the southwest. Analysis of the depth-averaged currents at sites along the reef crest and within the channel, revealed a dominant shoreward flow averaging 10–20 cm s^{-1} directed across the shallow (< 2 m deep) reef with a return flow out the deeper channel (Figure 2a). The strength of these flows were strongly correlated with offshore significant wave heights ($R \sim 0.8\text{--}0.9$), indicating that wave breaking was the dominant forcing mechanism driving the circulation of this section of Ningaloo (Figures 2b–d). Cross-reef currents along the southern reef section were typically $\sim 50\%$ faster than measured across the northern reef section (Figure 2b,d).

Measured wave setup, shown for two representative sites on the reef and within the lagoon (Figure 3), indicate that maximum setup near the reef crest varies from ~ 0 for $H_{0,s} < 0.7$ to as large as 0.5 m when $H_{0,s} \sim 2$ m. Interestingly, the lagoon also sets up dramatically, with typical values ranging from 60–80% of observed maximum reef values. The relatively large lagoon setup observed on this fringing reef is thus very different from what occurs within the expansive (unbounded) lagoons of atolls and barrier reefs, where the mean lagoon water level is typically the same as offshore. Such lagoon setup must be present in Ningaloo (and other fringing reefs) to provide a pressure gradient to overcome the frictional resistance as water is driven back to the ocean through the relatively shallow and rough lagoon and channel of this system. By significantly reducing the cross-reef mean water level gradients, the wave-driven flows on Ningaloo are much weaker than currents typically observed on atolls and barrier reefs for the same range of incident wave conditions (for a review, see Gourlay and Colleter, 2005). Despite these fairly weak flows, the flushing time of the lagoon (inferred from the total lagoon volume and cross-reef transport) is still relatively fast (5–8 hours).

Preliminary numerical simulations of the 2006 experiment period, indicate good agreement between observed and modeled current speeds and directions, albeit with some over-prediction in the strength of the wave-driven flows (not shown, to be discussed). Notably, the model also predicts much weaker cross-reef currents over the northern reef section. The modeled 2-D setup field (averaged over the simulation period) reveals a high degree of spatial variability (Figure 4). In particular, lagoon setup within the much shallower northern lagoon is, on average, much greater than within the deeper southern lagoon, thus elucidating why cross-reef currents measured on the northern reef section are so much weaker. In general, the momentum balance on the lagoon-channel return flow clearly plays a dominant role in controlling the magnitude of the wave-driven flows on fringing reefs; this momentum balance has typically been neglected in existing analytical model of reef wave-driven circulation.

Acknowledgements

Funding for this project was provided by the Western Australian Marine Science Institution and an Australian Research Council Discovery Grant (DP0770094) to R.J.L. We thank Wojciech Klonowski and Merv Lynch at Curtin University for providing access to preliminary hyperspectral bathymetry data.

References

- Brinkman, R.M. (1998), *AIMS data report: Ningaloo Reef (November–December 1997)*. Technical Report, March 1998, Australian Institute of Marine Science.
- Gourlay, M.R., Colleter, G. (2005), Wave-generated flow on coral reefs – an analysis for two dimensional horizontal reef-tops with steep faces, *Coastal Engineering*, 52, 353–387.
- Hearn, C.J., Hatcher, B.G., Masini, R.J., Simpson, C.J. (1986), *Oceanographic processes on the Ningaloo Coral Reef, Western Australia*. Environmental Dynamics Report ED-86-171. Centre for Water Research, Western Australia.
- Hearn, C.J. (1999), Wave-breaking hydrodynamics within coral reef systems and the effect of changing relative sea level, *Journal of Geophysical Research*, 104(C12), 30007–30019.
- Monismith, S.G. (2007), Hydrodynamics of Coral Reefs, *Annual Review of Fluid Mechanics*, 39, 37–55.
- Symonds, G., Black, K.P., Young, I.R., (1995), Wave-Driven Flow over Shallow Reefs, *Journal of Geophysical Research-Oceans*, 100(C2), 2639–2648.
- Taylor, J.G., Pearce, A.F. (1999), Ningaloo Reef currents: implications for coral spawn dispersal, zooplankton and whale shark abundance, *Journal of the Royal Society of Western Australia*, 82, 57–65.

Observations of the structure and dynamics of wintertime mid-shelf fronts

DAVID S. ULLMAN¹, DANIEL CODIGA¹, LAUREN DECKER¹, SCOTT STACHELHAUS¹,
S. BRADLEY MORAN¹, DAVID HEBERT¹, CHRISTOPHER KINCAID¹,
MICHELLE ALESZCZYK¹, JOSH KOHUT²

1. Graduate School of Oceanography, University of Rhode Island, 215 South Ferry Road, Narragansett RI 02882, USA
email: d.ullman@gso.uri.edu, dcodiga@gso.uri.edu, lbdecker@gmail.com,
sstach@gso.uri.edu, bmoran@gso.uri.edu, dhebert@gso.uri.edu,
ckincaid@gso.uri.edu, michelle@gso.uri.edu
2. Institute of Marine and Coastal Sciences, Rutgers University, 71 Dudley Road, New Brunswick NJ 08901-8521, USA
email: kohut@marine.rutgers.edu

Keywords: shelf circulation, horizontal dispersion

ABSTRACT

Hydrographic fronts oriented roughly along isobaths at mid-shelf locations have been observed along a number of coastal margins during the winter months. The mechanism(s) responsible for the formation of these fronts and their influence on cross-shelf transport are not presently understood. An intensive observational campaign was completed during the winter of 2007 in the mid-shelf front zone of the New York Bight off the U.S. east coast. The front separates cool, low salinity inshore waters from warmer, saltier offshore waters and an along-shore current jet is observed concurrent with the front. Cross-shelf mean and eddy heat fluxes are computed using the moored time series of velocity and temperature. Mean fluxes, arising from a mean upwelling circulation cell are larger than eddy fluxes. Eddy fluxes are dominated by subtidal fluctuations, with the effect of tidal fluctuations negligible. Cross-shelf dispersion is estimated from measurements of the cross-isobath variation in the activities of ²²⁸Ra. The effective cross-shelf diffusivity inshore of the mid-shelf front is larger than its value offshore of the front suggesting that the front is a boundary between a vigorously mixed inshore region and a more quiescent offshore zone.

Introduction

Analyses of fronts detected in satellite images of sea surface temperature (SST) have shown the presence of persistent frontal zones at mid-shelf locations along a number of coastlines (Hill and Simpson, 1989; Ullman and Cornillon, 1999; Hickox et al, 2000; Chang et al, 2006). These frontal zones, detected in satellite SST at approximately the 50 m isobath during winter only, are distinct from, and inshore of the stronger and more widely studied shelf break fronts that are also present along most coastal margins. From an analysis of historical hydrographic data, Ullman and Cornillon (2001) determined that the mid-shelf front off the northeast U.S. coast was a salinity front in the dynamic sense, separating cooler, fresher inner shelf waters from warmer, saltier offshore waters. Cross-frontal temperature differences, although providing the means of detection in SST imagery, actually served to decrease the cross-front density contrast. Ou et al. (2003) proposed that mid-shelf fronts can be formed over a sloping shelf due to spatial variability in the effective horizontal diffusivity due to tidal shear dispersion processes.

An observational effort in the mid-shelf frontal zone of the New York Bight (U.S. east coast) during the winter of 2007 was aimed at describing the vertical structure and temporal variability of the frontal hydrographic and velocity fields and determining the spatial variability in cross-shelf diffusivity. The overall goal is to determine the formation mechanism of these fronts and to evaluate the degree to which they serve as barriers to cross-shelf property exchange. This paper describes preliminary results from several avenues of analysis of the 2007 data sets.

Observations

The observational program consisted of a combination of shipboard measurements, deployment of moored instrumentation and autonomous gliders, and collection of remotely sensed data in the mid-shelf region of the continental shelf off southern New Jersey, USA. Numerous vertical sections of velocity, from a shipboard acoustic Doppler current profiler (ADCP), and hydrography, using a towed undulating vehicle (ScanFish) equipped with CTD sensors, were obtained on three R/V Endeavor cruises during the winter of 2007. On several cross-shelf ScanFish lines (see Figure 1) covering the zone between the 20 m and 70 m isobaths, surface water was collected from the ship's seawater intake at intervals of a few kilometers for analysis of the activity of Radium isotopes. Bottom mounted ADCPs were deployed at four locations (Figure 1) spanning the historical position of the surface manifestation of the mid-shelf front, and all returned data from an approximately three-month period (mid January to mid-April). Wave-driven profiling CTDs were deployed in the vicinity of the four moorings, however they failed to profile properly and did not return useful data. Temperature data were obtained from three thermistor chains located along the main ADCP mooring line (Figure 1). A Slocum glider equipped with a CTD obtained cross-shelf hydrographic sections during the periods between the three Endeavor cruises. Finally, the region of interest is located within the coverage zone of the Mid-Atlantic Regional Coastal Ocean Observing System HF radar network, which provided surface current maps for the winter of 2007 as well as for several prior years. Satellite SST imagery from the MODIS sensor aboard the Terra and Aqua satellites was obtained from NASA.

Temperature data were obtained from three thermistor chains located along the main ADCP mooring line (Figure 1). A Slocum glider equipped with a CTD obtained cross-shelf hydrographic sections during the periods between the three Endeavor cruises. Finally, the region of interest is located within the coverage zone of the Mid-Atlantic Regional Coastal Ocean Observing System HF radar network, which provided surface current maps for the winter of 2007 as well as for several prior years. Satellite SST imagery from the MODIS sensor aboard the Terra and Aqua satellites was obtained from NASA.

Results

Velocity records from the ADCPs show strong wind-forced variability of currents. Mean velocities at the four moorings over the first ~40 days (Figure 1) are less than 10 cm s^{-1} in magnitude but show evidence of a baroclinic jet structure in the vicinity of the 50 m isobath. Near surface flow is predominantly along isobaths to the southwest, peaking at the central mooring, with indications of a weak offshore component. Near bottom flows are generally onshore and upshelf (towards the north). Detided shipboard ADCP sections (not shown) often show a southwestward, surface intensified jet associated with the hydrographic front that is consistent with the structure shown in Figure 1.

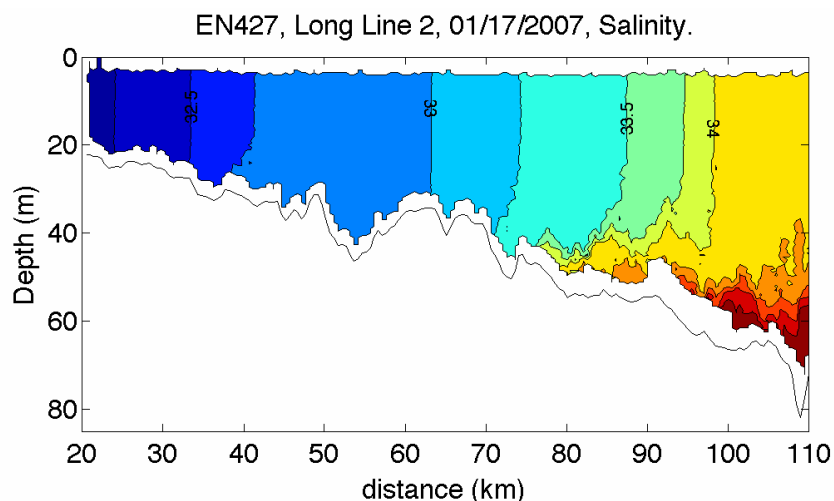


Figure 2. Cross-shelf salinity section from a ScanFish tow along the green line shown in Figure 1 during cruise 1. The bottom is denoted by the solid line.

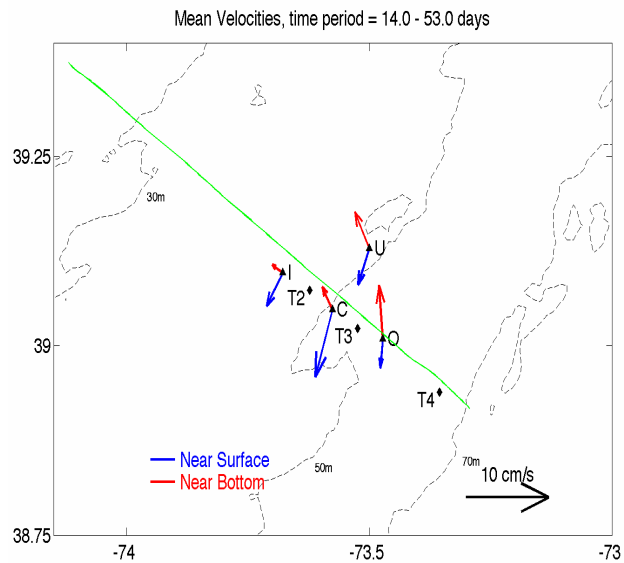


Figure 1. Mean ADCP near surface and near bottom currents during 14 January–22 February 2007. Black diamonds denote Thermistor chain moorings. The ScanFish transect line is shown in green.

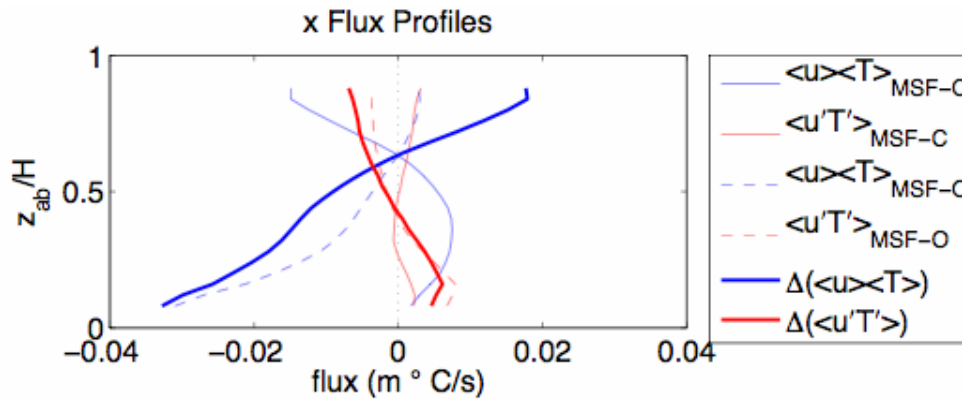


Figure 3. Vertical profiles of cross-shelf temperature flux at moorings C (solid curves) and O (dashed curves). The heavy solid curves show the flux differences between the two moorings (O minus C), an estimate of the flux divergence.

A cross-shelf ScanFish salinity section from the January 2007 cruise shows the typical upward- and offshore-sloping frontal structure (Figure 2). In this example there is a ~30 m deep surface mixed layer with highest horizontal gradients located approximately 90 km from the coast. Gradients at depth are stronger (roughly 1 psu per 10 km) with the front intersecting the bottom at roughly the 50 m isobath location (80 km offshore). There is also evidence of a weaker front about 30 km from the coast with salinities lower than 32.5 psu. This inshore front is also observed in satellite SST imagery (not shown) and appears to be temporally persistent. Although space considerations preclude their inclusion here, the multiple front cross-sections obtained during the three cruises (in addition to glider sections) show significant variability both in the position and structure of the front. Vertical mixing associated with strong wind events was observed on occasion to almost entirely eliminate the vertical structure seen in Figure 2.

Low pass filtered ADCP current observations at moorings C and O (Figure 1) were combined with low pass filtered temperature, interpolated to the ADCP locations from the thermistor chains, to estimate advective heat fluxes averaged over the time period 14 January–22 February 2007. After subtraction of an overall mean temperature the heat (actually temperature) flux $\langle uT \rangle$ is decomposed into contributions from the mean quantities and from correlations between fluctuating quantities. In the cross-shelf (x) direction this is written as:

$$\langle uT \rangle = \langle u \rangle \langle T \rangle + \langle u'T' \rangle, \quad (1)$$

where the $\langle \rangle$ denotes a record average and the primes denote fluctuations. The terms on the right-hand side of Equation (1) are denoted as the mean and eddy fluxes respectively.

In the cross-shelf direction, mean fluxes arise due to the presence of a mean upwelling circulation pattern (seen in Figure 1) and are larger in magnitude than the corresponding eddy fluxes (Figure 3). The mean flux is convergent (divergent) in the lower (upper) part of the water column implying a warming (cooling) tendency. Eddy fluxes are marginally significant and are positive in the lower part of the water column, indicating an up-gradient flux of heat by the fluctuations. In the lower layer, the eddy flux is divergent, implying a cooling tendency. Eddy fluxes computed using the raw unfiltered time series gave essentially the same results suggesting that these fluxes predominantly arise from subtidal fluctuations.

Large volume water samples taken from the ship's seawater intake at intervals of 4-5 km along two cross-shelf transects during the first cruise were analyzed for ^{228}Ra ($t_{1/2} = 5.75$ years) activity using the procedures described by Kelly and Moran (2002). The dominant inputs of radium to the coastal ocean are riverine and groundwater discharge. With assumptions of steady state, alongshore uniformity, and negligible cross-shelf advection, the across-shelf profile of ^{228}Ra activity is determined by a balance between supply at the coast, cross-shelf diffusion, and radioactive decay. The solution of such a model is an exponential decay of ^{228}Ra activity with distance from the coast, with an e -folding scale given by $(t_{1/2} K_x)^{1/2}$. A plot of $\ln(^{228}\text{Ra})$ versus offshore distance (Figure 4) shows two regimes: the region inshore of 80 km with relatively slow offshore decay ($K_x = 226 \text{ m}^2 \text{ s}^{-1}$) and the region offshore of 80 km characterized by rapid offshore decay ($K_x = 37 \text{ m}^2 \text{ s}^{-1}$). The break in slope delimiting the two regimes is located roughly at the position of the salinity front in Figure 2, suggesting that the front is a boundary between a rapid mixing zone inshore and a region of less intense horizontal mixing offshore.

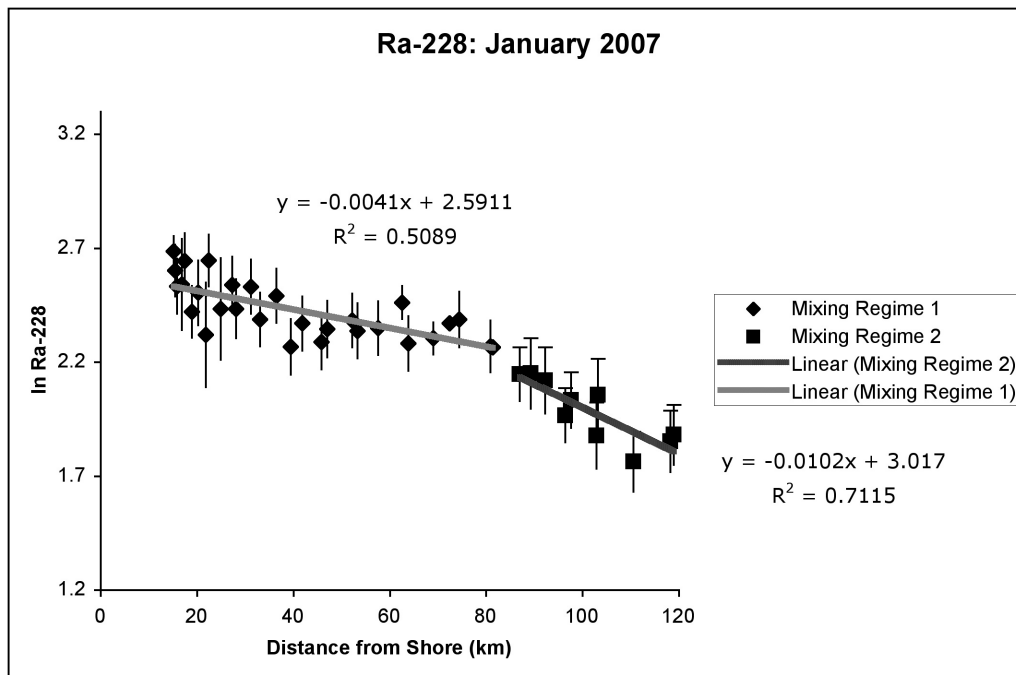


Figure 4. Natural log of ^{228}Ra activity versus distance from the coast for water samples on two long lines during the first cruise. The gray lines are the best fit straight lines to data points in each of the two regimes.

Conclusions

A mean down-shelf (in the direction of Kelvin wave propagation) surface intensified flow is observed during winter 2007. The horizontal structure of the mean current suggests the presence of a jet centered roughly at the location of the historical mean front (50 m isobath). The current observations also show a mean upwelling circulation in the cross-shelf plane. This circulation advects warm water onshore near the bottom and cool water offshore near the surface. Subtidal currents in the frontal zone fluctuate strongly in response to wind variability. However cross-shelf eddy heat fluxes arising from these fluctuations are small compared with mean fluxes. Eddy fluxes are dominated by subtidal variability in temperature and current with tidal fluctuations playing a minor role. This suggests that the tidal diffusivity frontogenesis mechanism proposed by Ou et al. (2003) is likely not important in the formation of the midshelf front. Measurements of ^{228}Ra as a function of cross-shelf position suggest that the mid-shelf front may represent the boundary between a region of high horizontal mixing inshore and a weaker mixing region offshore.

References

- Chang, Y., Shimada, T., Lee, M.-A., Lu, H.-J., Sakaida, F., Kawamura, H. (2006), Wintertime sea surface temperature fronts in the Taiwan Strait, *Geophysical Research Letters*, 33, L23603, doi:10.1029/2006GL027415.
- Hickox, R., Belkin, I., Cornillon, P., Shan, Z. (2000), Climatology and seasonal variability of ocean fronts in the East China, Yellow and Bohai Seas from satellite SST data, *Geophysical Research Letters*, 27, 2945–2948.
- Hill, A.E., Simpson, J.H. (1989), On the interaction of thermal and haline fronts. The Islay front revisited, *Estuarine, Coastal and Shelf Science*, 28, 495–505.
- Kelly, R.P., Moran, S.B. (2002), Seasonal changes in groundwater input to a well-mixed estuary estimated using radium isotopes and implications for coastal nutrient budgets, *Limnology and Oceanography*, 47, 1796–1807.
- Ou, H.W., Dong, C., Chen, D. (2003), Tidal diffusivity: A mechanism for frontogenesis, *Journal of Physical Oceanography*, 33, 840–847.
- Ullman, D.S., Cornillon, P.C. (1999), Satellite-derived sea surface temperature fronts on the continental shelf off the northeast U.S. coast, *Journal of Geophysical Research*, 104, 23459–23478.
- Ullman, D.S., Cornillon, P.C. (2001), Continental shelf surface thermal fronts in winter off the northeast U.S. coast, *Continental Shelf Research*, 21, 1139–1156.

Tidal circulation on the continental shelf

CLINTON D. WINANT

Scripps Institution of Oceanography, University of California, San Diego,
9500 Gilman Drive, La Jolla CA 92093-0209, USA
email: cwinant@ucsd.edu

Keywords: tides, circulation, continental shelf, estuaries

ABSTRACT

In this talk I want to examine why it is that estuarine physicists focus so much on barotropic tidal and tidally averaged circulation, while descriptions of continental shelf circulation often dismiss this component as unimportant. I will begin by reviewing recent descriptions of barotropic and baroclinic circulation driven by tides in semi-enclosed basins, and show that when these results are extended to the open continental shelf, they can explain features such as vertically sheared alongshore fluctuating flow accompanied by enhanced mixing and lateral circulation over the inner shelf, steady tidally averaged circulation along the edge of ocean basins and internal tide generation in the inner shelf.

Barotropic tidal circulation

In estuaries the tidally fluctuating flow tends to corkscrew into and out of the basin as sea level rises and falls with the tide. The lateral component is comparable in magnitude to the axial flow, as long as friction is not too large. This circulation is due to the imbalance between the cross-channel sea level gradient, that is in near geostrophic balance with the Coriolis acceleration associated with the vertically averaged axial flow, and the Coriolis acceleration associated with the vertically sheared axial flow. During flood condition for example, the lateral Coriolis acceleration near the surface exceeds the pressure gradient, tending to accelerate the lateral flow, while the converse is true near the bottom. Extending these results to the continental shelf suggests that over the inner-shelf (the region where surface and bottom frictional layers overlap, there is a similar, corkscrew like lateral exchange, driven by the barotropic tides. This constant vertical stirring may explain the enhanced vertical mixing that appears to lie at the root of nearshore productivity.

Barotropic tidally averaged circulation

In semi-enclosed basin, on time scales longer than tidal periods (residual circulation), fluid is drawn into the basin on the right side of an observer looking toward the closed end (in the northern hemisphere), and the return flow is on the opposite side. A steady lateral circulation is superposed on this steady axial flow, with upwelling over the deeper part of each section and downwelling near the sides. The residual flow is driven by a combination of advective terms, including the lateral advection of axial momentum associated with the Coriolis acceleration, and Stokes forcing. Tidally-averaged fluid parcel trajectories are determined by integrating the Lagrangian mean velocities. With or without rotation these trajectories vary considerably depending on small differences in initial position as well as on basin shape and other parameters of the problem. These results, extended to the shallow margins of larger ocean basins, are consistent with a cyclonic current system, running around the periphery of the basin, and concentrated over the inner-shelf. The Davidson current along the California coast, and the south-eastward drift that characterize the eastern coast of the USA may be examples of these barotropic features.

Conclusions

Observational and model results of the barotropic tidal circulation in estuaries, lagoons and other semi-enclosed basins suggest that the barotropic tide may be responsible for as yet unexplained features of the circulation over the open continental shelf. It is equally likely that baroclinic tidal circulation and mixing observed over open coasts can be explained in terms of known features of the baroclinic tides in estuaries.

Near-resonant response of the coastal ocean to sea breeze wind forcing in the Georgia Bight near the critical latitude

CATHERINE R. EDWARDS, HARVEY E. SEIM

Department of Marine Sciences, University of North Carolina at Chapel Hill,
340 Chapman Hall CB 3300, Chapel Hill NC 27599-3300, USA
email: credward@email.unc.edu, hseim@email.unc.edu

Keywords: diurnal-inertial resonance, sea breeze, critical latitude, shelf dynamics

ABSTRACT

Recent analysis indicates that non-tidal diurnal currents approach 30 cm s^{-1} on the shelf of the Georgia Bight, with appreciable diurnal variance persisting from April through October. These diurnal motions appear to be inertial oscillations (IOs) and near-inertial internal waves, forced by sea breeze/land breeze (SBLB) and other diurnal winds, resonant with the inertial frequency at 30°N . Near this critical latitude, diurnal/inertial currents can exceed 25 cm s^{-1} more than 120 km offshore and are surface-intensified, with IOs in the lower layer 180° out of phase with those in the upper layer.

Observational wind and current data from 1999–2007 are analyzed from a moored array in the Georgia Bight, between $29\text{--}32^\circ\text{N}$, where linear theory predicts a maximum of SBLB magnitude and offshore extent. The presence of the Gulf Stream offshore of the Georgia Bight may also contribute significantly to the magnitude of diurnal winds. The spatial structure, variability, and phase of diurnal/inertial currents are described and compared to those of diurnal wind forcing as both the atmospheric forcing and ocean response pass through the critical latitude for diurnal/inertial resonance. Ocean response appears to be strongly controlled by bottom friction, with increasing diurnal/inertial variance with distance offshore; preliminary analysis of surface currents from HF radar suggests continued increase past the shelf break into the Gulf Stream. Diurnal variance observations indicate SBLB winds on the order of $1\text{--}2 \text{ m s}^{-1}$ at least 125 km offshore, several times the typical offshore scale; diurnal winds using a mesoscale meteorological model suggest an estimate of 250 km offshore extent. The structure of observed and modeled wind fields compare well with the predictions of linear SBLB theory, and suggest significant divergence and convergence of the diurnal wind field that varies on time scales of days to weeks. The ubiquity of enhanced diurnal/inertial currents over much of the shelf, the vertical structure of these sea-breeze forced currents, and the phase-locking to the diel cycle may have significant implications for cross-shelf larval transport.

Introduction

While the barotropic M_2 tide is thought to dominate the current variance on the shelf of the Georgia Bight, diurnal variability has recently been observed to approach that of semidiurnal barotropic tide on synoptic and seasonal time scales. Seasonal variability of tidal currents can often be attributed to the presence of internal tidal energy derived from the barotropic tide under seasonal stratification (e.g., Holloway, 2001). Recent work has indicated a strong seasonal signal in the diurnal current, but the source of this diurnal variability does not appear to be tidal. The vertical structure of these currents is surface-intensified, with a shallow zero-crossing, below which currents change 180° in phase from that of the surface currents, and a subsurface local maximum of diurnal variance at about mid-depth. Near-surface currents approach 30 cm s^{-1} , and are persistent from April through October. The source of this variability may be attributed to sea breeze wind forcing of the coastal ocean at the critical latitude, where the inertial frequency coincides with that of the diurnal. Enhanced inertial currents have been reported elsewhere near the critical latitude: off the Namibian coast (Simpson et al., 2002), and in the Gulf of Mexico (Chen, 1996, DiMarco et al., 2001).

The atmosphere will also have a resonant response to diurnal thermal forcing at the critical latitude. Linear sea breeze/land breeze (SBLB) theory predicts a maximum of magnitude and offshore extent at 30°N/S , with a minimum of ellipticity as the SBLB ellipses become more inertial/circular (Rotunno, 1983; Yan and Anthes, 1987). Theories given by the literature disagree about whether or not the phase of SBLB with respect to the diurnal heating cycle may change at the critical latitude (Rotunno, 1983; Niino, 1987), but no observational analysis has been reported to test either hypothesis.

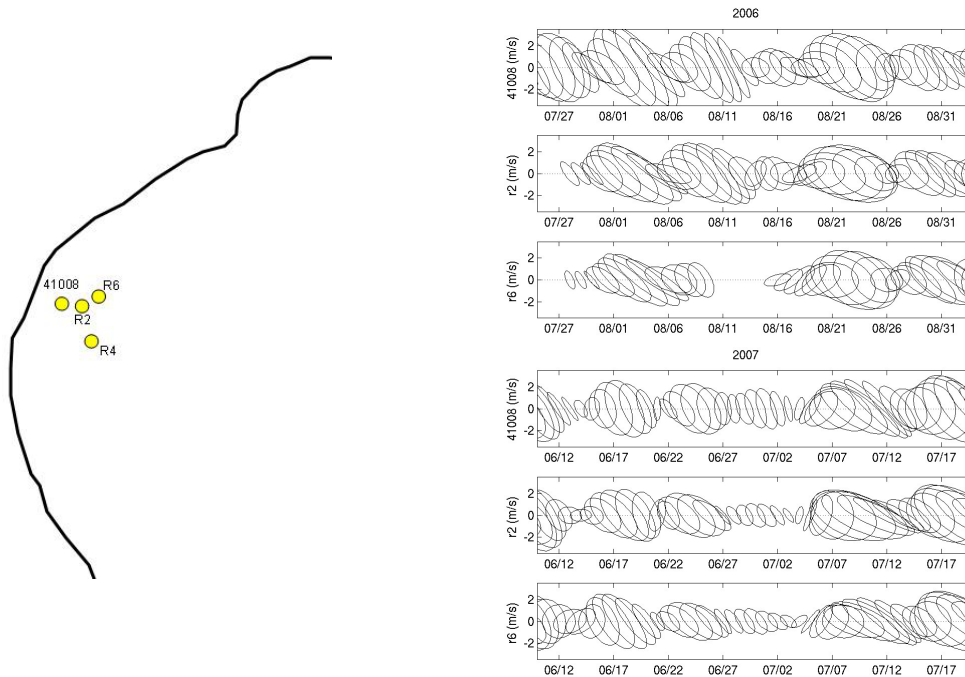


Figure 1. Left: Locations of wind and current observations on the shelf as part of the SABSOON array. NDBC coastal stations are not shown. Right: Best-fit wind ellipses to month-long time series of diurnally filtered observed wind for a quasi- cross-shore transect from 41008-R2-R6 for 27 August–1 September 2006 (upper panels) and 15 June–15 July 2007 (lower panels).

To understand the coastal response, the structure and variability of SBLB are explored through analysis of observational and modeled winds on the shelf of the Georgia Bight. Spatial patterns of SBLB are compared to linear theory. The structure and variability of the coastal ocean's response is described and compared to that of the SBLB wind forcing. Lastly, implications for larval transport and behavior on the shelf of the Georgia Bight are discussed.

Sea breeze/land breeze (SBLB)

The SBLB system is described using a combination of analysis of observations and modeled winds. Wind observations in the Georgia Bight are collected at in-shore coastal stations maintained by the National Data Buoy Center (NDBC) and at several moorings and towers on the shelf as part of the South Atlantic Bight Synoptic Offshore Observing Network (SABSOON) array (Figure 1, left). Wind and currents are available at NDBC buoy 41008 (water depth 15 m) and SABSOON mooring R2 (25 m), with wind at R6 (32 m) and currents at R4 (41 m).

The observations are not sufficient to completely describe the along- and cross-shore structure of SBLB in the Georgia Bight. Therefore, the description of large-scale features of the SBLB system relies on analysis of diurnal variability of near-surface wind fields given by the operational forecasting model Non-hydrostatic Mesoscale Model – Weather Research and Forecasting system (NMM-WRF). Further details of NMM-WRF model physics, data assimilation scheme, and computed fields are given by Skamarock et al. (2005).

The 10-m horizontal velocity field from the model reanalysis stage is filtered to the diurnal using a high (8-10th) order Butterworth filter, and the variance computed by month for summer months 2006 and 2007, shown in Figure 2. Diurnal variance of observed indicate SBLB winds on the order of $1-2 \text{ m s}^{-1}$ at least 250 km offshore, several times the offshore scale given by conventional wisdom. The structure of observed and modeled wind fields compare well with the predictions of linear SBLB theory, and suggest an additional effect of coastline curvature moving the local maximum slightly offshore to the inner to mid-shelf.

However, the temporal resolution of the model reanalysis fields (6 hr) is not sufficient to describe SBLB orientation, elliptical shape, or phase, and observations can provide this finer description of the SBLB system and its variability. The right panels of Figure 1 show best-fit ellipses to the diurnally filtered ($D1 = 20-28$ hours) observed wind over two month-long time series in 2006 and 2007. Diurnal wind is generally

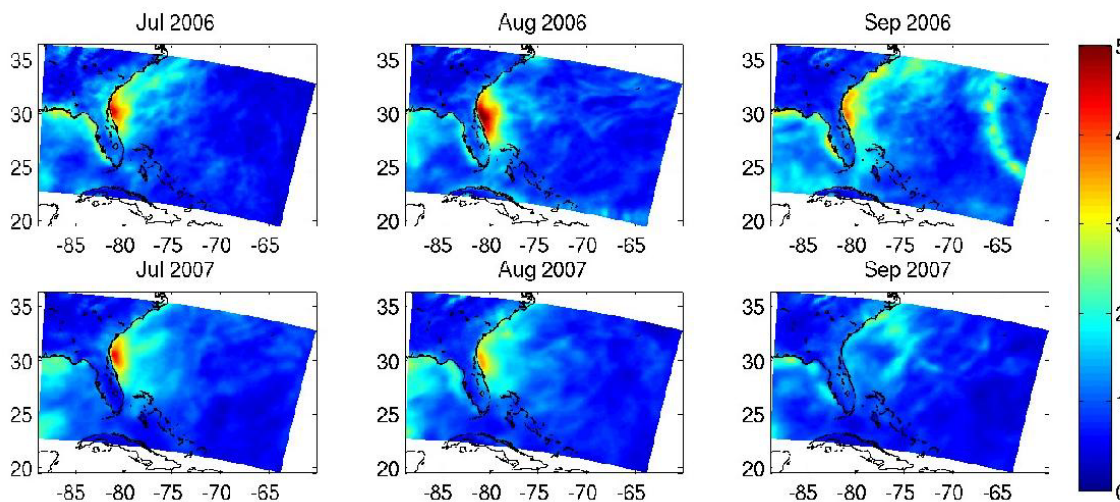


Figure 2. Diurnal wind variance in NMM-WRF model 10-m wind field, calculated by month. Variance is given in $\text{m}^2 \text{s}^{-2}$.

oriented cross-shore, with a wind speed approaching 5 m s^{-1} at its maximum, but wind ellipse size, ellipticity, orientation, and magnitude vary on a 7–10 day time scale, consistent with the synoptic time scale of summer in the Georgia Bight. The three observation locations form a quasi-cross-shore transect, and can be used to describe the cross-shore structure of SBLB. Figure 1 shows cross-shore coherence to be variable in time; 2007 SBLB is generally coherent, with a slight decrease of diurnal wind offshore. However, 2006 SBLB is much more variable in space and time, with less organized structure of the diurnal ellipses. This divergence and convergence of the diurnal wind field varies on time scales of days to weeks, and may lift or depress the pycnocline at the diurnal frequency. Analysis of SBLB phase (not shown) suggests that changes in phase with latitude are modified by coastline curvature, and may contribute to divergence and convergence of SBLB over the shelf.

Coastal ocean response to SBLB

Barotropic tidal currents are removed from the record using the method of complex empirical orthogonal functions described by Edwards and Seim (2008). The resultant ‘baroclinic’ velocity time series is then filtered at each depth to pass the diurnal band ($D1 = 20\text{--}28$ hours). Summertime maximum variances at R2 and R6 correspond to near-surface current variability of $6\text{--}10 \text{ cm s}^{-1}$ over the 3-month filtered records, but contours of ‘baroclinic’ filtered currents (Figure 3) indicate that these near-surface diurnal currents can approach 30 cm s^{-1} , the current magnitude of the semidiurnal barotropic tidal currents that dominate current variance on the shelf.

Ocean response appears to be strongly controlled by bottom friction, with rapid attenuation of near-inertial energy with diminished diurnal forcing. Diurnal/inertial variance increases with distance offshore; preliminary analysis of surface currents from HF radar suggests continued increase past the shelf break into the Gulf Stream. Comparison to the wind records in Figure 1 indicate a spin-up or spin-down time on the order of days.

Near-inertial internal waves propagate through the mid-shelf locations at R2 and R4. During 2007, when the wind field is generally coherent over the shelf, the internal waves appear to propagate offshore, consistent with the generation mechanism proposed by Davies and Xing (2003, 2002). Lines of constant phase over the month tilt upward, signifying downward energy propagation, and the clear transfer atmospheric diurnal energy into the surface ocean. However, August 2006 presents a more disorganized SBLB system, and the direction of propagation of the disturbance is less clear, and suggests multiple sources of near-inertial internal waves, likely in locations where the surface wind field converges or diverges on the diurnal frequency.

Over brief time periods (e.g., 30–31 August), upward energy propagation is observed, suggesting that the near-inertial internal waves may have reflected off of bottom topography. These reflection events often follow periods in time where the vertical structure departs from the surface-intensified mode-1 structure that dominates the record, and appears to cast the signal into higher modes. The higher modal structure may be the result of interference of near-inertial internal waves from multiple sources.

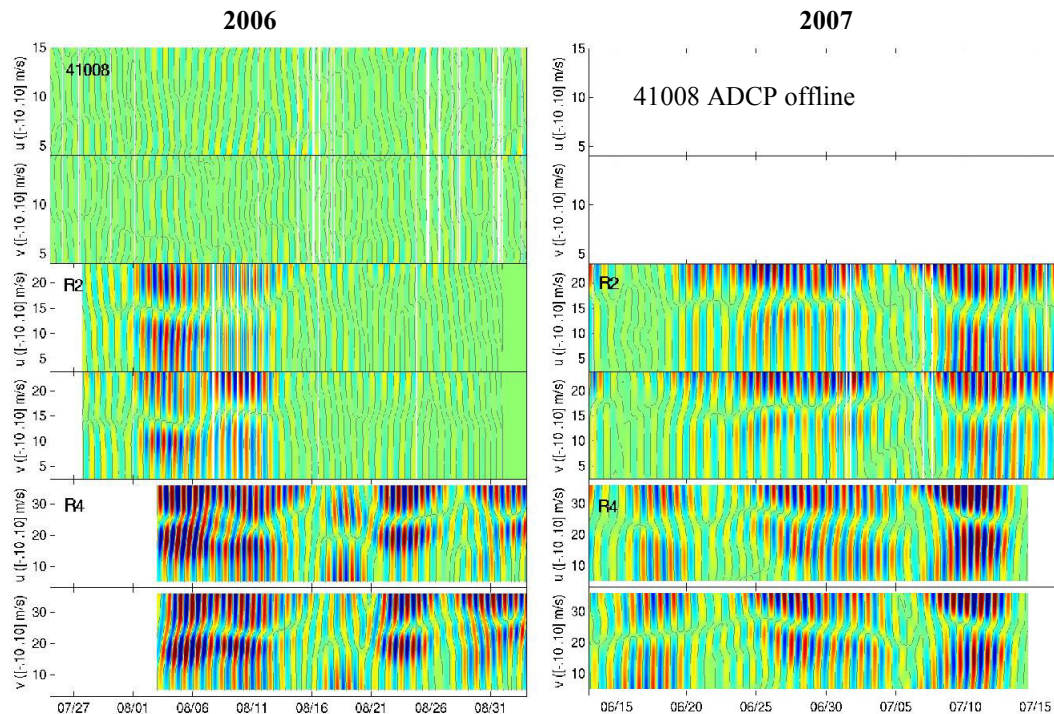


Figure 3. Month-long time series of D1 filtered non-tidal currents for the quasi-cross-shore transect from 41008-R2-R4. The left panels show currents from 27 August–1 September 2006, and right panels show 15 June–15 July 2007 (lower panels).

There may be significant implications for larval transport on the shelf of the South Atlantic Bight. Previous modeling work estimating larval transport in the region found that larval behavior did not appear to be a significant control on larval settlement location; alongshore currents were the greatest factor in larval transport on the shelf. However, the phase locking of the surface-intensified inertial oscillations and internal waves on the Georgia shelf to the diel cycle is unique to the critical latitude. The 180° vertical phase difference induced by coastal wall effects not only provides new pathways of transport in the cross-shore direction, but cross-shore transport requires larval behavior to achieve net movement on- or offshore.

References

- Chen, C., Xie, L. (1997), A numerical study of wind-induced, near-inertial oscillations over the Texas-Louisiana shelf, *Journal of Geophysical Research*, 102(C7), 15583–15593.
- Davies, A., Xing, J. (2002), Influence of coastal fronts on near-inertial internal waves, *Geophysical Research Letters*, 29(23), 1–4.
- Davies, A., Xing, J. (2003), Processes influencing wind-induced current profiles in near coastal stratified regions, *Continental Shelf Research*, 23, 1379–1400.
- DiMarco, S., Howard, M., Reid, R. (2000), Seasonal variation of wind-driven diurnal current cycling on the Texas-Louisiana continental shelf, *Geophysical Research Letters*, 27, 1017–1020.
- Edwards, C.R., Seim, H.E. (2008), EOF analysis as a method to separate barotropic and baroclinic velocity structure in shallow water, *Journal of Atmospheric and Oceanic Technology*, 25, 808–821.
- Holloway, (2001)
- Niino, H. (1987), The linear theory of land and sea breeze circulation, *Journal of the Meteorological Society of Japan*, 65, 901–921.
- Rotunno, R. (1983), On the linear theory of the land and sea breeze, *Journal of the Atmospheric Sciences*, 40, 1999–2009.
- Simpson, J., Hyder, P., Rippeth, T., Lucas, I. (2002), Forced oscillations near the critical latitude for diurnal-inertial resonance, *Journal of Physical Oceanography*, 32, 177–187.
- Skamarock, W.C., Klemp, J.B., Dudhia, J., Gill, D.O., Barker, D.M., Wang, W., Powers, J.G. (2005), *A description of the advanced research WRF version 2*, NCAR Tech Note, NCAR/TN-468+STR, 88pp. [Available from UCAR Communications, P.O. Box 3000, Boulder CO 80307, USA and online at: http://box.mmm.ucar.edu/wrf/users/docs/arw_v2.pdf]
- Yan, H., Anthes, R. (1987), The effect of latitude on the sea breeze, *Monthly Weather Review*, 115, 936–956.

Internal set-up, sub-tidal circulation and transport driven by shoaling and breaking internal tides

JAMES A. LERCZAK

College of Oceanic and Atmospheric Sciences, Oregon State University,
104 COAS Administration Building, Corvallis OR 97331-5503, USA
email: jlerczak@coas.oregonstate.edu

Keywords: internal waves, shoaling, buoyancy flux, momentum flux

ABSTRACT

We use a fully-nonlinear, non-hydrostatic, rotating, two-dimensional (cross-shelf/vertical) numerical model to study on-shore propagating internal tides and associated high-frequency internal waves on a linearly-shoaling continental shelf. Large amplitude, internal tides, high-frequency internal waves and internal undular bores are frequently observed to propagate onshore on continental shelves. Above wave troughs, near-surface onshore current speeds approach the wave propagation speed and the waves have been observed to contribute to the onshore transport of barnacle larvae with upward-swimming capability. Observations suggest that nonlinear internal waves: contribute significantly to horizontal mass and buoyancy fluxes on the inner shelf; influence the cross-shelf density structure either through mixing or in response to internal radiation stresses driven by the waves; drive a low-frequency, cross-shelf circulation; and drive an along-shelf geostrophic flow that partially balances a ‘set-up’ of the pycnocline. Here, we quantify the momentum and buoyancy budgets and mass transport associated with the waves at the time scale of the waves and averaged over several wave packets, and determine the amplitude and structure of the cross-shelf and along-shelf sub-tidal currents driven by the waves. The model is forced offshore with an internal tide and the response of the shelf is studied as a function of forcing amplitude, shelf bottom slope, stratification and turbulence closure parameterization. Model runs show that waves significantly influence the sub-tidal circulation and density field on the inner shelf. For example, in a domain with a steep bottom slope ($\alpha = 0.01$) and forcing amplitude consistent with internal waves observed on the southern California shelf, the dominant sub-tidal cross-shore momentum balance is between nonlinear terms (internal radiation stress divergences), cross-shore baroclinic pressure gradients and the Coriolis term. The internal waves drive a sub-tidal cross-shore and along-shore circulation, both with amplitudes of about 5 cm s^{-1} .

Introduction

Internal tides and large amplitude, high-frequency internal waves are observed to propagate towards the coast on many continental shelves (Jackson, 2004; Helfrich and Melville, 2006). Various field studies suggest that the cross-shore mass fluxes associated with nonlinear internal waves can be a dominant mechanism by which larval invertebrates, plankton and nutrients are transported towards the coast (Pineda, 1999; Leichter et al., 2003; Lennert-Cody and Franks, 1999; Shanks, 1987) in certain regions of the coastal ocean, particularly where wind-driven coastal upwelling is weak. Analytical and numerical studies of shoaling, nonlinear internal waves have shown that single, large-amplitude internal waves can transport surface waters, and the materials contained within them, large distances (Lamb, 1997, 2002). As the surface currents within the solitary wave approach the propagation speed of the wave ($U_{max} \rightarrow c$), a trapped-core can form that can, in principle, transport the water within the core indefinitely (Lamb, 2002; Aigner et al., 1999). Lamb (1997) has shown that, even prior to breaking ($U_{max} < c$), nonlinear waves with scales typical of those observed in the coastal ocean, can transport mass several kilometers in the direction of propagation. Assuming shoreward propagating internal wave packets are generated once every tidal cycle, as is often the case. Surface transport velocities associated with these packets are on the order of 10 cm s^{-1} , when averaged over several tidal cycles ($5 \text{ km} / 12.42 \text{ h} = 11 \text{ cm s}^{-1}$).

This ‘back-of-the-envelope’ estimate of surface transport velocity is comparable to cross-shore upwelling transport currents in regions of strong coastal upwelling (Lentz, 1992) and suggests that internal waves can be an important term in the cross-shore mass, buoyancy and momentum budgets (Hogg, 1972). Here, we explore the contribution of shoaling nonlinear internal waves in the coastal ocean to the cross-shore and along-shore momentum budgets in the coastal ocean using a two-dimensional, rotating, nonlinear, non-hydrostatic numerical model.

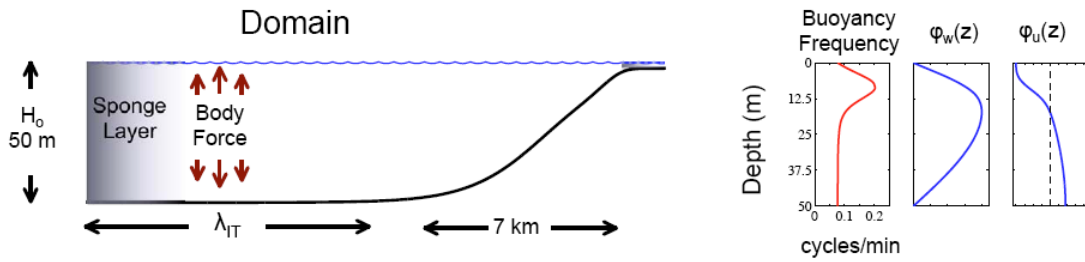


Figure 1. Numerical model domain (left panel). The right panels show vertical profiles of the buoyancy frequency of the initial stratification and the vertical and horizontal structure functions for a mode-one internal tide. The model is forced at the M_2 tidal frequency by applying an oscillatory body force having a vertical shape the same as the vertical structure function, ϕ_w , at the offshore end of the domain.

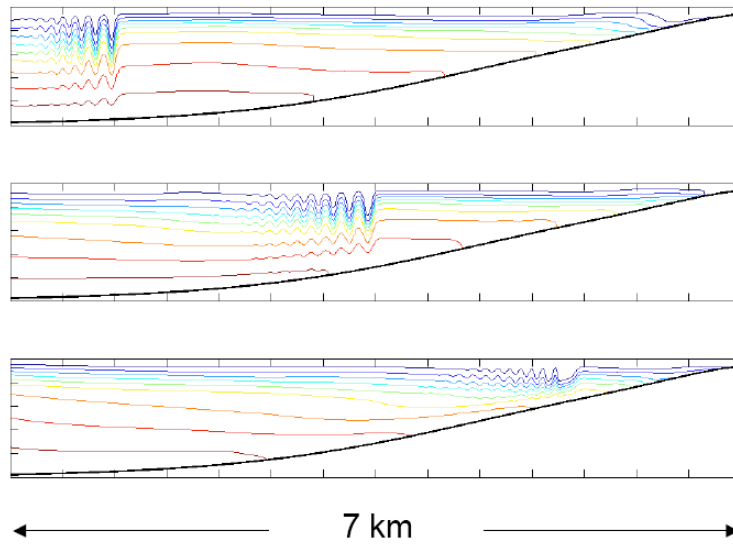


Figure 2. Example of an undular bore propagating towards the coast from the numerical simulations.

Numerical model

The nonlinear, non-hydrostatic numerical model solves the 2.5 dimensional Boussinesq equations on a two-dimensional (x, z) orthogonal curvilinear grid, using a cell-centered, second-order, fractional-step projection method (Bell and Marcus, 1992), and a second-order Godunov-type method for computing the nonlinear advection terms. The subgrid turbulence closure used is based on the Richardson Number dependent mixing scheme of Munk and Anderson (1948). Rotation is included in the model, however no along-shelf gradients are permitted. The numerical code was written by Karl Helfrich (WHOI).

The domain consists of a flat continental shelf with a depth of 50 m, extending a distance of one internal tidal wavelength (Figure 1). Shoreward of the flat region, the bottom shoals over a distance of 7 km, with a uniform slope of 0.01. Afterward, the domain is flat again, with a depth of 2.5 m. Sponge layers on either side of the domain have absorb kinetic energy that radiates towards the open boundaries. The model is set-up with a stratified fluid having a constant buoyancy frequency in the bottom 25 m of the water column (Figure 1). A pycnocline is present at a depth of 10 m, and the buoyancy frequency is reduced towards the surface. The bottom slope of the shoaling region and the stratification roughly match summer-time conditions on the southern California continental shelf.

The model is forced with a body force acting on the vertical momentum equation, having the vertical structure of a mode-one internal wave ($\phi_w(z)$, Figure 1) and a forcing frequency of the M_2 internal tide. This internal tide propagations onshore and evolves into an undular bore that shoals towards the coast (Figure 2).

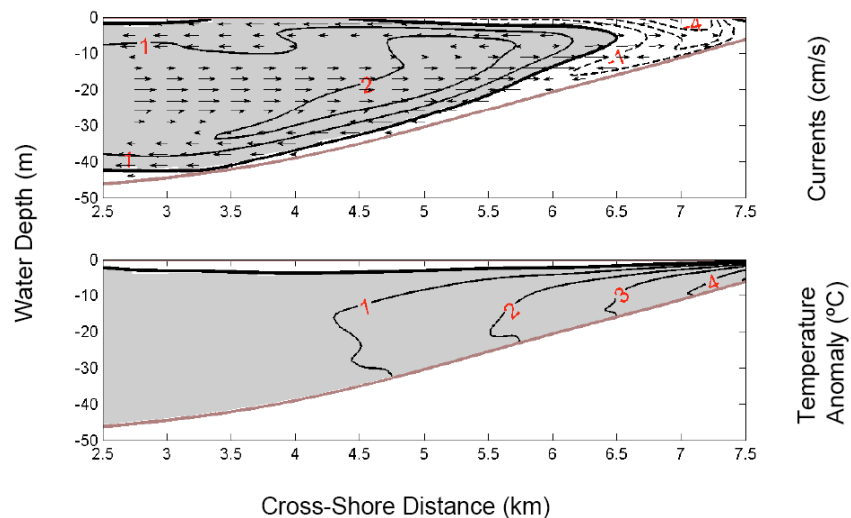


Figure 3. Upper panel: tidally-averaged cross-shore (arrows) and along-shore (contours) circulation. The maximum cross-shore current is about 5 cm s^{-1} and the contour interval is 1 cm s^{-1} . Lower panel: tidally-averaged, temperature anomaly (the difference between the tidally-averaged temperature and the initial temperature. Averaging was over eight M_2 tidal cycles.

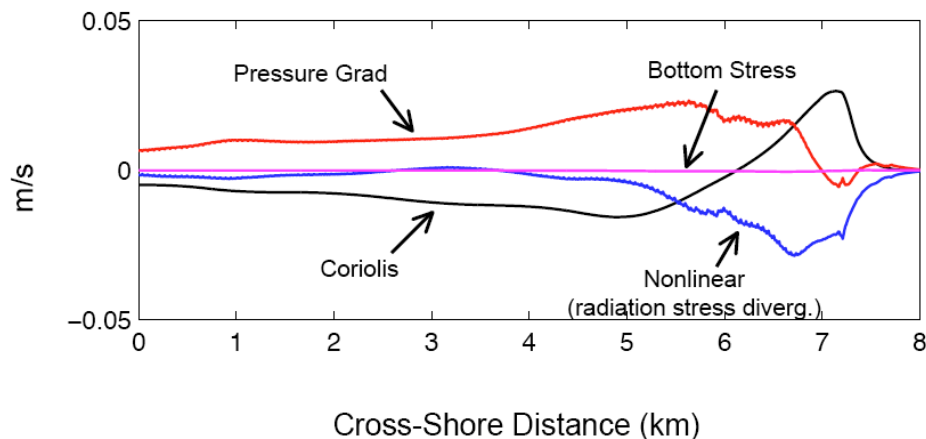


Figure 4. Vertically- and tidally-averaged terms in the cross-shore momentum equation vs cross-shore distance. Averaging is over eight tidal cycles. The three dominant terms in the balance are Coriolis, pressure gradient and the nonlinear radiation stress divergence associated with the shoaling nonlinear internal waves.

Results

The tidally-averaged (Eulerian), cross-shore circulation over the shoaling region is onshore at mid-depths with an amplitude of about 5 cm s^{-1} (Figure 3a). Near-surface and near-bottom currents are offshore. Along-shore currents are to the left (when facing the coast) in the outer portion of the shoaling region, and have an amplitude of about 2 cm s^{-1} (Figure 3b). In the inner-shelf (water depths $< 20 \text{ m}$), along-shore flow is to the right, with an amplitude exceeding 4 cm/s . We define the cross-shore temperature anomaly as the tidally-averaged temperature minus the initial (unperturbed) density field (Figure 3b). Below five meters, the water column is anomalously warm, and increasing in temperature towards the coast, with a cross-shore temperature gradient of four degrees over 2.5 km . In the upper 5 m of the water column, the temperature is anomalously cold.

In order to assess the dominant balances in the cross-shore momentum budget, we vertically- and tidally-average each of the terms in the cross-shore momentum equation (Figure 4). In water depths greater than 30 m ($x < 5 \text{ km}$), the dominant balance is between the cross-shore pressure gradient and the Coriolis term associated with the along-shore flow. In water depths less than 30 m ($x > 5 \text{ km}$), nonlinear transport of

momentum becomes important and the momentum balance is between the cross-shore pressure gradient, Coriolis and the nonlinear radiation stress divergence.

Conclusions

Cross-shore transport associated with shoaling, nonlinear internal waves is likely to be an important transport mechanism, and may be a dominant mechanism in regions where upwelling winds are not significant (e.g., the California coast south of the southern California Bight). This numerical modeling study suggests that transport of mass and momentum by shoaling internal waves drives a significant cross-shore and along-shore Eulerian circulation. The waves tend to ‘pile-up’ warm water on the inner shelf, which we refer to as the ‘internal set-up’, the pressure gradient associated with this internal set-up is balanced by Coriolis and the cross-shore radiation stress divergence due to the shoaling, nonlinear internal waves. The influence of internal waves on the background density and on the current fields should be taken into account when quantifying cross-shore fluxes of tracers (e.g., plankton, nutrients, and pollutants).

References

- Aigner, A., Broutman, D., Grimshaw, R. (1999), Numerical simulations of internal solitary waves with vortex cores, *Fluid Dynamics Research*, 25, 315–333.
- Bell, J.B., Marcus, D.L. (1992), A second-order projection method for variable-density flows, *Journal of Computational Physics*, 101, 334–348.
- Helfrich, K.R., Melville, W.K. (2006), Long nonlinear internal waves, *Annual Review of Fluid Mechanics*, 38, 395–425.
- Hogg, N.G. (1971), Longshore current generation by obliquely incident internal waves, *Geophysical Fluid Dynamics*, 2, 361–376.
- Jackson, C.R. (2004), *An Atlas of Internal Solitary-like Internal Waves*, Global Ocean Associates.
- Lamb, K.G. (1997), Particle transport by nonbreaking, solitary internal waves, *Journal of Geophysical Research*, 102, 18641–18660.
- Lamb, K.G. (2002), A numerical investigation of solitary internal waves with trapped cores formed via shoaling, *Journal of Fluid Mechanics*, 451, 109–144.
- Leichter, J.J., Stewart, H.L., Miller, S.L. (2003), Episodic nutrient transport to Florida coral reefs, *Limnology and Oceanography*, 48, 1394–1407.
- Lentz, S.J. (1992), The surface boundary layer in coastal upwelling regions, *Journal of Physical Oceanography*, 22, 1517–1539.
- Lennert-Cody, C.E., Franks, P.J.S. (1999), Plankton patchiness in high-frequency internal waves, *Marine Ecology Progress Series*, 186, 59–66.
- Munk, W.H., Anderson, E.R. (1948), Notes on a theory of the thermocline, *Journal of Marine Research*, 7, 276–295.
- Pineda, J. (1999), Circulation and larval distribution in internal tidal bore warm fronts, *Limnology and Oceanography*, 44, 1400–1414.
- Shanks, A.L. (1987), The onshore transport of an oil spill by internal waves, *Science*, 235(4793), 1198–1200.

Identification and structure of baroclinic tides off the southeast coast of the United States

HARVEY E. SEIM, CATHERINE R. EDWARDS, THOMAS SHAY, FRANCISCO WERNER

Department of Marine Sciences, University of North Carolina at Chapel Hill,
340 Chapman Hall CB 3300, Chapel Hill NC 27599-3300, USA
email: hseim@email.unc.edu, credward@email.unc.edu, tshay@email.unc.edu,
cisco@unc.edu

Keywords: internal tides, modal structure, current profiles

ABSTRACT

Despite conditions favorable for generation of internal tides, detection of semidiurnal baroclinic tides on the shelf and slope of the US southeast coast has been difficult because of the presence of strong flows on the shallow shelf. However, recent observational and model studies from a coastal observatory system are beginning to provide evidence for their existence. Multi-year records from a cross-shelf array of current profilers are used to document the strength and variability of the internal tide on the shallow shelf. An empirical orthogonal function analysis is used to both isolate the barotropic tide, which has a pronounced bottom boundary layer structure, and to quantify the modality and amplitude of the baroclinic tide at semidiurnal frequencies. Gravest modes dominate the signal, with amplitude increasing with water depth. There are few signs of the development of solitons on the shelf except during period of abnormally strong stratification. Several short-term glider deployments confirm the modal structure and provide detailed mass field observations. These patterns of variability suggest a generation site near the shelf break. Because the presence of the Gulf Stream at the shelf break makes mooring deployments difficult and costly, a recently developed regional-scale circulation model is used to look for evidence of an internal tide generation site seaward of the mooring array and for propagation of the internal tide into the Sargasso Sea. Constraints on propagation imposed by the presence of the Gulf Stream are explored.

Introduction

The South Atlantic Bight (SAB) is a region where the major axis of semi-diurnal tidal currents is oriented across isobaths over the continental slope and shelfbreak (Blanton et al., 2004). The presence of the Blake Plateau (water depth 800–1000 m) makes the total depth change at the continental slope less extreme than in other parts of the world but it still has the potential for generating a significant internal tide. A considerable complication to estimating the potential magnitude of the internal tide is the presence of the Gulf Stream flowing along the slope which 1) enhances offshore stratification below the depth of the shelfbreak and 2) causes the pycnocline to shoal dramatically over the slope. Both factors complicate estimation of the potential for internal tide generation because they violate common assumptions in semi-analytical treatments (Vlasenko et al., 2005).

We are aware of a single published observational account of internal tides on the inner shelf for a small region in the SAB in the context of fisheries studies (Shank, 1988). Two studies have suggested their presence over a broad scale, however; the first a study of chlorophyll imagery that suggested internal tides as a possible explanation for the presence of enhanced chlorophyll along the shelfbreak (Ryan and Yoder, 1996), the second a study of the barotropic tides in the SAB that found a significant seasonal variation in tidal amplitude and phase at the coastline that may indicate a seasonally varying mechanism for internal tide generation in the region that shunts barotropic tidal energy into the internal tide during certain times of year (Blanton et al., 2004).

We here begin to establish a framework for examining the internal tides off the southeastern United States. The first element is evidence for the presence of internal tides on the shelf from current moorings and a glider survey; the second is model evidence for internal tides from a regional-scale model.

Evidence of an internal tide

A number of current meter moorings have been maintained on the shelf off of Georgia since 2000 (Seim et al., 2003). Because the shelf is shallow (<50 m depth) and experiences 1–2 m amplitude tides, current variance on the shelf is dominated by tidal-frequency fluctuations. Stratification is not particularly strong and hence the bottom boundary layer influence extends through a significant fraction of the water column. It is therefore important to correctly account for the structure of the barotropic tide before quantifying the magnitude of currents associated with the internal tide. We have used an empirical orthogonal function (EOF) analysis to define the vertical modal structure of the currents (Edwards and Seim, 2008) and identify the gravest mode with the barotropic tide. Higher vertical modes are assumed to contain the variance associated with internal processes, including internal tides. Summing the higher modes and band-passing in the semidiurnal band reveals a seasonally and spatially varying internal tidal current dominated by a mode 1 and 2 (one or two nodes in the vertical) structure. The multi-year records permit examination of seasonal and interannual variability in the magnitude of the signal and can be considered a first step in developing an internal tide climatology for the shelf. Moderate amplitude, tidal-frequency internal wave motions dominate the records; solitary-wave like signals are rare and occur at times of abnormally strong stratification, as during summer of 2003 (Aretxabaleta et al., 2006). Near the shelf break, seasonally-averaged magnitudes are greatest, with a magnitude of about 3 cm s^{-1} , but exhibiting considerable seasonal and interannual variability (e.g. Figure 1). Maximum values are found below mid-depth, suggesting that the internal tide may exist preferentially as a wave of elevation on the outer shelf. Further onshore magnitudes slowly decrease and the magnitude distribution adjusts to nearly equal surface and bottom values.

Several glider deployments near the shelfbreak have also confirmed the presence of an internal tide. A month-long survey in August 2006 in which the glider stayed in approximately the same location, yielding a time series of temperature and salinity profiles, exhibits semi-diurnal frequency pycnocline displacements of several meters which vary with the spring-neap cycle. A subsequent deployment in which the glider occupied a more inshore location for several days, then transited to the Gulf Stream, confirmed the presence

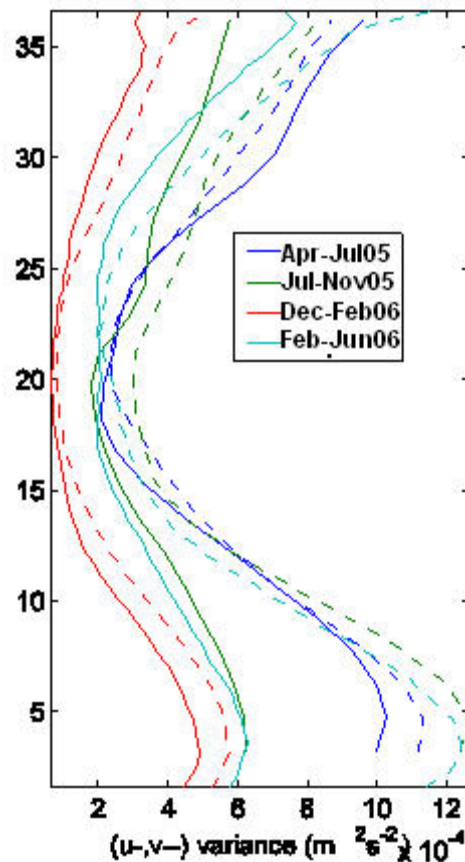


Figure 1. Vertical profiles of current variance computed over several seasons from semidiurnal band-passed current observations collected near the shelf break. Vertical axis is meters about the bottom; solid lines are for shore-parallel currents and dashed lines for shore-normal. Note the greater current variance in the lower half of the water column and the significant seasonal variability.

of an internal tide at mid-shelf, and suggested a much larger amplitude, and possibly more non-linear, wave field near the inshore edge of the Gulf Stream.

Evidence for generation of an internal tide on the slope and at the shelf break is present in output from a regional-scale implementation of a finite-element model nested within a basin-scale model of the North Atlantic. However, evidence for propagation of the internal tide is poorly represented in the model because of coarse resolution seaward of the shelf break. The regional-scale model used is QUODDY, which resolves the tides but is hydrostatic. The mass field and subtidal boundary conditions used for bi-weekly integrations are taken from a HYCOM simulation of the North Atlantic and provide a realistic estimate of the Gulf Stream in the region. Examination of model output from four cross-sections at varying latitudinal positions reveals variance maxima over the slope in most fields. The variance is dominated by signals at tidal frequencies, and the spatial structure is enhanced near bottom along nearly linear trajectories paralleling the upper slope; other structures are also apparent that may be associated with Gulf Stream dynamics. There is no obvious signal propagation away from the variance maximum, which is likely the result of poor spatial resolution in the model. Other sources of model fields are available and will be explored. One promising source is ADCIRC solutions run on a revised finite-element grid with much higher resolution seaward of the shelf break, but the implementation is not yet finalized.

References

- Aretxabaleta, A., Nelson, J.R., Blanton, J.O., Seim, H.E., Werner, F.E., Bane, J.M., Weisberg, R. (2006), Cold event in the South Atlantic Bight during summer of 2003: Anomalous hydrographic and atmospheric conditions, *Journal of Geophysical Research*, 111, C06007, doi:10.1029/2005JC003105.
- Blanton, B., Werner, F., Seim, H., Luettich Jr., R., Lynch, D., Smith, K., Voulgaris, G., Bingham, F., Way, F. (2004), Barotropic Tides in the South Atlantic Bight, *Journal of Geophysical Research*, 109, C12024, doi:10.1029/2004JC002455.
- Edwards, C.R., Seim, H.E. (2008), EOF analysis as a method to separate barotropic and baroclinic velocity structure in shallow water, *Journal of Atmospheric and Oceanic Technology*, 25, 808–821.
- Ryan, J.P., Yoder, J.A. (1996), Long-term mean and event-related pigment distributions during the unstratified period in South Atlantic Bight outer margin and middle shelf waters, *Continental Shelf Research*, 16(9), 1165–1183.
- Seim, H., Bacon, B., Barans, C., Fletcher, M., Gates, K., Jahnke, R., Kearns, E., Lea, R., Luther, M., Mooers, C., Nelson, J., Porter, D., Shay, L., Spranger, M., Thigpen, J., Weisberg, R., Werner, F. (2003), SEA-COOS – A Model for a Multi-State, Multi-Institutional Regional Observation System, (*Marine Technology Society*) *MTS Journal*, 37(3), 92–101.
- Shanks, A.L. (1988), Further support for the hypothesis that internal waves can cause shoreward transport of larval invertebrates and fish, *Fishery Bulletin*, 86, 703–714.
- Vlasenko, V., Stashchuk, N., Hutter, K. (2005), *Baroclinic tides, theoretical modeling and observational evidence*, Cambridge University Press, New York, 351pp.

